POLITECNICO DI TORINO

Master Degree course in Biomedical Engineering

Master Degree Thesis

A Review of Quantifying Drug Diffusion in Human Tissues for Assessing Drug Dispersion in the Body

Supervisors
Dr. Giulia Grisolia
Prof. Umberto Lucia

Candidate
Matilda Laborante

Academic Year 2024-2025

Ai piccoli che affrontano la vita con il cuore spezzato
a causa di un male, a volte incurabile,
eppure continuano a sorridere.

Abstract

Understanding the mechanisms and effectiveness of drug diffusion in human tissues is critical for advancing precision medicine and optimizing therapeutic strategies. This thesis presents a comprehensive bibliographic and methodological review of current approaches for evaluating drug diffusion, emphasizing the integration of pharmacokinetics, thermodynamics, and state-of-the-art imaging technologies. Central to this investigation is the role of magnetic resonance imaging (MRI), with a particular focus on diffusion-weighted imaging (DWI) and dynamic contrast-enhanced (DCE) sequences, which serve as powerful, non-invasive tools for visualizing drug dispersion, assessing tissue permeability, and monitoring pharmacodynamic interactions in vivo.

This work inquiries into the application of mathematical and physical models to describe and predict drug transport phenomena. Models based on Fick's law of diffusion and Darcy's law for fluid flow are examined alongside tracer-kinetic models and thermodynamic concepts such as Gibbs free energy. These frameworks provide a theoretical basis for simulating molecular movement across complex biological barriers and heterogeneous tissue environments. Emphasis is placed on the importance of combining empirical data from imaging studies with computational simulations to achieve more accurate and meticulous predictions of drug behavior.

Special attention is dedicated to pediatric pharmacotherapy, a field that presents unique challenges due to anatomical and physiological variability, limited availability of patient data, and strict ethical constraints on invasive procedures. The use of non-invasive imaging modalities and computational models becomes especially valuable in this context, offering safer alternatives for assessing drug efficacy and optimizing dosing regimens in vulnerable populations.

Furthermore, the thesis explores the clinical and translational potential of emerging technologies, including the use of nanoparticles for targeted delivery and the application of artificial intelligence (AI) for image analysis, parameter estimation, and model personalization. Illustrative case studies and optimized imaging protocols are discussed to demonstrate real-world applications and highlight areas for future development.

By integrating multidisciplinary methodologies - from biophysics and pharmacology to medical imaging and computational modeling - this research proposes a comprehensive framework aimed at enhancing the precision, efficacy, and safety of drug administration in both adult and pediatric populations. The findings and recommendations presented herein aim to support the development of more individualized therapeutic strategies and contribute to the evolving landscape of precision medicine.

Contents

Chapter 1

Introduction

1.1 Medicinal Drug

> *A medicinal product (medicine)[1] is a substance or combination of substances that is used for the treatment or prevention of diseases in human beings. With the aim of safeguarding public health, the market authorisation, classification, and labelling of medicines has been regulated in the EU since 1965. Since 1995, the evaluation of most medicines has been centralised through the European Medicines Agency (EMA) to streamline approvals and maintain a stable supply of medicinal products.*

Definition found on the European Parliament website [37]. In Italy, medicinal products are regulated by the Agenzia Italiana del Farmaco (AIFA) [17] and defined in line with the European Directive 2001/83/EC [56]. This directive governs the community code relating to medicinal products for human use. Article 1(2) of the directive states:

> Medicinal product shall mean:
>
> a) any substance or combination of substances presented as having properties for treating or preventing disease in human beings; or
>
> b) any substance or combination of substances which may be used in or administered to human beings either with a view to restoring, correcting or modifying physiological functions by exerting a pharmacological, immunological or metabolic action.

In the United States, medicinal drugs are regulated by the Food and Drug Administration (FDA) under the Federal Food, Drug, and Cosmetic Act (FDCA). According to Section 201(g) [46]:

---

[1] *Throughout this thesis, the terms* drug, medical drug, medicine, *and* medicinal product *are used interchangeably, unless explicitly stated otherwise. This equivalence reflects common usage in biomedical literature and aims to enhance readability without loss of scientific precision.*

> The term *drug* means (A) articles recognized in the official United States Pharmacopoeia, official Homoeopathic Pharmacopoeia of the United States, or official National Formulary... and (B) articles intended for use in the diagnosis, cure, mitigation, treatment, or prevention of disease in man or other animals... and (C) articles (other than food) intended to affect the structure or any function of the body of man or other animals.

From a structural point of view, each drug consists of (a) an active ingredient, responsible for the therapeutic effect, acts therapeutically on the cells of the living being concerned; and (b) one or more excipients, which perform supporting functions such as stabilising, preserving, improving bioavailability or facilitating administration [6, 7]. The active ingredient is the component of medicines on which its curative action, the actual medicine. Excipients, on the other hand, are inactive components of the medicinal, devoid of any pharmacological action; their function is to protect the active ingredient from external agents that could damage it (heat, cold, moisture or other substances), damage it (heat, cold, humidity or other chemicals), to increase the volume to allow the preparation of tablets or any other pharmaceutical form, to stabilise solutions, suspensolutions or suspensions by avoiding sedimentation of the active ingredient at the bottom of the container, to facilitate the absorption of the active ingredient in the body, to make medicines taste more pleasant, etc.

In Italy, the notion of a medicine also includes [7]:

- immunological medicinal products which include vaccines, toxins, serums or allergens, in particular *agents used for the purpose of inducing active immunity or passive immunity and agents used for the purpose of diagnosing the state of immunity*,
- homeopathic medicines,
- radiopharmaceuticals,
- radionuclide generators and precursors,
- kits: any preparation to be combined with radionuclides in the final radiopharmaceutical, usually before administration,
- medicines derived from human blood or plasma, whole blood, i.e. blood taken from a donor, does not fall within the notion of medicinal product,
- medicines for advanced therapies: gene therapy drugs, somatic cell therapy and tissue engineering products. The latter consist of cells or tissues of human or animal origin or both.

Once authorised by AIFA, the marketing authorisation (MA) is valid for five years. At this point, one can proceed with the primary packaging and packaging, which is called *labelling*. Detailed information on the drug is written on the package leaflet.

Medical drugs can be classified according to multiple criteria. In Italy, according to AIFA, medicines can be classified as:

- prescription medicines,
- medicines subject to medical prescription to be renewed time by time,
- medicines subject to special medical prescription,
- medicines subject to restrictive medical prescription, including:
  - medicines sold to the public on prescription by hospitals or specialists,
  - medicines that may only be used in a hospital environment or hospital or similar environment,
  - medicinal products that can only be used by specialists,
- non-prescription medicines including:
  - over-the-counter or self-medication medicines,
  - remaining non-prescription medicines.

According to the pharmaceutical form [62], medicines can be solid (tablets, capsules), liquid (syrups, injectable solutions), semi-solid (creams, ointments) or gaseous (aerosols). The choice of pharmaceutical form and route of administration (oral, intravenous, topical, transdermal, etc.) has a decisive influence on the pharmacokinetics of the drug and, in particular, on its ability to reach the site of action in therapeutically effective concentrations.

From a therapeutic perspective, medical drugs are divided into analgesics, antibiotics, antineoplastics, antivirals, immunosuppressants, among others. From the point of view of mechanism of action, they can be divided into agonists, antagonists, modulators, enzyme inhibitors, etc.

Chemical structure also provides a criterion for classification: small molecules, biological drugs (monoclonal antibodies, vaccines), synthetic peptides, and emerging nanotechnologies are distinguished. This heterogeneity reflects the increasing complexity of the diseases to be treated and the need for increasingly targeted and personalised therapeutic approaches [40].

Specifically, Vargason et al. [80] analyzed five classes of therapeutic who led to the creation of medicines: small molecules, nucleic acids, peptides, proteins, and cells. These classes can be seen in figure 1.1. After these analysis, the authors identify, furthermore, three core paradigms that have been employed to address drug delivery challenges across different classes of therapeutics: modifying the drug itself, changing the surrounding environment of the drug, and designing an interface (namely, a drug delivery system) that manages the interactions between the drug and its microenvironment to enhance delivery.

For all medical drugs, delivery must aim to maximize therapeutic efficacy while minimizing off-target effects. This involves ensuring that the drug reaches and is released at

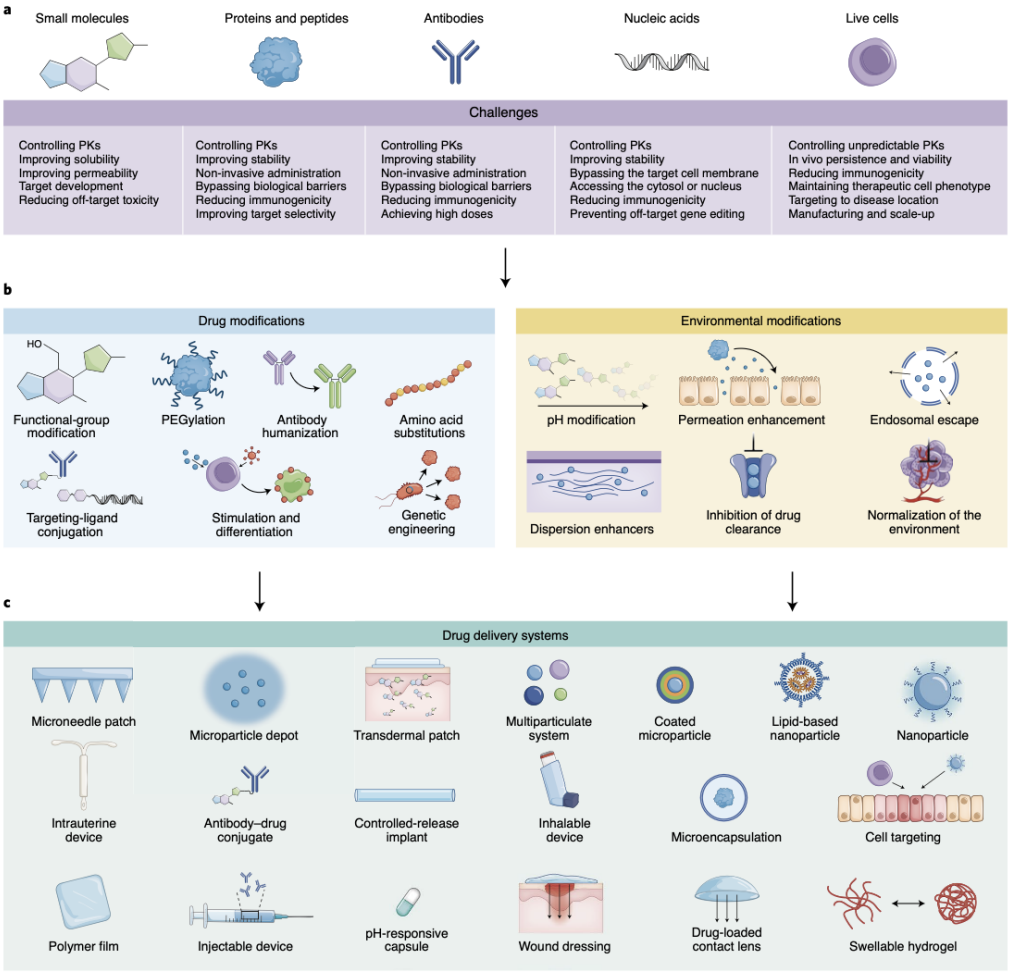

Figure 1.1: Classification of medical drugs by Vargason et al. [80].

the intended site in the body - either passively or actively - while avoiding unwanted distribution elsewhere. Achieving this requires control over pharmacokinetics, which governs how the body absorbs, distributes, metabolizes, and excretes the drug. By studying and manipulating pharmacokinetics, it is possible to reduce drug toxicity, enhance accumulation at the target site, and ultimately to improve patient acceptance and compliance. The table in the appendix (Table 1) shows the challenges faced by Vargason et al.

1.1.1 Pharmacokinetics

Pharmacokinetics [23] is the branch of pharmacology that studies how drugs are distributed in the body, specifically analysing how and when a pharmacologically active substance is absorbed, distributed, metabolised, and eliminated. Understanding these processes is crucial to correctly design a drug therapy, as the concentration of the drug at the site of action determines both the efficacy and toxicity of the treatment.

Important is the concept of the therapeutic window, which is the interval between the minimum effective concentration and the concentration at risk of toxic effects. A drug with a wide therapeutic window will be safer to administer, as it will tolerate larger concentration changes without compromising therapy.

The modern approach to drug administration is no longer based solely on empirical experience, but is based on general biological principles that regulate the behaviour of substances in the body. Through the study of pharmacokinetics, it is possible to predict with good accuracy the course of plasma and tissue concentrations of a drug depending on its chemical-physical characteristics, the route of administration and the patient's pathophysiological state. In this way, the physician can plan the most appropriate dosage to achieve the desired effect while minimising the risk of adverse events.

There are four main pharmacokinetic processes: absorption, distribution, metabolism and elimination (also known by the acronym ADME). These events are closely influenced by the ability of the drug to cross cell membranes, which in turn depends on the lipophilic/hydrophilic partition coefficient and any active or facilitated transport mechanisms. Each stage of pharmacokinetics represents a critical node that can profoundly affect bioavailability and, consequently, the efficacy of drug treatment.

Absorption

Absorption is the first step a drug takes to reach the systemic circulation, unless it is administered directly intravenously. It comprises all those processes, passive and active, that allow the drug to pass from the site of administration into the bloodstream.

The predominant mechanism is passive diffusion, governed by Fick's law (discussed in detail in the following chapter 2.3.1.), though active transport, facilitated diffusion or endocytosis mechanisms may also be involved.

Factors determining the efficiency of absorption are the partition coefficient (lipophilicity/hydrophilicity of the drug), solubility, absorbent surface area, permeability of biological barriers, and the degree of vascularity of the site.

The small intestine, due to its large surface area and rich blood supply, is the main site of enteric absorption. Furthermore, gastric emptying and the presence of food can significantly influence oral bioavailability, i.e. the fraction of the administered dose that reaches the systemic circulation unaltered.

Distribution

Once absorbed, the drug is distributed through the circulatory stream to the different tissues of the body. This process is not uniform and depends on various factors, including tissue perfusion, binding of the drug to plasma proteins, capillary permeability and the chemical and physical characteristics of the drug.

The capillary endothelium represents a selective barrier, whose permeability varies in different body districts: highly permeable in the liver, very selective in the brain where it forms the blood-brain barrier (BBB). The latter severely limits the entry of hydrophilic drugs, while favouring lipophilic ones. The placental barrier also has peculiar

characteristics that allow the passage of numerous drugs from mother to foetus, a crucial aspect in pharmacotherapy during pregnancy.

Metabolism

Metabolism, or biotransformation, comprises the processes by which the body chemically modifies the drug, often to facilitate its elimination. The liver is the main organ involved, due to the presence of numerous enzymes (particularly of the cytochrome P450 system) capable of transforming drugs into inactive metabolites or sometimes into active compounds (pro-drugs).

Metabolisation can alter the drug's partition coefficient, making it more hydrophilic and thus more easily eliminated. However, high hepatic activity can significantly reduce the bioavailability of some orally administered drugs. This is the so-called first-pass effect.

Elimination

Elimination is the process that leads to the removal of the drug from the body and can occur through urine (renal circulation), faeces (biliary system), exhaled air (pulmonary route), saliva, sweat and breast milk. The kidney is the main organ responsible for the elimination of hydrophilic drugs, which are filtered by the glomerulus and then reabsorbed or excreted along the nephron. Lipophilic drugs often have to be metabolised first to be eliminated effectively.

The rate at which a drug is eliminated affects its plasma half-life and thus the frequency of administration. Alterations in liver or kidney function may compromise the efficacy and safety of therapy, leading to drug accumulation and adverse effects.

1.2 Scientific Context and State of the Art

The evaluation of drug delivery in human tissues is a multidisciplinary field involving biomedical engineering, pharmacokinetics, materials science, and many others. Several approaches, both experimental and computational, have been developed to understand and model drug transport mechanisms in biological tissues. In this section, the main contributions in the literature will be reviewed, highlighting the progress and the challenges still open.

Mathematical models (2.3.1) are fundamental tools for describing drug diffusion in human tissues. The Fick equation (2.3.1) is often used as a basis for modelling passive transport, but more complex models have been developed that take into account tissue anisotropy and drug-tissue interactions and other issues. A very significant example in this sense is the Higuchi model (2.3.2) introduced in the 1960s by Takeru Higuchi. Even though many years have passed, its use is still very widespread in this field.

Furthermore, advanced computational models, such as those based on finite elements (2.3.5), were used to simulate drug diffusion in complex tissues, taking into account the mechanical and structural properties of the tissue microenvironment. Each interaction is fundamental to understand the right mechanism and perform a correct study.

Modern discoveries in the field of computer science can be a valuable tool in the study of this field of research. For example, van Herten et al. [79] introduces physics-informed neural networks (PINNs) to perform myocardial perfusion magnetic resonance (MR) quantification. The controversial field of artificial intelligence will be discussed in the chapter 4.2 and how it was introduced into this field of research will be indicated. The use of *data-driven* models, which combine experimental data with machine learning algorithms, is emerging as an effective strategy to predict drug distribution in complex physiological conditions.

Experimental techniques are essential to validate computational models and obtain quantitative data on drug diffusion. In Chapter 3, some examples will be presented to validate this statement. Magnetic resonance imaging (MRI) is one of the most used techniques to monitor drug distribution in tissues in real-time. But other techniques will also be mentioned, sometimes used in combination for better precision and optimization of therapy. For example, data obtained from imaging techniques, such as MRI or PET, can be used to calibrate and validate numerical simulations, allowing a more accurate representation of drug diffusion in tissues.

Other techniques, such as Raman spectroscopy and confocal microscopy, have been used to analyze drug distribution at the cellular and subcellular level, providing a more detailed view of drug-tissue transport and interaction mechanisms as demonstrated by Esmonde-White et al. [21].

The development of controlled release systems is essential to optimize drug diffusion in tissues. Drug nanocrystals and nanoparticles (NPs), for example, offer significant advantages in terms of solubility and bioavailability. These elements are also fundamental in the field of imaging and to be precise on a specific target.

Despite significant progress, several challenges remain in assessing drug diffusion in human tissues. The complexity of biological tissues, interindividual variability, and the difficulty in obtaining precise in vivo parameters represent significant obstacles.

This work fits into this context, proposing an integrated approach that combines advanced computational models with experimental data (3), in order to improve the understanding of drug diffusion mechanisms and optimize delivery strategies.

1.3 Purpose of Thesis

The primary aim of this thesis is to explore and critically analyze the current methods used to assess drug diffusion in human tissue, with a particular focus on technologies that bridge pharmacokinetics and medical imaging. This research is primarily bibliographic in nature, aiming to consolidate and evaluate the state-of-the-art knowledge in this field, while also identifying potential areas for future investigation.

Special attention is given to methods involving the analysis of pharmacokinetics, particularly the role of Gibbs free energy in modeling drug release kinetics. Furthermore, the thesis investigates the use of magnetic resonance imaging (MRI) as a non-invasive tool to monitor drug dispersion, alongside experimental setups that can simulate in vivo conditions and help validate diffusion models.

A key aspect of this research is to examine the technologies currently employed by

clinicians to monitor and assess drug delivery effectiveness, evaluating both their strengths and limitations. The study also aims to highlight open issues in this domain, including the need for more precise, real-time monitoring tools and personalized approaches to drug diffusion assessment.

In pediatric cases, the challenge is even greater, as infants are especially vulnerable and many standard assessment techniques are either too invasive or ethically constrained. In this part of the discussion, a small socio-economic aspect will also be revealed.

Finally, illustrative case studies - whether from literature or proposed as conceptual frameworks - will be used to contextualize the theoretical findings and underline their clinical relevance.

Context and Motivations

This work was born from a dual interest that has matured over time: on the one hand, scientific curiosity towards the world of drugs, consolidated during the years of study; on the other, a personal attention towards the world of childhood, cultivated thanks to continuous experiences as a childcare provider during the university course. The theme chosen for this work reflects not only an academic interest in the methods of investigation of drugs in human tissue, but also a personal sensitivity that has matured over the years. The encounter with literature in the pediatric field has aroused a particular involvement, also thanks to the experiences lived as a babysitter, making this investigation not only scientifically stimulating, but also humanly significant.

Chapter 2

Materials and Methods

2.1 Diffusion and Convection

The transport of drugs within the body is a complex process involving several physical and biological mechanisms. Among these, diffusion and convection represent the main phenomena through which drugs are distributed in tissues. Understanding these mechanisms is crucial for the optimisation of drug therapies and the development of controlled release systems.

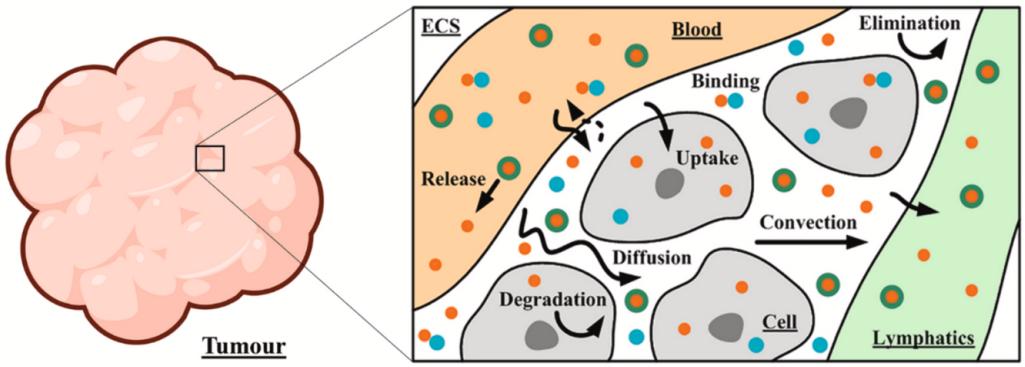

Figure 2.1: Schematical diagram of the key drug-tumour interactions in the tissue [8].

Diffusion

Diffusion is a fundamental transport mechanism in biological systems, referring to the movement of molecules from a region of higher concentration to a region of lower concentration, driven by the concentration gradient. This passive process does not require energy input and is described by Fick's laws of diffusion 2.2, which allow quantification of molecular flux based on parameters such as concentration gradient, diffusion coefficient, surface area, and barrier thickness. The diffusion coefficient itself depends on molecular properties (such as size and shape), the viscosity of the medium, and temperature.

In the context of drug delivery, passive diffusion is especially relevant in systems designed for controlled release, such as hydrogels or polymeric matrices, where the drug moves through the material and into surrounding tissues over time. Similarly, diffusion across biological barriers - such as epithelial layers or mucus - plays a critical role in determining drug absorption and bioavailability.

On the other hand, active transport mechanisms involve the movement of molecules against a concentration gradient and require energy input, typically in the form of adenosine triphosphate (ATP), the cell's primary energy carrier. These processes are mediated by specific transporter proteins and are essential for the uptake of certain drugs, especially those that are not able to cross membranes by passive diffusion alone.

In the evaluation of drug diffusion in human tissues, distinguishing between passive and active transport mechanisms is crucial, as they impact both the modeling approach and the interpretation of experimental data. While passive diffusion can often be described with mathematical models based on Fick's laws, active transport requires more complex kinetic models that account for saturation, energy dependence, and specific molecular interactions. Understanding these mechanisms is key to optimizing drug delivery strategies and accurately predicting drug distribution within tissues.

Convection

Convection is the transport of mass due to fluid motion, often induced by a pressure gradient. This mechanism is described by Darcy's law 2.13. Convection can overcome the limitations of diffusion, especially in dense tissues or in the presence of biological barriers.

Convection-Enhanced Delivery (CED) [95] is a technique that uses convection to improve the distribution of drugs in the central nervous system. Through the insertion of catheters and the application of positive pressure, it is possible to directly infuse the drug into the brain tissue, bypassing the blood-brain barrier (BBB). This methodology has been studied for the treatment of pathologies such as glioblastoma, epilepsy and Parkinson's disease.

In many biological systems, diffusion and convection act simultaneously, influencing drug distribution. For example, in tumor tissues, high vascular permeability can favor convection, while extracellular matrix density can limit diffusion. Understanding the interaction between these two mechanisms is crucial to design effective drug delivery strategies.

The integration of mathematical models and experimental data allows the experts to understand and predict the behavior of drugs in biological systems, facilitating the development of more effective and targeted therapies.

The solute transport in biological systems can be assumed to be a combination of convection and diffusion in the porous medium. Here, Arifin et al. [4] present the concept of percolation theory for the solute transport in the porous medium is applied with additional feature of solute elimination kinetics. The drug elimination due to degradation and uptake by the tissue cells, species conservation also involves the possible source of drug transported from the vasculature and loss due to convective to the lymphatic system.

For the drug transport, they used:

$$\frac{\partial C_i}{\partial t} = D_{e:tissue}\nabla^2 C_i - \nabla \cdot (r_F \boldsymbol{v} C_i) + F_s - F_{s1} - R(C_i) \tag{2.1}$$

The first two terms of the equation capture the diffusion and convective contributions, the third and fourth terms describe the possible drug source and the last term is the rate of drug degradation and uptake in the tissue.

Another example of this strong link between these two concepts is represented by Yuan et al. [95] present a convection-diffusion reaction equation that encompasses convection and diffusion specifically for drug delivery in the brain, reported below 2.16. This equation is an excellent example of how these phenomena are intrinsically linked and are never isolated from each other.

2.2 Perfusion

Perfusion [65] is a key physiological parameter describing blood flow through tissue, usually expressed in milliliters per minute per gram of tissue (mL/min/g). This process is crucial for the transport and distribution of systemically administered drugs, as it determines the amount and speed at which the active substance reaches the target tissues. In particular, perfusion directly affects the distribution phase of the drug after absorption, influencing local concentration and therapeutic efficacy.

In the context of pharmacokinetic modeling, perfusion is often incorporated into so-called perfusion-limited models, in which the rate at which the drug penetrates the tissues is limited primarily by blood flow rather than by the permeability of cell membranes [44]. Advanced imaging techniques, such as dynamic contrast-enhanced magnetic resonance imaging (DCE-MRI) or positron emission tomography (PET), now allow a non-invasive estimate of perfusion in vivo, supporting both diagnosis and therapeutic monitoring [76].

In the case of tissues with low perfusion, such as some neoplasms or fibrotic areas, medical drug diffusion can be significantly compromised, limiting the efficacy of the treatment. For this reason, the evaluation of perfusion represents a key aspect in therapeutic planning and in the development of controlled release systems [35].

2.3 Laws and Mathematical Models in Drug Delivery

The conduct of medical drugs in biological tissues is governed by fundamental physical laws and mathematical models that make it possible to simulate and predict the behaviour of active ingredients in complex biological systems. This chapter provides an overview of the main equations and models used to describe these phenomena, with a focus on controlled release in the articles analysed.

2.3.1 Fundamental Laws of Diffusion

Fick's Law

As mentioned previously, diffusion is a fundamental process in many areas, such as oxygen transport in tissues, drug delivery and solute exchange in biological membranes. Fick's

laws mathematically describe mass flow due to a concentration gradient.

Fick's first law [50] states that diffusive flow J of a solute through a medium is proportional to the concentration gradient:

$$J = -D\frac{dC}{dx} \tag{2.2}$$

Where:

- J is the diffusion flux [mol·m^{-2}·s^{-1}],
- D is the diffusion coefficient [m^2/s],
- $\frac{dC}{dx}$ is the concentration gradient along the x-direction [mol·m^{-3}·m^{-1}].

This law applies under stationary conditions, i.e. when the concentration does not vary over time.

Fick's second law [4], or diffusion equation, describes the time evolution of the concentration of a solute in a medium and is derived from the application of the law of conservation of mass combined with Fick's first law:

$$\frac{\partial C}{\partial t} = -D\frac{\partial^2 C}{\partial^2 x} \tag{2.3}$$

Where:

- $\frac{\partial C}{\partial t}$ represents the time variation of the concentration,
- $\frac{\partial^2 C}{\partial^2 x}$ is the second derivative of the concentration with respect to position.

This equation is used in non-stationary conditions, where the concentration varies with time.

Both laws assume that the medium is homogeneous, isotropic, free of chemical reactions and that the diffusion coefficient D is constant.

Laplace's Law

When a steady state is reached, Fick's second law reduces to Laplace's equation [41],

$$\nabla^2 C = 0 \tag{2.4}$$

where C represents the drug concentration. This simplified form is applicable in constant release systems, such as reservoirs, where the drug distribution in the tissue reaches an equilibrium.

The Laplace equation also appears in other contexts relevant to biomedical engineering. For example, in the study of electroporation, Granot et al. [29] consider the electric field generated inside the tissues, modeled through an extension of the classical form of the equation:

$$\nabla((\sigma + \varepsilon_0\varepsilon)\nabla\varphi) = 0 \tag{2.5}$$

Where:

- φ is the electric potential,

- σ, is the extracellular conductivity,
- ε, is the relative permittivity (dielectric constant),
- ε_0 is vacuum permittivity.

In this case, the equation describes the distribution of the electric field taking into account the electrical composition of the tissue, which is essential for modeling the effect of electromagnetic fields on the transport of molecules.

The Laplace operator [41], also known as the Laplacian, is a differential operator defined as:

$$\nabla^2 f = \frac{\partial^2 f}{\partial x^2} + \frac{\partial^2 f}{\partial y^2} + \frac{\partial^2 f}{\partial z^2} \tag{2.6}$$

It measures the divergence of the gradient of a function and appears naturally in equations describing diffusion, heat transfer or electric field phenomena in conductive materials.

Finally, the Laplace transform [50] is a useful mathematical tool for solving linear differential equations, especially in dynamic (non-stationary) models. The transform allows to move from the temporal domain to the complex domain, facilitating the analysis of temporal drug release systems, especially in compartmental models.

$$\mathcal{L}f(t) = \int_0^\infty e^{-st} f(t), dt \tag{2.7}$$

2.3.2 Drug Release Models

Higuchi Model

First proposed by Takeru Higuchi in 1961 [6], Higuchi's model describes the release of drugs from a homogeneous matrix system where the mechanism is primarily governed by Fickian diffusion. It assumes a pseudo-steady-state concentration gradient within the matrix and is particularly applicable to systems where the initial drug concentration significantly exceeds its solubility within the carrier medium (i.e., $C_0 \gg C_s$).

The model predicts that the cumulative amount of drug released, M_t, is proportional to the square root of time, yielding the well-known relation $M_t = k_H\sqrt{t}$, where k_H is the Higuchi release constant. This square root time dependence is often interpreted as evidence of diffusion-controlled kinetics in planar, spherical, and cylindrical geometries [4, 50, 77].

Higuchi's theory, originally developed for semi-solid and topical formulations, is now widely applied in modeling release from various modern drug delivery systems including microspheres, nanoparticles (NPs), and hydrogels, owing to its simplicity and empirical success across a broad spectrum of drug-polymer interactions [4]. However, it is important to note that despite frequent application, many studies assume Higuchi kinetics even when actual boundary and physicochemical conditions deviate from those originally required by the model [50].

Tracer-Kinetic Modelling

Tracer-kinetic modeling [95] plays a critical role in biomedical imaging and pharmacokinetics by providing a quantitative framework to describe the transport and interaction of drugs or contrast agents within biological systems. This approach is particularly prominent in techniques such as dynamic contrast-enhanced magnetic resonance imaging (DCE-MRI), dynamic susceptibility contrast MRI (DSC-MRI), and positron emission tomography (PET), where temporal signal changes following tracer administration are interpreted using compartmental models governed by systems of ordinary differential equations (ODEs).

In the context of DCE-MRI, pharmacokinetic parameters such as the volume transfer constant (K^{trans}), the extravascular extracellular space fraction (v_e), and the plasma volume fraction (v_p) are estimated using models like the Tofts or extended Tofts model [34], which capture the dynamics of tracer diffusion and permeability across capillary membranes. These models assume a linear relationship between contrast concentration and signal intensity and require accurate knowledge of the arterial input function (AIF) to compute tissue-specific uptake curves.

In parallel, in brain-targeted drug delivery - particularly through convection-enhanced delivery (CED) [95] - tracer-kinetic modeling extends beyond perfusion-based imaging and incorporates multiphysics principles to simulate the infusion and distribution of therapeutic agents in the interstitial space. The complexity of brain tissue, characterized by its anisotropic structure (e.g., oriented axonal fibers in white matter), poroelastic properties, and highly heterogeneous microarchitecture, demands advanced mechanistic models that couple fluid dynamics, solid mechanics, and molecular diffusion across spatial scales. At the tissue level, transport is often modeled using Darcy's law to account for flow through porous media, while diffusion processes are governed by Fick's law or extended convection-diffusion-reaction equations that include reaction kinetics for drug binding and metabolism. For example, the delivery of a tracer or therapeutic agent into brain parenchyma involves not only its convection-driven dispersion but also potential uptake by neural cells and interactions with extracellular matrix components, which may be described by Michaelis-Menten or enzyme kinetic models.

Computational simulations based on these tracer-kinetic principles are increasingly employed to optimize drug infusion protocols, minimize backflow, and predict therapeutic coverage in the brain. These simulations incorporate patient-specific parameters such as infusion pressure, catheter placement, hydraulic permeability, and tissue compliance, all of which influence the spatial-temporal distribution of infused agents. In imaging-based applications, such as DCE-MRI or arterial spin labeling (ASL), tracer-kinetic models not only enhance the physiological interpretability of imaging biomarkers but also enable the non-invasive quantification of perfusion, permeability, and metabolic rates. Moreover, the integration of tracer-kinetic modeling with high-resolution imaging and advanced techniques such as hyperpolarized NMR spectroscopy further enhances sensitivity to metabolic fluxes and dynamic changes in living systems. Together, these models represent a powerful interdisciplinary approach, combining mathematical rigor, biophysical insight, and clinical utility to improve our understanding and control of drug delivery and diagnostic imaging.

Release Kinetics Models

In addition to the Higuchi's model, which describes drug release as a diffusion-controlled process with a square root time dependence, several other mathematical models are extensively used to characterize drug release kinetics.

Zero-order kinetics assumes a constant drug release rate independent of concentration, suitable for systems with a constant driving force such as osmotic pumps or reservoirs with saturation at the release interface [77].

First-order kinetics, in contrast, describes release rates proportional to the remaining drug content, commonly used for water-soluble drugs in porous matrices. The Korsmeyer-Peppas model [26] is a semi-empirical approach useful for identifying the release mechanism when it is not purely Fickian; it introduces the release exponent n to distinguish between Fickian diffusion, anomalous (non-Fickian) transport, and Case-II transport mechanisms. Case-II transport refers to a specific type of drug release mechanism that is not governed by simple Fickian diffusion, but rather by polymer relaxation or swelling-controlled processes and typically occurs in polymeric systems, especially those that swell significantly in the presence of biological fluids. [77]. More complex systems may require modeling approaches that integrate both diffusion and erosion, as seen in the Peppas-Sahlin model.

As reviewed by Mircioiu et al. [50], modeling drug release from supramolecular drug delivery systems often requires careful consideration of boundary and initial conditions due to the involvement of mass transfer phenomena and interface dynamics. Analytical solutions to diffusion equations are obtainable only under simplified geometries and conditions. Hence, empirical and semi-empirical models often remain the preferred approach for practical applications.

2.3.3 Thermodynamics in Drug Delivery

Thermodynamics [54], the study of energy transformations, plays a pivotal role in modern drug discovery by providing quantitative insights into biomolecular interactions. In drug discovery, the primary interest lies in the heat changes that occur when a drug molecule binds to a biological target. These interactions can be characterized by measuring the changes in enthalpy (ΔH), entropy (ΔS), free energy (ΔG), and dissociation constant (K_D), thereby shedding light on the forces driving binding and recognition.

Isothermal titration calorimetry (ITC) has become the gold standard in this context, allowing direct measurement of the heat changes during binding events without the need for labeling. Other methods such as surface plasmon resonance (SPR) or fluorescence spectroscopy allow indirect measurement through the van't Hoff analysis, offering flexibility in experimental design but introducing greater complexity in data interpretation.

This chapter would like to explore the theoretical foundation, methodologies, and practical applications of thermodynamics in drug discovery. Emphasis is placed on lead optimization strategies, enthalpy - entropy compensation (EEC), and enthalpy as a probe in fragment-based drug design (FBDD).

The fundamental thermodynamic relationship for a binding interaction is:

$$\Delta G = \Delta H - T \cdot \Delta S \tag{2.8}$$

Where:

- ΔG is the Gibbs free energy change,
- ΔH is the enthalpy change,
- T is the absolute temperature (Kelvin),
- ΔS is the entropy change.

The dissociation constant K_D is linked to ΔG by:

$$\Delta G = RT \ln K_D \tag{2.9}$$

where R is the gas constant (1.987 cal·mol^{-1}·K^{-1}).

ITC measures heat changes during molecular interactions. The experiment involves titrating a ligand into a solution containing the protein, with each injection resulting in a measurable heat pulse. The integrated heat signal is plotted to generate a binding isotherm, from which the parameters K_D, ΔH, and stoichiometry n are derived.

The change in heat capacity ΔC_p, which is informative of desolvation and conformational changes, can be determined by measuring ΔH at different temperatures:

$$\Delta C_p = \frac{d\Delta H}{dT} \tag{2.10}$$

Indirect methods derive thermodynamic parameters from temperature-dependent changes in K_D. The integrated van't Hoff equation is:

$$\ln\left(\frac{K_2}{K_1}\right) = \frac{\Delta H}{R}\left(\frac{1}{T_1} - \frac{1}{T_2}\right) \tag{2.11}$$

However, deriving accurate ΔH and ΔS values this way is sensitive to experimental errors, particularly in affinity measurements across temperature ranges.

Thermodynamic profiling can inform the rational design of drug candidates. Freire [24] observed that best-in-class drugs, such as HIV protease inhibitors and statins, exhibit the most favorable binding enthalpies. This observation supports a strategy where thermodynamics guides structural modifications.

Some general rules are frequently applied:

1. Hydrogen bonds contribute favorably to enthalpy.
2. Hydrophobic interactions contribute favorably to entropy.
3. Conformational changes often result in entropy loss.

By observing shifts in thermodynamic profiles, chemists can assess whether a chemical modification enhances binding through specific interactions.

EEC describes the phenomenon where gains in binding enthalpy are offset by losses in entropy, resulting in little net change in ΔG. It is common during lead optimization and

complicates straightforward interpretation of thermodynamic data. For example, adding a hydrogen bond may increase ΔH, but rigidify the complex, thus reducing ΔS.

Fragment-based drug discovery (FBDD) involves identifying small molecules with weak affinity but favorable enthalpic profiles. Fragments tend to bind through strong, geometrically optimal hydrogen bonds, often resulting in enthalpy-driven interactions.

As fragments are optimized into larger molecules, entropy becomes more significant due to loss of conformational freedom. Monitoring enthalpy helps preserve key interactions during fragment growing.

Due to the weak binding of fragments, ITC experiments often require high concentrations and careful design. Low c-values (where $c = [P]K_D$) are challenging but can be mitigated using displacement titrations or competition assays.

Single-injection thermal extinction (SITE) experiments provide rapid assessments of relative enthalpy for fragment binding, supporting screening campaigns.

Many biological systems feature complex binding modes, including multiple binding sites, allostery, or coupled equilibria. ITC, especially when combined with global fitting and orthogonal techniques (e.g., NMR, X-ray crystallography), allows characterization of such systems.

By fitting multiple ITC datasets simultaneously, researchers can extract thermodynamic parameters for each interaction equilibrium, even in cases involving cooperativity or multivalent binding.

Despite its promise, thermodynamic optimization in medicinal chemistry is not yet widely adopted in prospective design due to:

- Measurement variability (e.g., concentration errors).
- Difficulties in interpreting entropy and enthalpy contributions.
- EEC and entropy-enthalpy transduction (EET).
- Limited structural and dynamic data.

Future use will depend on integrating thermodynamic data with structural biology and computational modeling, alongside better experimental designs and industry-academia collaboration.

Thermodynamics provides critical insights into drug-target interactions, especially in early-stage lead identification and optimization. ITC stands out for its ability to deliver detailed and label-free thermodynamic profiles. However, full exploitation of these data requires understanding the complex interplay between enthalpy, entropy, and structural dynamics. As our tools and models improve, thermodynamically guided drug discovery will become a more practical and powerful strategy.

2.3.4 Other Physical Laws

Starling's Law

Starling's law describes the fluid flow balance between plasma and interstitium, influencing the tissue distribution of drugs.

Arfin et al. [4] use the Starling equations when they talk about simulation of drug delivery in tissues, in the specific case of correlation between release profile and elimination kinetics to predict transport. They use the mass conservation (continuity) equation for interstitial fluid flow that can be formulated by incorporating Starling's law to describe the fluid exchange between the vasculature, interstitium, and lymphatic system:

$$\frac{\partial \rho}{\partial t} + \nabla \cdot (\rho \boldsymbol{v}) = \rho(F_V - F_L) \tag{2.12}$$

With:

- $F_V = L_p \left(\frac{S}{V}\right) [p_V - p_i - \sigma_T(\pi_V - \pi_i)]$,
- $F_L = L_{p,L} \left(\frac{S_L}{V}\right) [p_i - p_L]$.

In their model, the right-hand side of the continuity equation includes both a source term, representing fluid influx from the blood vasculature, and a sink term, accounting for fluid drainage into the lymphatic system. The source term is defined by the hydraulic conductivity from the vasculature (L_p), the vascular surface area per unit tissue volume (S/V), and the difference in hydrostatic and osmotic pressures between the vasculature and the interstitium. The sink term is similarly defined, using parameters specific to lymphatic drainage, including the lymphatic hydraulic conductivity ($L_{p,L}$), lymphatic surface area per unit volume ($\frac{S_L}{V}$), and the pressure gradient between the interstitium and lymphatic vessels. Both terms incorporate the osmotic reflection coefficient (σ_T), and the osmotic pressures of the vasculature (π_V) and interstitium (π_i). This formulation captures the dynamic fluid exchange that governs interstitial fluid balance.

Darcy's Law

When analysing transport in porous tissues such as tumour tissues or in hydrogel systems, Darcy's law is applied to describe fluid filtration. It states that the volumetric flow $\vec{q}$ is proportional to the pressure gradient ∇p:

$$\vec{q} = -\frac{\kappa}{\mu} \nabla p \tag{2.13}$$

Where:

- κ is the permeability of the porous medium,
- μ is the dynamic viscosity of the fluid.

In the context of drug delivery via microspheres, Darcy's law is implicitly used in the model of tissue diffusion, especially in simulating extracellular transport after drug release. Arifin et al. [4] models the tissue as a porous medium through which the drug diffuses once released.

Koch et al. [41] explicitly apply Darcy's law to model interstitial fluid flow in tissues, coupling it with 1D equations for capillary flow (based on the Hagen-Poiseuille law 2.3.4). The Darcy equation is expressed in the form:

$$-\nabla \left(\frac{\rho_I}{\mu_I} \kappa \nabla p_t\right) = \hat{q}_m \delta_A \tag{2.14}$$

Where:

- ρ_I is constant density,
- $\hat{q}_m$ is the transmural mass flux [kg $s^{-1}m^2$] and $\hat{q}_m = \rho_I L_p S_v (p_v - p_{t,W})$,
- δ_A is Dirac delta function.

However, this law is applicable only for simulating interstitial fluid flow under quasi-steady-state conditions, wherein the fluid exchange between the tissue and the circulatory system has reached dynamic equilibrium [80].

Macroscopically, the tissue, which can be either normal or tumor tissue, is ideally assumed as an isotropic porous medium, so it can be described by Darcy's law for the balance of linear momentum in the tissue interstitium. Arfin et al. talk about the full-form of the momentum equation expressed as follows:

$$\frac{\rho}{\varepsilon}\left(\frac{\partial \boldsymbol{v}}{\partial t} + \boldsymbol{v}\cdot\nabla\boldsymbol{v}\right) = -\nabla p_i + \left(\frac{\mu}{\varepsilon}\right)\nabla^2\boldsymbol{v} + \rho\boldsymbol{f} - \left(\frac{\mu}{k}\right)\boldsymbol{v} - \frac{1}{2}C_V\rho\,|\boldsymbol{v}|\,\boldsymbol{v} \tag{2.15}$$

Hagen-Poiseuille

For laminar flow in capillary vessels or microchannels of delivery devices, the Hagen-Poiseuille law provides an estimate of flow rate as a function of viscosity and tube geometry.

This law is used by Koch et al. [41] in the case of reference to blood, considered as a Newtonian fluid with constant density ρ_B, and dynamic viscosity μ_B. They have developed a method for modeling tissue perfusion on the capillary scale.

Navier-Stokes

To describe the dynamics of blood flow, particularly in large vessels or in the presence of turbulence or pulsations, the Navier-Stokes equations are used.

These equations are used by Mircioiu et al. [50] and Yuan et al. [95]. In particular, the second study group present a convection-diffusion reaction equation, within a study of a mathematical model concerning the brain and the blood-brain barrier (BBB):

$$\frac{\partial(\phi C_n)}{\partial t} + \frac{\partial(\rho C_{Sn})}{\partial t} + \nabla\cdot(\boldsymbol{u}_F C_n) = \nabla\cdot[(\boldsymbol{D}_n + \boldsymbol{D}_{Sn})\nabla C_n] + R(C_n) \tag{2.16}$$

Where:

- n is the species of drug particles,
- ϕ is the tissue porosity,
- C_n [mol/l] is the particle concentration in the fluid phase,
- C_{Sn} [mol/unit] dry weight of the cells] is the amount absorbed by the cells,
- $\rho = (1-\phi)\rho_S$ is the dry bulk density,

- ρ_S is the cell density,
- t is time,
- $\boldsymbol{u}_F$ is the flow velocity,
- $\boldsymbol{D}_n$ [m^2/s] is the particle diffusion tensor in the fluid phase,
- $\boldsymbol{D}_{Sn}$ is that in the solid phase,
- $R(C_n)$ defines the biochemical reaction processes of the drug particles.

In the equation, the term $(\boldsymbol{u}_F C_n)$ represents the convection, the term $[(\boldsymbol{D}_n + \boldsymbol{D}_{Sn})\nabla C_n]$ the diffussion and the last term $R(C_n)$ represents reaction.

Fourier-Kirchhoff

In the case of thermal diffusion coupled with drug delivery (e.g. thermotherapy), the Fourier-Kirchhoff law is used to model heat distribution as in the case of Mircioiu et al. [50].

Biomedical signal and image processing frequently uses advanced mathematical tools, including Fourier transform and deconvolution techniques. These methodologies, although conceptually distinct, find joint application in numerous areas of bioengineering, such as in the removal of artefacts from diagnostic images or in the spectral analysis of physiological signals. Janhng et. al. [34] refer to the Fourier-based methods to perform the deconvolution and Baudino [6] use the Fourier transform to perform the infrared spectroscopy (FT-IR) as Brindle et al. [11] also use the transform in NMR.

Newton

Newton's law of viscosity is used to describe the rheological behaviour of biological fluids and to estimate shear forces in microfluidic devices.

Mircioiu et al. [50] report Newton's law of cooling in case of boundary condition.

$$\frac{\partial C}{\partial n} + \alpha(C_s - C_0) = 0 \tag{2.17}$$

Furthermore, Yuan et al. [95] quote the Newton's second law to describe the trajectory of the particles to describe it mathematically:

$$F = \frac{d}{dt}(m\boldsymbol{v}) \tag{2.18}$$

Both Yuan et al. and Koch et al. [41] refer to the behavior of Newtonian fluid when considering blood.

Lambert-Beer Equation

The Lambert-Beer law [77] is fundamental to spectrophotometric analysis, providing a quantitative relationship between absorbance and the concentration of a solute in solution. This linear relationship is mathematically expressed as

$$A = KC \tag{2.19}$$

where A is the absorbance, C is the concentration of the analyte, and K is a constant that encompasses the molar absorptivity and path length of the cuvette.

In in vitro studies, especially for the evaluation of drug release from delivery systems, this equation enables the indirect quantification of active molecules in receptor solutions over time, offering a non-invasive and reproducible method to assess release kinetics.

As discussed by Trucillo [77], UV-Vis spectrophotometry based on the Lambert-Beer law is widely used to monitor drug concentrations in the context of drug delivery models, where accurate quantification is essential for characterizing release profiles and fitting experimental data to mathematical models of diffusion and transport. In particular, the absorbance data, typically recorded at the specific wavelength characteristic of the drug molecule, are used to calculate the cumulative release and to assess encapsulation efficiency, both of which are critical parameters in evaluating the effectiveness of polymeric carriers.

This approach was also employed in the experimental part of this thesis, where caffeine-loaded nanocarriers were monitored using UV-Vis spectroscopy to analyze their transdermal release through Franz diffusion cells [6].

2.3.5 Simulation Tools

Finite Element Method (FEM)

The finite element method (FEM) allows differential equations on complex geometries, such as those derived from CT or MRI images, to be solved numerically.

The FEM has become an indispensable computational tool in biomedical engineering, particularly for simulating the mechanical behavior of complex biological tissues and medical devices. In the study by Shu et al. [68], FEM was used to model microneedle array insertion into a multi-layered, anisotropic, hyperelastic human skin model that incorporated realistic in vivo characteristics such as prestress and material nonlinearity. Their simulations demonstrated that increasing skin pretension from 0% to 10% strain reduced microneedle penetration force by approximately 13% and local deformation by 22%, highlighting the sensitivity of insertion mechanics to skin biomechanics.

In the context of tissue engineering, Vasquez et al. [81] applied FEM alongside a Taguchi design of experiments approach to optimize 3D-printed PLA scaffolds with varying pore sizes and porosities, achieving a balance between mechanical integrity and biological performance.

Similarly, Williamson et al. [52] employed patient-specific FEM models to evaluate the structural integrity of customized orthopedic implants fabricated through additive manufacturing. Their simulations, based on CT-derived geometries of ovine femora,

provided valuable insights into stress distribution and implant fixation strategies. These applications illustrate the critical role of FEM in the iterative design and analysis of biomedical systems, facilitating predictive modeling that complements experimental and clinical findings.

Boundary conditions

The Dirichlet and Neumann [41] conditions are fundamental for the correct formulation of physico-mathematical problems in drug release, especially in the presence of physiological barriers.

In the mathematical modeling of drug release kinetics from supramolecular drug delivery systems (SMDS), boundary conditions play a fundamental role in defining the behavior of diffusion-driven processes.

The paper by Mircioiu et al. [50] offers a comprehensive classification of boundary conditions based on their physical significance and mathematical form, drawing from established heat and mass transfer analogies. Classical boundary conditions include constant surface concentration (BC1), specified flux (BC2), impermeable barriers (BC3), and Newton-type radiative conditions (BC4), among others, such as moving boundary conditions (BC8), which account for dynamic interfaces due to immobilization or dissolution processes. These boundary types are instrumental in transforming general diffusion equations into analytically solvable models, particularly through simplifications that idealize complex physicochemical phenomena into forms compatible with separation of variables and integral transformation techniques. The authors highlight that identifying the correct boundary and initial conditions is essential not only for solution derivation but also for aligning mathematical models with real-world experimental or biological scenarios. Moreover, the paper emphasizes that multiple phenomenological settings can lead to identical boundary conditions, meaning the same mathematical solution might represent different physical systems, which underlines the importance of a careful interpretation of model assumptions and boundary definitions.

The synergy between classical physical laws and advanced computational models allows a detailed description of the process of drug release, diffusion and absorption. The adoption of these laws in the design of personalised therapeutic systems represents an ever-expanding frontier in biomedical engineering.

This discussion is certainly not exhaustive of the use of laws and models throughout the pharmaceutical world, but it does represent the complexity of the problems present. In the appendix at the bottom there is a collection of some examples of models used in drug delivery as in the tables 3 and 2. This shows how broad the topic is and how many studies have been done on it.

2.4 Medical Imaging

Bioimaging [60] can be classified in different ways, depending on the standard adopted as a distinguishing element. A principle particularly familiar to doctors consists in grouping

the different techniques based on the organ they intend to study. In fact, doctors generally specialize in the analysis of pathologies of a specific body district, using the various diagnostic techniques available. The choice of the most suitable instrument depends each time on the type of diagnostic question they want to answer.

Imaging techniques can also be distinguished based on their degree of invasiveness: they are defined as invasive when they involve the introduction of instruments into the patient's body (such as probes or catheters), and non-invasive when this does not occur. Another common distinction concerns the safety of the procedure, in particular the use or not of ionizing radiation. This aspect is really relevant because it determines whether the technique can also be used for long-term monitoring of the patient, without significant risks to health.

Electromagnetic radiation [51], which includes a broad spectrum of frequencies from radio waves to gamma rays, has numerous applications in the medical field, both for diagnosis and therapy. Depending on the frequency and wavelength, these waves have very different characteristics in terms of tissue penetration, spatial resolution and potential damage to biological tissues. While microwaves and infrared offer non-invasive activation modes with good localization. On the other end of the spectrum (X-rays or gamma rays), while ensuring high imaging and penetration capacity, can cause cytotoxic effects and therefore require controlled use. In this context, radiation-based medical imaging techniques, such as magnetic resonance imaging, computed tomography (CT) and PET, exploit different portions of the spectrum to obtain morphological and functional information of extraordinary precision.

The work of Seoni et al. [66] was taken as a reference point for the conceptual subdivision of the following paragraph.

2.4.1 Radiology

This imaging modality [66] includes computed tomography (CT) imaging, magnetic mesonance imaging (MRI), and mammography.

This mode faces significant challenges due to variations in image acquisition parameters and protocols across different imaging centers and devices due to radiation. The images produced may present construction problems, inconsistencies in the data due to the lack of uniformity of the protocols, accuracy and reliability.

Magnetic Resonance Imaging (MRI)

Molecular diffusion is a fundamental physical phenomenon in the metabolic processes of biological tissues, since it regulates the transport of molecules within a medium due to thermal agitation. Under physiological conditions, water represents approximately 70% of the tissue volume [89], constituting the main vehicle of diffusion. The free movement of water molecules is prevented by the presence of cellular membranes and intracellular organelles that make biological tissues non-homogeneous. Therefore, the phenomenon of diffusion is made complex and highly informative on the structural and pathological characteristics of the tissue.

In isotropic media, diffusive motion can be described by Fick's first law discussed in chapter 2.3.1. For free diffusion and infinite medium, the solution to this equation has a Gaussian form. Einstein's relation relates the variance of random motion to the diffusion coefficient D (m^2/s) [78, 95]:

$$\langle(\vec{r} - \vec{r}_0)^2\rangle = 6Dt \tag{2.20}$$

Where the first term represents the mean squared displacement (MSD). It is a statistical measure of how far, on average, a particle has moved away from its initial position $\vec{r}_0$. t is the time spent.

Nuclear magnetic resonance (NMR) is the only non-invasive technique capable of studying molecular diffusion in vivo at the cellular level. Diffusion-sensitive MRI sequences exploit the principle of Intra-Voxel Incoherent Motion (IVIM) [28], which highlights the incoherent motion of molecules within a voxel.

The most commonly used basic sequence is the Stejskal-Tanner sequence [8, 78], consisting of Spin-Echo pulses with the addition of two bipolar diffusion gradients:

$$\frac{M}{M_0} = \exp\left(-\gamma^2 G^2 \delta^2 D \left(\Delta - \frac{\delta}{3}\right)\right) \tag{2.21}$$

Where:

- γ: gyromagnetic ratio,
- G: gradient intensity,
- δ: duration of the gradient,
- Δ: time between gradients,
- D: diffusion coefficient.

For a more complete analysis, the Bloch-Torrey equation is introduced, which extends the Bloch equations [78] by including the diffusion term:

$$\frac{\partial \vec{M}}{\partial t} = \gamma \vec{M} \times \vec{B} - \frac{M_x \hat{i} + M_y \hat{j}}{T_2} - \frac{(M_z - M_0)\hat{k}}{T_1} + \nabla \cdot (D \nabla \vec{M}) \tag{2.22}$$

Under controlled experimental conditions, the solution can be simplified by obtaining exponential attenuation of the diffusion-weighted signal:

$$M(TE) = M_0 \exp(-bD) \tag{2.23}$$

where the b-value parameter is defined as:

$$b = \gamma^2 G^2 \delta^2 \left(\Delta - \frac{\delta}{3}\right) \tag{2.24}$$

Free diffusion occurs in homogeneous media without obstacles. The mean free path follows Einstein's law, as previously stated. Restricted diffusion occurs in the presence of impermeable barriers that limit molecular displacement. The apparent diffusion coefficient D(t) decreases with time:

$$D(t) = D_0 \left(1 + \frac{C}{\sqrt{t}}\right) \tag{2.25}$$

Molecules must circumvent obstacles, making the path more tortuous (diffusion hinders). The concept of tortuosity is introduced ζ:

$$D = \frac{D_{\text{free}}}{\zeta^2} \tag{2.26}$$

Anisotropic diffusion occurs when molecular mobility varies with direction. In this case, the coefficient becomes a 3×3 tensor.

Diffusion weighted imaging (DWI) images are obtained by adding diffusion gradients to conventional MRI sequences. Low-diffusion zones appear hyperintense, while free diffusion zones appear hypointense.

For a quantitative measure, apparent diffusion coefficient (ADC) [8, 15, 16, 28, 32, 34, 53, 78] maps are introduced, where the ADC is obtained voxel by voxel:

$$ADC = \frac{1}{b_2 - b_1} \ln\left(\frac{S(b_1)}{S(b_2)}\right) \tag{2.27}$$

These maps allow a quantitative assessment of diffusion, independent of relaxation times T_1 and T_2. ADC changes reflect cellular changes, e.g. cytotoxic swelling reduces intracellular diffusion.

The study of diffusion by MRI represents a powerful diagnostic resource, capable of providing microstructural information that cannot be obtained by other techniques. DWI sequences and ADC maps have transformed the approach to neuroradiological imaging and continue to evolve with increasing spatial and temporal resolution.

In addition to diagnosis, diffusion-weighted magnetic resonance imaging (DWI) and contrast-enhanced magnetic resonance imaging (DCE-MRI) have been widely used to assess drug distribution in tissues. In particular, DCE-MRI allows to analyze vascular permeability, perfusion and extracellular volume, which are fundamental elements to understand drug penetration in a pathological tissue.

A landmark study is that of Tofts et al. [76], who proposed a pharmacokinetic model for the quantitative analysis of DCE-MRI data. The parameters obtained, such as K^{trans} (transfer coefficient), v_e (extracellular volume), and v_p (plasma volume), allow to infer the diffusion efficacy of a systemically administered drug.

In the preclinical setting, Bhandari et al. [8] used DCE-MRI to quantify the penetration of anticancer drugs in murine models of glioma, highlighting how pharmacokinetic parameters can change following treatments that modify the blood-brain barrier.

Modalities

Jahng et al. [34] present three MRI modalities for the assessment of cerebral perfusion but also applicable to other contexts: DSC-MRI (Dynamic Susceptibility Contrast MRI), DCE-MRI (Dynamic Contrast-Enhanced MRI) and ASL (Arterial Spin Labeling). Each of these methods is based on different principles and has peculiar characteristics that make them suitable for specific clinical and research contexts.

DSC-MRI is a technique based on the use of a contrast agent introduced from the outside, typically a paramagnetic agent containing gadolinium such as Gd-DTPA, gadolinium-diethylenetriaminepentaacetate (see paragraph 2.5). This contrast agent is injected, often, intravenously in the form of a bolus, and the images are acquired very rapidly during the first passage of the contrast through the cerebral circulation. The emitted signal depends on the T_2 or T_2^* relaxation times, which undergo a transient decrease due to the magnetic susceptibility effect induced by gadolinium. For this reason, the technique is also known as bolus tracking MRI. DSC-MRI is widely used to obtain information on cerebral perfusion, in particular on cerebral blood volume (CBV), cerebral blood flow (CBF) and mean transit time (MTT).

The second technique, DCE-MRI, is also based on the injection of a contrast agent, but unlike DSC-MRI, the acquired signal depends on the T_1 relaxation time, which tends to shorten in the presence of gadolinium, resulting in an increase in the signal in T_1-weighted images. This technique involves the rapid and repeated acquisition of T_1 images to monitor signal changes in tissues over time. Contrast diffuses from the vascular compartment into the extravascular extracellular space (EES), at a rate that depends on tissue perfusion and capillary permeability. DCE-MRI therefore allows not only to evaluate perfusion, but also to estimate parameters related to vascular permeability, proving useful especially in oncology and in the study of the blood-brain barrier.

Finally, ASL represents a completely non-invasive method, as it does not require the use of contrast media. In this case, arterial blood water is used as an endogenous tracer: the blood arriving at the brain is magnetically *labeled* (spin labeling), and the perfusion signal is obtained by subtracting the images acquired with and without labeling. The result reflects the absolute blood supply to the brain tissue. However, since the signal difference between the two images is very low (less than 1%), ASL suffers from a relatively low signal-to-noise ratio. Despite this limitation, the possibility of repeating the test several times without side effects makes it particularly suitable for longitudinal studies, both in research and in clinical practice.

Magnetic Resonance Spectroscopy (MRS)

In-cell NMR offers information on metabolites and proteins in the physiological intracellular environment at the atomic level. In vivo magnetic resonance spectroscopy (MRS) provides qualitative measurements of metabolites under study in specified areas of living organisms [57]. MRS is a complementary technique to MRI that allows non-invasive analysis of the chemical composition of tissues, detecting metabolites such as choline, lactate and creatine. In the context of drug delivery, MRS allows indirect monitoring of the presence and effect of a drug through changes in the metabolic profile of the target tissue [90].

Although less sensitive than other molecular imaging techniques, MRS is valuable for the study of tumor metabolism and for the early assessment of therapeutic response.

Example of Machine

In their work Granata et al. [28] used a 1.5 Tesla system (Magnetom Symphony, upgraded with the Total Imaging Matrix Package, Siemens, Erlangen, Germany) equipped with both body and surface coils, which can be seen in the figure 2.2. This machine was used to evaluate liver metastases treated with targeted chemotherapy agents. Imaging studies were conducted at two time points: baseline (T_0), with a mean of 5 days before treatment, and follow-up (T_{14}), which took place 14 days after the completion of the first chemotherapy cycle.

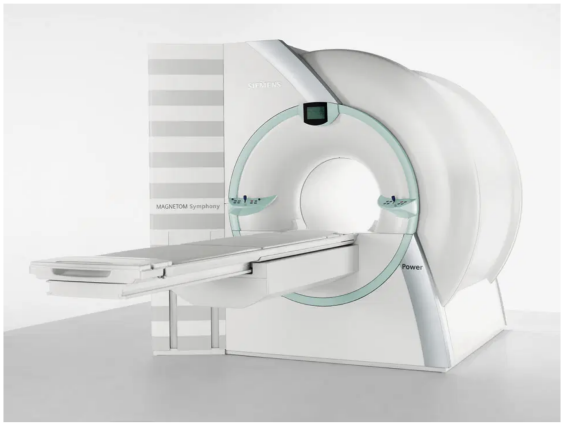

(a) MAGNETOM Symphony, a system with TIM technology at 1.5T.

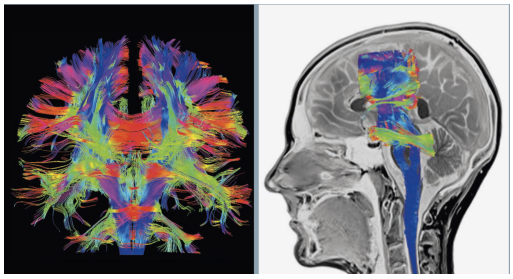

(b) Example of images obtained.

Figure 2.2: High-performance MRI system with cutting-edge technology. 0.2 ppm magnet homogeneity on 40 cm DSV for extremely precise images, with a large FoV of 50×50×50 cm. Thanks to Zero Helium Boil-Off technology, operational efficiency is maximum. High gradient performance up to 80 mT/m @ 200 T/m/s, even simultaneously. Includes TimTX TrueShape for excellent RF flexibility and the Tim 4G + Dot system with 64 or 128 reception channels. 60 cm gantry diameter, optional High Power Shim and high-power image reconstruction for superior diagnostic quality [69].

The imaging protocol included a range of sequences to comprehensively evaluate the anatomy and treatment response:

- Unenhanced, coronal, free-breathing TRUFI T_2-weighted scans. These fast imaging sequences with steady-state free precession (TRUFI) provided high-resolution anatomical details.

- Triggered-breathing HASTE T_2-weighted scans. Acquired using a half-Fourier single-shot turbo spin-echo (HASTE) technique, these axial images offered fast acquisition while minimizing motion artifacts.

- Axial T_2-weighted scans with or without fat saturation (spectral adiabatic inversion recovery - SPAIR). These helped highlight tissue contrast and reduce fat signal interference.

- End-expiratory breath-hold in-phase and out-of-phase axial T_1-weighted scans. Used to evaluate tissue composition and detect fat or hemorrhage.

- Axial diffusion-weighted imaging (DWI). Conducted with a free-breathing, single-shot echo planar sequence using seven different b-values (0, 50, 100, 150, 300, 600, and 800 s/mm^2) to assess tissue cellularity and detect changes in diffusion related to treatment response.

This comprehensive MRI protocol enabled detailed assessment of both anatomical structures and functional changes associated with therapy.

Computed Tomography (CT)

Computed tomography (CT) [4,8,34,47,53,59,66,82] is a powerful imaging technique that plays an important role in visualizing anatomical structures and assessing physiological processes within the body. By acquiring X-ray attenuation data from multiple angles and reconstructing it into cross-sectional images, CT enables detailed analysis of tissue composition and structure.

Beyond conventional anatomical imaging, advanced CT modalities such as dynamic contrast-enhanced CT (DCE-CT) offer functional insights that are particularly relevant to the study of drug diffusion. DCE-CT involves the serial acquisition of images following the administration of an iodinated contrast agent, allowing for the quantification of tissue perfusion, vascular permeability, and extracellular volume - parameters that closely influence drug delivery and distribution. The technique is especially useful in oncology, cardiology, and neurology, where understanding blood flow and capillary leakage is critical for evaluating drug uptake and therapeutic efficacy. In this context, DCE-CT serves as a non-invasive surrogate for assessing how drugs may diffuse through vascular and interstitial compartments, providing valuable data for pharmacokinetic modeling and personalized treatment planning.

Two other new techniques worth mentioning are micro-computed tomography (μ-CT) [95] that works on a smaller scale and with significantly higher resolution, it allows examining the internal structure and three-dimensional ultrasound computed tomography (3D USCT) [33] that is a promising breast imaging technology that captures high-quality images, speed of sound, reflection, and attenuation data quickly and reliably, it offers fast, full-volume breast scans in just 4 minutes, making it suitable for clinical use.

Mammography

Mammography [12, 66] is a critical imaging modality for breast examination and cancer screening. It utilizes low-dose X-rays to detect early signs of breast cancer.

It works by compressing the breast between two plates to spread the tissue and acquire high-resolution, two-dimensional images, typically in craniocaudal (CC) and mediolateral oblique (MLO) views. This compression helps reduce motion, improve image quality, and minimize radiation dose. While mammography has been instrumental in reducing breast cancer mortality through early detection, it is not without limitations - namely, high false

positive rates, which can lead to unnecessary biopsies, and false negatives, which may result in missed diagnoses.

Despite its clinical relevance, mammography is not the focus of this thesis, so it is only mentioned for scientific completeness.

2.4.2 Nuclear Imaging

Nuclear medical imaging [60] aims to study biochemical and physiological processes within the body. The images obtained show the distribution of a biologically active molecule, bound to a radioactive isotope, which is introduced into the patient's body mainly intravenously, but also through inhalation or ingestion.

Ionizing radiation is characterized by a high energy content that allows it to break the chemical bonds of the molecules with which it interacts, thus altering their chemical structure. This radiation propagates in a vacuum without changing its characteristics. However, when it passes through a material, it can transfer part of its energy to the atoms of the medium. This transfer can cause the expulsion of an electron from an atom, generating two ions with opposite charges: it is precisely this phenomenon that gives them the property of being *ionizing*.

A radioisotope (or radionuclide) is an atom with an unstable nucleus, due to an excess of protons or neutrons. To return to a stable state, the radionuclide transforms spontaneously through a process called radioactive decay, which can involve the variation of the chemical species of the atom itself. This process occurs randomly at the level of the single atom, but can be described in a predictable way at the macroscopic level.

Assuming that there is an initial quantity N_0 of radionuclides of a certain element at time $t = 0$, the number $N(t)$ of atoms still radioactive over time decreases according to an exponential law:

$$N = N_0 e^{-\lambda t} \tag{2.28}$$

determined by the decay constant λ, specific for each radionuclide.

A fundamental parameter to describe this behavior is the half-life, which represents the time necessary for half of the radioactive nuclei initially present to decay. The half-life $T_{\frac{1}{2}}$ is linked to the decay constant by the relationship:

$$T_{\frac{1}{2}} = \frac{\ln 2}{\lambda} \tag{2.29}$$

The different existing radionuclides have very variable half-lives. For example, the radionuclides used in PET (Positron Emission Tomography) have half-lives of a few hours, while those used in SPECT (Single Photon Emission Tomography) can have half-lives of up to one or two days.

The radioactive decay of a radionuclide can generate several types of radiation, not just one. In particular, alpha (α), beta minus (β^-), beta plus (β^+), and gamma (γ) decays can be observed, each associated with the emission of a specific radiation.

Gamma decay (γ decay) does not involve a change in the composition of the nucleus (i.e. in the number of protons or neutrons), but occurs after another type of decay that has left the nucleus in an excited state. When the nucleus returns to the ground state, it releases the excess energy in the form of a gamma photon.

Example of γ reaction:

$$^{123}I \rightarrow ^{123} Te + \gamma \tag{2.30}$$

In β^+ decay, a proton in the nucleus spontaneously transforms into a neutron, emitting a positron (β^+) and an electron neutrino. Since the total number of nucleons (protons + neutrons) remains the same, the mass number does not change, but the atomic number decreases by 1, since a proton is lost.

Example of β^+ reaction:

$$^{68}Ga_{31} \rightarrow ^{68} Zn_{30} + \beta^+ + \nu \tag{2.31}$$

where ν is the neutrino.

Radioactivity can be natural, if the radionuclide occurs spontaneously in nature, induced artificially, through specific nuclear processes. The main articial ones are:

- Radiochemical processes. An example is the production of metastable technetium-99 (Tc-99m) from molybdenum-99 (Mo-99):

$$^{99}Mo \rightarrow ^{99m} Tc \rightarrow ^{99} Tc + \gamma(140keV) \tag{2.32}$$

- Bombing with neutrons (neutron activation). Stable nuclei capture neutrons and become unstable. This type of reaction requires a nuclear reactor or a particle accelerator:

$$n + ^{98} Mo \rightarrow ^{99} Mo + \gamma \tag{2.33}$$

- Charged particle bombardment. Used mainly to generate radionuclides that decay by β^+, such as those used in PET.

Inside the body, the positron slows down due to Coulomb interactions with the electrons of the tissue. When it has lost all its energy and has reached thermal equilibrium with the electrons of the medium it is passing through, the positron undergoes the process of annihilation. The distance between the point of emission of the positron and the point where annihilation occurs is called the positron range.

The positron, resulting from β^+ decay, has a very short half-life in biological tissue. It rapidly loses energy through inelastic interactions with the atomic electrons of the tissue. After dissipating most of its energy, the positron combines with an atomic electron to form positronium, an unstable entity similar to a hydrogen atom, which has a half-life of about 10^{-10} seconds. After this, the process of annihilation occurs. During annihilation, the mass of the positron and electron is converted into electromagnetic energy. This energy is released in the form of two colinear gamma photons, emitted simultaneously in opposite directions, called *back to back* photons. The process can be schematized as:

$$e^+ + e^- \rightarrow \gamma + \gamma \tag{2.34}$$

The characteristics of the annihilation process are the basis of the PET imaging technique. Annihilation photons, being very energetic, have a good chance of leaving the human body and can therefore be detected by external devices, unlike the positron which is absorbed locally.

If the two gamma photons are detected simultaneously (within an interval called the *coincidence time window*) by two detectors placed outside the body, since the emission angle (180°) and the positions of the detectors are known, it is possible to trace the point of annihilation inside the body. This point is located on the line that joins the two detectors, called the line of response (LOR).

Since the positron travels only a short distance before annihilating, it can be assumed that the site of radioactive decay is located along the LOR. This type of localization is called electronic collimation, unlike the mechanical collimation used in SPECT. Thanks to electronic collimation, PET achieves a better and more uniform spatial resolution and a higher efficiency than SPECT, while also allowing quantitative analysis of the images.

The annihilation point is therefore a good indicator of the location of the radioactive atom in the body. In addition, all positron-emitting radionuclides, regardless of the element or the positron energy, always produce two collinear 511 keV photons. This allows the PET scanner to detect different radionuclides with the same emission energy. In contrast, in the SPECT, the energy of the gamma photons depends on the radionuclide used, making it necessary to detect photons with a broad energy spectrum.

When a photon passes through a material medium, it can interact with it through different mechanisms. The main interaction processes are:

- Photoelectric effect (PE). The photon transfers all its energy to an electron strongly bound to the atom. The electron is expelled from the atom with an energy equal to the difference between the energy of the incident photon and the binding energy of the electron. The vacancy left by the ejected electron is filled by an external electron, resulting in the emission of characteristic X-rays or Auger electrons.

- Incoherent scattering or Compton effect (CE). The photon gives up only part of its energy to a loosely bound electron, which is ejected (Compton electron). The residual energy is conserved in a scattered photon, which changes direction with respect to the initial photon.

- Coherent scattering or Rayleigh scatter (RS). The photon interacts elastically with the atom, without appreciably losing energy. The energy of the photon is not sufficient to ionize or excite the atom.

- Pair production (PP) This process occurs only if the photon energy is greater than 1.022 MeV, equivalent to the mass of an electron and a positron.

- Photonuclear reactions (PR). These occur at energies greater than 6 MeV. The photon interacts with the nucleus of the atom causing the emission of neutrons, protons or other subnuclear particles. Due to the high energy required, this type of interaction is secondary to the other mechanisms.

The gamma radiation emitted by the sample analyzed is detected by specialized detectors, which convert it into electrical signals that can be used to reconstruct images. These detectors must be able to perform a extremely rapidly conversion, since gamma photons come from uncontrollable radioactive sources, which can emit significant amounts of radiation only for very short periods.

A detector used in PET or SPECT is structured to follow a precise information conversion path, and is typically composed of:

- Collimator: selects the direction of the incident gamma photons, improving the spatial resolution of the image.
- Scintillator crystal: converts the energy of the gamma photons into visible light.
- Photomultiplier tubes (PMT): transform the visible light produced in the crystal into amplified electrical signals.
- Electronic equipment: processes and displays the data to reconstruct the image of the analyzed area.

Detectors can be small, with a small crystal and a single photomultiplier, or larger and more complex, with a large crystal and multiple PMTs. The latter are the so-called gamma cameras. The single gamma camera was one of the first functional imaging tools: this type of examination is known as planar scintigraphy. However, planar scintigraphy has been progressively abandoned in favor of more advanced techniques such as SPECT and PET, since, being a projective and not tomographic method, it provides only two-dimensional images, insufficient for a detailed functional analysis.

Single Photon Emission Computed Tomography (SPECT)

Single photon emission computed tomography (SPECT) [1, 4, 29, 34, 50, 57, 59, 67, 77, 95] is a imaging technique based on the administration of radiopharmaceuticals containing gamma-emitting isotopes, such as Technetium-99m (Tc-99m) or Iodine-123. After the injection of the tracer, the gamma photons emitted by the tissues are detected by one or more gamma camera. These systems acquire planar projections from different angles around the patient, allowing the 3D tomographic reconstruction of the distribution of the radiopharmaceutical within the body. In figure 2.3 there is an example of the result of this operation.

SPECT imaging [44] allows to obtain functional and metabolic information on the tissues under examination in a non-invasive manner, proving particularly useful in clinical fields such as cardiology (e.g. myocardial perfusion), neurology (e.g. cerebral perfusion), oncology (e.g. tumor localization), as well as in the evaluation of renal function and pulmonary ventilation/perfusion. In the pharmacological field, SPECT allows monitoring the spatial-temporal distribution of labeled molecules, since they maintain the same metabolic behavior as unlabeled substances but are traceable thanks to the emitted radiation.

Compared to traditional planar scintigraphy, SPECT provides more detailed images thanks to the removal of anatomical overlaps, similarly to what happens in CT compared to conventional radiology. However, the spatial resolution of SPECT (about 7-8 mm) remains lower than PET (4-5 mm), and several degrading phenomena affect the quality of the images obtained [60]:

- Collimator blur: due to the imperfect selection of the direction of the photons due to the finite size of the collimator holes. This leads to a non-uniform loss of

(a) Symbia Intevo by Siemens

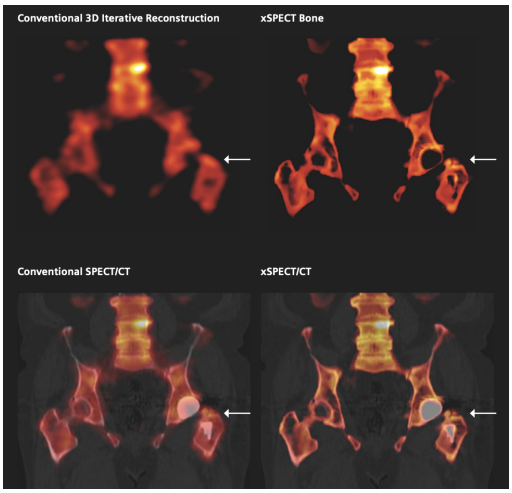

(b) Image comparison.

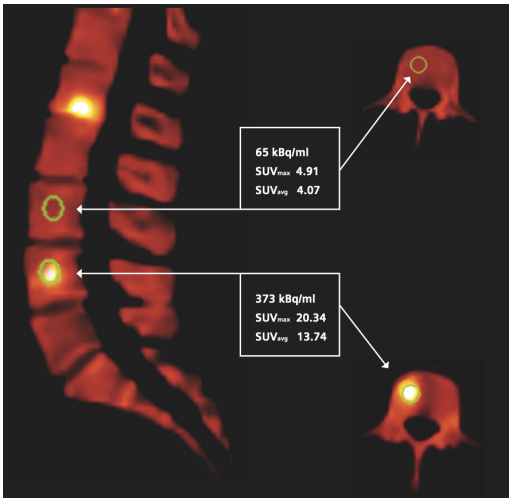

(c) Example of obtained image.

Figure 2.3: The Symbia Intevo has advanced Spiral CT System: Featuring 2-, 6-, and 16-slice configurations, HD digital detectors, and an open 70 cm gantry for enhanced patient comfort. Includes intuitive controls, autocontour infrared positioning, integrated ECG, and ergonomic bed design for streamlined, patient-friendly imaging [70].

resolution, which complicates the effectiveness of standard deconvolution techniques and causes interslice cross-talk phenomena, i.e. the overlapping of information between adjacent slices.

- Attenuation: the loss of photons that, although emitted in the direction of the detector, are absorbed or deviated due to interaction with body tissues.
- Scatter: occurs when photons are deviated by body structures and detected in the wrong directions, thus leading to spatially distorted information.
- Noise: statistical noise related to the low number of photons detected per unit of

time.

Traditionally, tomographic reconstruction in SPECT investigations has been performed using filtered backprojection (FBP), a two-dimensional algorithm that works on single axial sections, then stacked to reconstruct the volume. In this approach, compensation techniques for degrading phenomena are inserted at the data preprocessing or postprocessing level of the reconstructed image. However, these corrections are based on simplified models of the acquisition physics and are therefore approximate and ineffective.

To overcome these limitations, iterative volumetric reconstruction methods are increasingly used. These methods operate on the entire volume simultaneously, providing a more realistic modeling of the acquisition process and improving the quality and diagnostic accuracy of images.

A common strategy consists of overiterating (i.e. exceeding the theoretical optimum of the iterative algorithm) followed by postfiltering with a Gaussian filter. This allows to effectively attenuate noise artifacts without excessively compromising spatial resolution. Among the most widespread iterative algorithms is expectation maximization (EM), based on a Poissonian statistical modeling of the data. However, due to its slow convergence, EM is not practical in the clinical setting. To overcome this problem, ordered subsets expectation maximization (OSEM) was developed, which divides the data into subsets and applies the EM algorithm to each of them, significantly improving the convergence speed without compromising its quality.

Positron Emission Tomography (PET)

Positron emission tomography (PET) [4,29,34,44,57,60,77,95] is an advanced functional imaging technique that allows us to visualize and quantify physiological and metabolic processes in the human body. Unlike morphological imaging techniques, such as CT and MRI, PET aims to measure the function of organs and tissues, providing essential information for early diagnosis, therapeutic planning and monitoring of response to treatments.

PET uses radiopharmaceuticals labeled with positron-emitting radionuclides (β^+) such as fluorine-18, carbon-11 or oxygen-15. These isotopes, selected for their short half-lives and biocompatibility, are incorporated into biological molecules (e.g. sugars, amino acids) that distribute in tissues according to their pharmacokinetic characteristics.

The temporal coincidence is essential to identify pairs of photons originating from the same annihilation. A time window, typically 4-10 ns, determines whether two events are true coincidences or single events. Events accepted as coincidences are assigned to a LOR and contribute to the image reconstruction.

Events detected by a PET system are classified as:

- Trues (T): true coincidences, in which both photons arise from the same annihilation without undergoing interactions in the body.

- Scatter (S): one or both photons undergo Compton scattering, generating an incorrect LOR.

- Random (R): two uncorrelated photons (from two different annihilations) are recorded within the time window, creating a completely arbitrary LOR.

The sum of the observed events (P) is therefore:

$$P = T + R + S \tag{2.35}$$

Random events increase with radioactive activity and represent a significant source of noise. Their incidence can be reduced by shortening the time window, which is only possible with very fast detectors.

Modern PET scanners (example in figure 2.4) generally adopt a ring configuration with tens of thousands of small detectors arranged in blocks (typically 6×6 or 8×8). The detectors are made of high-efficiency materials (such as LSO or BGO), capable of providing spatial resolutions of the order of 4-6 mm. PET does not require mechanical collimators, which makes it more efficient than SPECT and capable of better quantitative accuracy and image quality. Alternative configurations also exist, such as dual-head gamma cameras with coincidence electronics, used for low-cost applications, although with lower performance.

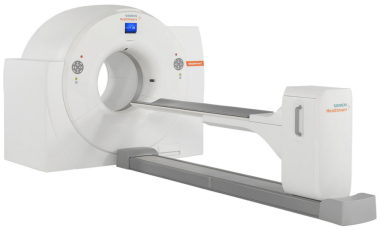

(a) The Biograph mCT is a true dual-modality scanner that seamlessly integrates high-performance PET and CT technologies into a single compact system.

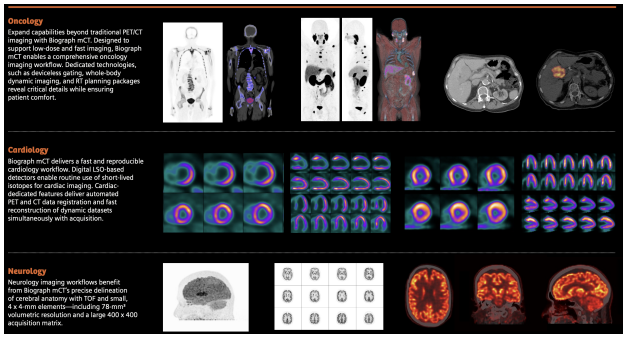

(b) Example of imaging with Biograph mCT.

Figure 2.4: The Biograph mCT delivers exceptional image quality with its high 78 mm^3 volumetric resolution and small 4×4 mm lutetium oxyorthosilicate (LSO) crystal elements, enhancing lesion detectability and enabling accurate, reproducible quantification. Advanced features such as true time-of-flight (TOF) imaging and FlowMotion^{TM} technology support both clinical precision and workflow efficiency. The system also offers versatile CT configurations, from 40 to 128 slices, incorporating low-dose innovations to help you provide care beyond the standard. [71].

In recent years, dedicated PET scanners for brain studies have been developed, characterized by a small diameter and high spatial resolution (<2.5 mm). The depth of interaction (DOI) is a critical parameter to correct the so-called parallax effect (radial elongation), which causes errors in event localization especially in peripheral regions. Advanced systems such as high resolution research tomograph (HRRT) use panels of LSO detectors with phoswitch technology, capable of determining the DOI and therefore significantly improving spatial precision.

Once the sinogram (the fundamental element for image reconstruction) has been acquired, it is necessary to proceed with image reconstruction. Reconstruction methods are mainly divided into two categories: analytical algorithms and iterative algorithms.

The main analytical method is filtered back projection (FBP), which performs the Fourier transform of the projections, filters them to attenuate the artifacts and backprojects them onto the image. This method, historically widely used for its simplicity and speed, however has poor resistance to noise and tends to produce star artifacts, especially in the presence of incomplete or noisy data.

To overcome these limitations, iterative algorithms have been developed, based on mathematical and statistical models of image formation. These algorithms, such as ordered subset expectation maximization (OSEM), allow for better reconstructive quality thanks to an approach that iteratively minimizes a cost function, taking into account the statistical nature of the acquired data. Although more computationally expensive, they are more robust to noise and able to reconstruct images even from partially incomplete datasets.

The use of OSEM-3D allows a high-quality volumetric reconstruction, while the application of rebinning allows the transformation of three-dimensional data into two-dimensional sinograms, allowing the use of the corresponding OSEM-2D algorithm, which is more computationally efficient.

PET represents one of the most sophisticated methods in nuclear medicine for functional imaging, offering high sensitivity, quantitative accuracy and the possibility of obtaining unique information on tissue metabolism. Despite the high costs and the need for specialized facilities (such as cyclotrons and radiopharmacy laboratories), its superior performance compared to other functional techniques such as SPECT make it an irreplaceable tool for research and advanced clinical practice.

2.4.3 Optical Imaging

This modality include digital pathology, fluorescence imaging, optical coherence tomography (OCT), and OCT angiography (OCTA) [66].

Digital pathology involves scanning and digitizing histological slides for computer-based analysis, enabling detailed and reproducible examination of tissue samples. The increasing demand for multi-centric studies in digital pathology is driven by the need to validate findings across institutions and ensure the generalizability of results. However, such studies face significant challenges due to variability in data acquisition, staining techniques, and imaging protocols across centers.

Fluorescence imaging plays a crucial role in disease research, drug discovery, and personalized medicine. Although multi-center studies using fluorescence imaging are expanding, they often encounter difficulties with image consistency due to differences in imaging devices, acquisition protocols, and analytical methods. These inconsistencies complicate the comparison of results across studies, potentially leading to unreliable or contradictory conclusions.

Optical Coherence Tomography (OCT)

Optical coherence tomography (OCT) [64, 67, 73, 87] is a high-resolution optical imaging technique that allows non-invasive imaging of tissues at the μm scale and real-time 3D imaging properties [10]. In addition to its diagnostic function, in recent years OCT has

found application in the functional assessment of tissues, including the study of perfusion and diffusion of pharmacological agents.

A promising area is the use of OCT to track the diffusion of nanoparticles (NPs) administered as contrast agents, as demonstrated by Stohanzlova et al. [73] in a study on a phantom model of biological tissue. In this work, the authors developed a perfused tissue phantom into which a bolus of gold nanorods of varying sizes was injected. OCT data were analyzed using mathematical deconvolution models to estimate the system's impulse response, enabling a description of the contrast agent's behavior as a function of flow. Among the models analyzed (exponential, gamma, lagged, and LDRW), the lagged model showed the best performance in terms of accuracy and fit to the experimental data.

Although this study was performed in a simulated environment, similar approaches have been applied to real tissues such as skin or ocular surfaces, where OCT's resolution and penetration depth are particularly effective in tracking local drug delivery. In dermatology, for instance, OCT has been used to assess the cutaneous absorption of topical corticosteroids by detecting changes in tissue scattering [87].

Advanced OCT modalities, such as Doppler-OCT or spectroscopic OCT, offer functional extensions by providing data on flow dynamics or molecule-specific absorption, further enhancing the capability of OCT for non-invasive drug diffusion monitoring.

OCT Angiography (OCTA)

Optical coherence tomography angiography (OCTA) [72] is a non-invasive imaging technique that allows for detailed visualization of retinal and choroidal vasculature without the need for dye injection. By detecting motion contrast from flowing blood cells, OCTA constructs high-resolution, depth-resolved images of the microvascular networks in the retina and optic nerve head. This technique enables clinicians and researchers to identify and monitor a range of ocular pathologies, such as diabetic retinopathy, age-related macular degeneration, and glaucoma, with greater precision and less patient discomfort compared to traditional fluorescein angiography. OCTA has become increasingly important in both clinical practice and research due to its rapid acquisition time and ability to reveal vascular abnormalities at early stages of disease.

Fluorescence and Bioluminescence

Optical imaging includes techniques such as fluorescence and bioluminescence, which are widely used in preclinical research for in vivo tracking of drugs, nanoparticles and cells. Fluorescence uses fluorophores excited by an external light source, while bioluminescence relies on the endogenous production of light by enzymatic reactions (e.g. luciferase).

These techniques offer very high sensitivity and specificity, especially when combined with targeted vectors (e.g. antibodies or peptides). They are ideal for temporal monitoring of drug distribution in animal models, thanks to their real-time acquisition capability [35].

The main disadvantage of optical imaging is the low penetration of light into tissues, which limits its application in the clinical setting. However, the use of near-infrared (NIR)

fluorophores and the development of activatable probes have improved the applicability in more complex animal models.

Raman Spectroscopy

Another technique mentioned above is Raman spectroscopy [22]. Since the main drug control agencies (FDA, EMA and also the Japanese one) wanted to encourage the improvement of production and quality control, it was decided to integrate real-time analysis and in this Raman spectroscopy is an excellent ally.

This analyses is a non-destructive optical technique that provides detailed information about the molecular composition and structure of a sample through its unique vibrational fingerprint. This method has gained widespread application across various fields due to its high specificity, minimal sample preparation, and ability to analyze solids, liquids, and gases. Since the 1980s, Raman spectroscopy has been increasingly employed in the pharmaceutical industry, particularly for the analysis of active pharmaceutical ingredients (APIs), allowing for the identification of compounds, monitoring of polymorphic forms, and assessment of content uniformity in formulations. Beyond pharmaceuticals, Raman spectroscopy plays a critical role in polymer characterization, bioprocess monitoring, and biomedical diagnostics, offering a versatile platform for both qualitative and quantitative analysis in complex systems.

Optical imaging has been made very accessible and user-friendly in recent years with the introduction of stable laser sources, high-speed fiber optics, volume holographic gratings, and low-noise detectors with charge-coupled devices that do not require constant realignment or sophisticated knowledge of optics. In addition, the instruments are equipped with integrated control, software, and sometimes contain supports such as artificial intelligence.

2.4.4 Ultrasound

Ultrasound (US) [9, 45] is an emerging technology in the field of controlled drug delivery and assessment of drug diffusion in biological tissues. Thanks to its ability to interact non-invasively with tissues [8], US can be used both to promote drug penetration (therapeutic US) and to monitor its distribution (diagnostic US).

One of the most promising techniques as gene therapy is sonoporation, a process by which exposure to low-frequency, high-intensity us induces the temporary formation of pores in cell membranes, facilitating drug entry into cells [92].

Furthermore, the use of contrast microbubbles in combination with US allows for localized improvement of vascular and tissue permeability, increasing the precision and efficiency of drug release (see CEUS). Microbubbles can also be used as vehicles for drug delivery, which is released in response to a specific ultrasonic stimulus, thus allowing spatial and temporal control of drug delivery [42]. Low-intensity focused US combined with microbubbles can temperately open the blood-brain barrier, enabling drugs to travel from the bloodstream into brain tumours for therapy [8].

From a diagnostic point of view, US can be used to monitor drug distribution in tissues in real-time, through advanced imaging techniques such as US molecular imaging. These approaches allow to dynamically evaluate drug diffusion, providing quantitative and qualitative data useful for optimizing therapeutic strategies [19].

Table 2.1: Typical values of density, propagation velocity and acoustic impedance for various biological tissues [14].

Material	**Density** [g/cm^3]	**Propagation Velocity** [m/s]	**Acoustic Impedance** [g/(cm$^2 \cdot s$)]
Air	0.0013	331	0.0004×10^5
Blood	1.055	1580	1.67×10^5
Bone	1.738	$2240 \pm 8\%$	$3.89 \times 10^5 \pm 8\%$
Fat	0.952	1450	1.38×10^5
Muscle	1.080	1580	1.70×10^5
Kidney	1.040	1560	1.62×10^5
Liver	1.060	1550	1.64×10^5
Spleen	1.040	1566	1.63×10^5

Figure 2.5: Vevo 2100 Ultrasound Imaging System (FujiFilm VisualSonics Inc., Toronto Canada) [32, 85]. The Vevo 2100 Imaging Platform - featuring high-frequency, high-resolution ultrasound with linear array technology and Color Doppler - delivers 30-micron resolution, frame rates up to 1000 fps, and advanced 3D imaging for preclinical research across multiple animal models and disciplines.

US refers to mechanical vibrations in the frequency range from about 20 kHz to GHz. Most medical applications employ frequency between 1 and 15 MHz.

The US technique often proves to be complementary to the X-ray diagnostic technique. The diagnostic information of X-rays depends on the different radiogenic absorption coefficients of tissues that are composed of elements of different atomic numbers and in different proportions. On the other hand, the ionizing aspect produced by the rays is related to therapeutic effects.

Ultrasonic techniques are based on the diversity of substances in relation to their density, propagation speed and absorption coefficients of mechano-elastic waves (the table 2.1 shows some typical values as an example). At present, not much is known about the therapeutic or indirect effects produced by US. However, the risk from the use of US is less than that associated with the use of ionizing radiation; this is particularly important in the case of diagnoses to be made on infants, children or pregnant women.

The application of US in medicine is essentially based on the propagation of longitudinal pressure waves. Such energy propagation can occur without material transport. In this oscillatory phase, there is transfer of energy from one particle to another. There is a relationship between the pressure to which a particle p is subjected, its velocity v, the density of the medium ρ and the speed of propagation of the ultrasound C in the medium:

$$p = v\ \rho C \tag{2.36}$$

This relationship is analogous to the electrical relationship, the Ohm's law, $V = IZ$ (voltage = current $\times$ impedance). This is also why the quantity ρC is called the characteristic impedance of the medium. Most biological media have a negligible imaginary part.

When a wave encounters two different media, effects similar to those that occur in optics (incidence, reflection, transmission) occur at the frontier between the two. The wave passing through the medium is attenuated along the direction of propagation according to the relation:

$$A = A_0 e^{-\alpha \cdot x} \tag{2.37}$$

where A is the amplitude of the wave and α being the absorption coefficient along the x direction. Given the high value of α for air, it is necessary to cover the transducer with appropriate fluid before applying it to the skin. This is in order to achieve a better fit between the different impedances. The absorption coefficient α depends on the frequency according to a relationship that, for biological tissues, can be approximated by:

$$\alpha = Kf \tag{2.38}$$

where K is a medium-dependent proportionality constant. It would therefore seem convenient to use low-frequency waves. The lower limit, however, is the need for a sufficiently focused ultrasound beam. The beam diverges by an angle θ given by:

$$sen\theta = \frac{0.61\lambda}{r} = \frac{0.61C}{rf} \tag{2.39}$$

where r is the radius of the transducer and λ the wavelength of the US. This relationship is valid at a certain distance from the transducer.

The tissues and structures of the human body are, in general, good conductors of elastic waves. The size of the smallest detectable structures is related to the wavelength

used, and the latter depends on the frequency and speed of propagation of the wave in the medium under examination:

$$\lambda = \frac{c}{f} \tag{2.40}$$

where λ is the wavelength, c is the speed in the medium and f is the frequency. The propagation velocity in water and most soft tissue has values between 1450 and 1600 m/s; an average value of 1540 m/s is normally assumed for c. With the use of elastic waves with frequencies in the order of MHz, it is possible to obtain information on structures with dimensions in the order of mm.

Similar to the optical case, an ultrasound wave passing through the separation zone between two media with different acoustic impedance is subject to a reflection and refraction phenomenon. The reflected components, appropriately detected, provide an indication of the structure of the tissue crossed by the ultrasound wave.

The elastic wave generated propagates through the tissues and is partially reflected by the discontinuities encountered along the way. The reflected components return towards the transducer itself and are detected with a certain delay with respect to the instant of emission of the ultrasonic wave. From the measurement of this delay, it is possible to trace the distance of the discontinuities from the transducer and thus realise a representation of the structure underlying the examined area.

The piezoelectric transducer can be regarded as a device with an electrical input and an acoustic output. Due to the presence of resonant elements, this device ultimately behaves like a bandpass filter. The most important characteristic of a medical diagnostic transducer is its bandwidth, i.e. its ability to reproduce an electrical signal as accurately as possible in an acoustic signal. A transducer for medical diagnostics has the back surface of the ceramic generally in contact with a compound of epoxy resins and high-density metal powder (tungsten, lead) which has an acoustic impedance $\rho_b C_b$ much closer to that of the ceramic. The acoustic energy fed into this material, which is called backing, is completely absorbed, given the high attenuation coefficient of these compounds. The front surface of the ceramic is in contact with the tissue by means of an epoxy resin plate, which is also filled with metal powders of $\frac{\lambda}{4}$ thickness. This plate, called a matching plate, acts like an impedance transformer so that if it is of the appropriate acoustic impedance, it will make the ceramic see the increased impedance. In figure 2.5 there is an example of a machine.

There are different ways of displaying the information acquired by means of return echoes. For example, there can be A-mode (Amplitude-mode) representation, B-mode (Brightness - mode) variant of A-mode, M-mode (time Motion mode), dynamic scanning systems, rotating transducer dynamic scanning systems, Doppler systems.

The A-mode representation system was the first to be used in ultrasound diagnostics, but is now considered outdated. In a B-mode representation system (brightness mode is equal brightness representation), each echo reflected from an interface corresponds, on the horizontal axis of the oscilloscope, to a dot that is as bright as the echo detected. This system is the basis of time motion or M-mode, as well as two-dimensional imaging. When the interface considered is that of a moving system (e.g. the anterior mitral flap), in B-mode we obtain luminous dots which move more or less rapidly along the horizontal axis, placing this axis vertically on a screen with a certain persistence and sliding it from

left to right at a constant speed, each luminous dot, if fixed, will describe a horizontal straight line, if mobile a curve, which will represent the displacement in time of that interface point in movement.

The return echoes obtained from the different types of transducers are processed in various ways to obtain one- and two-dimensional images. Since the signals picked up are very small, they must pass through an amplifier to become representable. This is characterised by a gain, calibrated in dB that can be varied by means of a general gain control. It is then necessary to act on the deepest echoes to bring them down to amplitudes that make it possible for them to be represented alongside the nearest ones. The gain control that takes into account the distance of the transducer from the surfaces under examination is the time gain compensation: it assigns a greater gain to the echoes coming from deeper separating surfaces than that assigned to the echoes relating to surfaces close to the transducer and thus counterbalances the increase in attenuation of the signal, both direct and reflected, that depends on the depth, type and number of structures crossed. At the same time, it will become necessary to bring the closer echoes to values proportional to those of the more distant echoes, decreasing their amplitude by means of a control referred to as near gain or bear suppression. Other useful controls for improving image quality are the reject and dynamic range controls. The reject allows all echoes below a set level to be cancelled, thus eliminating echoes due to background noise from the radio-frequency amplifiers that process the signal. The dynamic range conditions the quality of the two-dimensional image, determining the presence of more or less extensive shades of grey. The greyscale representation is a function of the dynamic range or the reception - amplification - representation system. The dynamic range relative to the representation screen is the ratio in dB, between the voltage that produces the brightest dot and that which produces a barely visible dot. Despite the limitations imposed by noise and maximum transmission power, the maximum usable dynamic range for received echoes in a pulsed system for medical-diagnostic applications is approximately 100 dB. It is divided between the amplitude variation of the echoes at a fixed distance and the attenuation due to the distance of the transducer. For a fixed range, the maximum possible amplitude variation of an echo is 30 dB, so 70 dB is used to compensate for the various attenuations.

In biomedical applications [94], the human body can be exposed to varying ultrasonic frequency ranges, including high-frequency US (1-20 MHz, commonly used for diagnostic purposes), medium-frequency (0.7-3 MHz), and low-frequency (20-200 kHz) regions. Low-frequency US is further classified into high-intensity (>5 W/cm^2, using a focused beam) and low-intensity (0.125-3 W/cm^2, using an unfocused beam). By adjusting parameters such as frequency and intensity, US can produce different interactions with biological tissues, inducing either thermal or non-thermal effects. These effects are key in activating US-sensitive biomaterials for a variety of therapeutic functions.

As US waves propagate through tissues, they undergo attenuation due to absorption and scattering, which decreases their amplitude with distance. Some waves change direction, while others are converted to heat, leading to a rise in temperature. These US-induced thermal effects are utilized in certain therapies, such as high-intensity focused ultrasound (HIFU) [80], which enables precise tissue ablation with minimal invasiveness

compared to other methods. HIFU's thermal effects can also trigger temperature-sensitive drug release and stimulate immune responses, making it a promising strategy for cancer treatment.

Contrast-Enhanced Ultrasound (CEUS)

Contrast-Enhanced Ultrasound (CEUS) [83, 88] uses microbubbles containing inert gases that, once injected into the bloodstream, increase the ultrasound reflectivity of vascularized tissues. Microbubbles can also be functionalized with specific ligands to achieve molecular targeting.

CEUS is a low-cost, safe and easily accessible technique, ideal for assessing tissue perfusion and monitoring drug release in real-time. It is used in oncology to study tumor vascularization and to monitor the efficacy of anti-angiogenic therapies.

The combination of CEUS with therapeutic approaches (sonoporation, drug release from microbubbles) opens new perspectives in the field of non-invasive drug delivery.

2.4.5 Emerging Techniques

Many techniques have been born in recent years, the result of research, necessity and desire to improve in this field.

Matrix-assisted laser desorption/ionization imaging mass spectrometry (MALDI-IMS) [91] is a perfect example. It is an ex vivo technique that allows to obtain spatial maps of the molecular distribution of drugs, metabolites or biomolecules on tissue sections. The analysis occurs by laser ionization followed by mass spectrometry, generating images with microscopic resolution. MALDI-IMS is particularly useful in the evaluation of tissue penetration of new drugs, in the preclinical phase, without the need for radioactive or fluorescent labeling.

Another example is given by the infrared thermography (IRT) that is a non-invasive imaging technique that allows to measure the surface temperature distribution of biological tissues. The use of highly sensitive thermal cameras allows to detect thermal changes induced by the absorption or diffusion of drugs, particularly in protocols in which the drug causes an alteration of local metabolism or blood perfusion [43, 61]. In the context of tissue pharmacokinetics, the thermal camera can be used to track in real-time the thermal variations following the administration of the drug, providing indirect information on its diffusion. For example, in studies on the efficacy of topical vasodilator or anti-inflammatory drugs, thermographic analysis has shown significant correlations between the intensity of the thermal response and the local concentration of the drug [5]. This technique is particularly useful in soft tissues, where thermal changes are more easily detectable, and has also shown promise in the context of transdermal or intradermal administration, where it can support the spatial and temporal assessment of the penetration of the active ingredient [2].

2.5 Contrast Agents

The use of contrast agents [4, 8, 28, 60, 62, 82] has revolutionised medical imaging, enabling more accurate visualisation of anatomical structures and physiological abnormalities. These agents enhance the contrast between tissues in images obtained by various diagnostic techniques such as radiography, CT, MRI and ultrasound. Contrast media can be classified according to the imaging technique for which they are used.

These agents are typically based on iodine or barium, elements with a high atomic number that effectively absorb X-rays.

- Iodine media. They can be ionic or non-ionic and are mainly used for CT. Examples include iopamidol, iohexol and ioversol.
- Barium sulphate. Used mainly for gastrointestinal studies, it is an insoluble salt that provides excellent contrast without being absorbed by the body [13].

In MRI, contrast agents act by modifying proton relaxation times.

- Gadolinium (Gd). Gadolinium-based agents, such as gadopentetate dimeglumine, are the most common. They are generally chelated to avoid toxicity, as free Gd is highly toxic. Gd is a paramagnetic contrast agent [34].
- Recently, attention has shifted to iron- or manganese-based agents as safer alternatives in patients with renal problems [63].
- Oily contrast medium: lipiodol [4].
- Hyperpolarized agents require injection to function [57].

Gas microbubbles are the most used in ultrasound. They are composed of inert gases such as perfluorocarbons or sulfur hexafluoride, encapsulated in a lipid or protein shell. They are used to study tissue perfusion and contrast in vessels. This variant is known as contrast-enhanced ultrasound (CEUS) [27].

In SPECT/PET, radiopharmaceuticals are used and they can be divided into diagnostic and therapeutic [3]. The first one applied [60] was Iodine 131 in the study of thyroid pathologies. Currently, Technetium 99 (^{99m}Tc) plays a fundamental role in SPECT diagnostics, representing over 90% of the radionuclides used. In particular, ^{99m}Tc is highly valued because it is cheap, easily produced locally and, above all, because it emits exclusively gamma radiation with an energy ideal for obtaining quality diagnostic images. Furthermore, thanks to its short half-life of only 6 hours, it inactivates rapidly, minimizing the environmental impact. Research in the radiochemical and radiopharmaceutical fields has led to the development of numerous compounds capable of binding to Technetium and selectively accumulating in specific organs, thus improving the effectiveness of diagnostic investigations. In the field of PET diagnostics, the most commonly used radiopharmaceutical is ^{18}F-fluorodeoxyglucose (FDG). This metabolism tracer is used on a large scale in oncology, cardiology and neurology, thanks to its ability to highlight areas of high glucose consumption, typical of many pathologies. In the tables 2.2 you can see examples of radiopharmaceuticals.

Table 2.2: Common radiopharmaceuticals used in PET and SPECT selected by Ricci [60].

PET Radiopharmaceuticals

Radiotracer	Function
^{18}F-FDG	Glucose metabolism
^{18}F-ESP	D_2 and 5-HT_2 antagonist
^{15}O-H_2O	Cerebral perfusion
^{11}C-Ammonia	Myocardial perfusion
^{11}C-Flumazenil	Benzodiazepine receptor
^{11}C-Raclopride	Dopamine D_2 receptor
^{11}C-FE-bCIT	Dopamine reuptake
^{11}C-Choline	Prostate cancer
^{11}C-Fluvoxamine	Serotonin reuptake
^{11}C-Palmitate	Fatty acid metabolism

SPECT Radiopharmaceuticals

Radiotracer	Function
^{99m}Tc-ECD	Cerebral perfusion
^{99m}Tc-IMP	Cerebral perfusion
^{99m}Tc-MIBI	Myocardial perfusion
^{123}I-β-CIT	Dopamine transporter
^{123}I-IBZM	D_2 receptor binding

The use of contrast media requires careful evaluation of the safety profile, particularly in subjects with renal dysfunction (iodinated contrast medium nephropathy or gadolinium nephrogenic systemic fibrosis). Clinical guidelines recommend the use of low osmolality agents and pre-test assessment of renal function [75].

Among the most promising innovations:

- Molecular contrast agents: directed at specific biological targets (receptors, enzymes, tumour cells).
- Nanoparticles. In particular, iron oxide nanoparticles for MRI and gold nanoparticles for CT and multimodal imaging.
- Hybrid techniques. Such as PET/MR or SPECT/CT, which require dual agents capable of being detected by multiple modalities [36].

Contrast media are an essential element of modern biomedical imaging. Their choice and use must take into account the diagnostic technique, the patient's clinical profile and the associated risks. Research continues to offer increasingly effective and safe solutions, pushing towards molecular and personalised imaging.

2.6 Nanoparticles

In recent decades, nanotechnology has acquired an increasingly important role in the biomedical landscape, giving rise to a new interdisciplinary field known as *nanomedicine* [20]. It deals with the use of materials with dimensions between 1 and 1000 nm for diagnostic, therapeutic and preventive purposes. In this context, nanoparticles (NPs) represent one of the most promising platforms, as they allow the targeted and controlled delivery of active ingredients, the reduction of systemic side effects and the improvement of the pharmacokinetic profile of drugs.

NPs can be divided, based on their chemical composition, into several main categories. Lipid nanoparticles, such as liposomes and solid lipid NPs (SLN), are among the most

widely used due to their biocompatibility and ability to encapsulate both hydrophilic and lipophilic compounds. Polymeric NPs, made with natural materials (such as chitosan or alginate) or synthetic materials (such as PLGA), offer high stability and the possibility of prolonged release. Equally interesting are inorganic NPs, based on metals or metal oxides, used mainly in the diagnostic field, and hybrid structures, which combine different materials to obtain synergistic properties.

From an applicative point of view, NPs are used in numerous clinical fields. In oncology [8, 95], for example, they allow the localized release of chemotherapeutics, reducing systemic toxicity and increasing the concentration of the drug at the tumor site. In the infectious disease field, nanoparticles are used to deliver antibiotics or vaccines (as in the case of mRNA vaccines for COVID-19, formulated with lipid NPs). Further applications are under development for gene therapy, administration of analgesics, treatment of neurodegenerative diseases and regenerative medicine.

Lipid-Based Nanoparticles

Lipid-based NPs [20] include liposomes, lipid NPs, and emulsions (examples in the appendix table 4). These systems are particularly favored in nanomedicine due to their biocompatibility, straightforward formulation processes, and the versatility to encapsulate a wide range of therapeutic agents.

Liposomes are primarily composed of phospholipids. They can form both unilamellar and multilamellar vesicles, enabling the encapsulation of hydrophilic, hydrophobic, and lipophilic drugs within the same system. Their structures can be engineered to enhance circulation time and improve targeted delivery by evading rapid clearance by the reticuloendothelial system.

Nano-emulsions consist of oil-in-water or water-in-oil mixtures, where the active pharmaceutical ingredient (API) is enclosed within oil droplets stabilized by surfactants and cosurfactants, all dispersed in an external aqueous phase. These emulsions often utilize excipients considered safe for human use and exhibit a high loading capacity for lipophilic drugs, although they may face challenges related to thermodynamic stability.

To address limitations found in conventional lipid-based carriers, newer forms such as solid lipid NPs (SLNs) and nanostructured lipid carriers (NLCs) have been developed. These advanced systems are capable of enhancing drug targeting, improving the bioavailability of poorly soluble compounds, and protecting labile therapeutic agents.

Lipid-based nanoparticles have been extensively researched across various therapeutic areas, including oncology and vaccine delivery (example with mRNA-based COVID-19 vaccines). Liposomes, in particular, are the most widely studied within pediatric medicine, where pharmacokinetic variations between children and adults have been observed. Despite their potential, the inclusion of pediatric populations in clinical trials involving liposomes remains limited. Among several hundred ongoing or upcoming studies, only a small fraction specifically involves participants under the age of 18, with most trials focusing on cancer therapy.

Other innovative lipid NP systems, such as in situ self-assembling NPs (ISNPs), have also shown promise. For instance, pediatric-friendly formulations of antiviral therapies using ISNPs have demonstrated enhanced drug bioavailability and tissue targeting in

preclinical studies. Additional research has explored the use of self-assembling nanoassemblies incorporating modified therapeutic agents, which have shown significant cellular uptake and potential antitumor activity in vitro.

Polymer-Based Nanoparticles

Polymer-based NPs [20] are colloidal systems composed of natural, semi-synthetic, or synthetic polymers, offering a wide range of structural configurations and functional properties. These systems encompass various forms, including dendrimers, polymeric micelles, polymersomes, nanospheres, and nanogels, each serving different clinical purposes.

These NPs can be either biodegradable or non-biodegradable. Biodegradable polymers are particularly favored in biomedical applications, especially in pediatrics, due to their ability to degrade in vivo through enzymatic or non-enzymatic pathways, producing biocompatible by-products. Their performance can be optimized by employing approved biodegradable polymers, utilizing in situ administration techniques, combining with other treatment modalities like immunotherapy or radiotherapy, or enabling controlled, on-demand release of therapeutic agents.

Common biodegradable polymers include polysaccharides such as hyaluronic acid, chitosan, dextrin, and alginate. For example, chitosan is recognized as safe for use in biomedical applications, including tissue engineering and pediatric drug delivery, although its approval has been challenged by concerns over source variability, purity, and potential immunogenicity.

Hyaluronic acid (HA) is suitable for nanomedicine applications. Its primary receptor, CD44, is overexpressed in many solid tumors, making HA a valuable component for targeted cancer therapies. In pediatric drug formulations, HA has been explored to enhance patient compliance by modifying dosage forms or reducing administration frequency.

Protein-based natural polymers, including albumin, lactoferrin, and apotransferrin, have also been utilized in drug delivery. Albumin, a major plasma protein, is hemocompatible and widely used in intravenous formulations. Lactoferrin, a natural iron-binding glycoprotein, exhibits a range of therapeutic activities including antiviral, anti-inflammatory, and anti-cancer effects. Its receptors are often overexpressed in tumors and brain endothelial cells, facilitating targeted delivery and transport across the blood brain barrier (BBB). Lactoferrin-based NPs have shown pH-sensitive drug release properties, enhancing therapeutic efficacy in acidic tumor microenvironments. Similar applications have been explored using apotransferrin, which also plays a role in iron transport.

Semi-synthetic and synthetic polymers are increasingly investigated. Polyethylene glycol (PEG) is widely applied due to its biocompatibility and ability to prolong circulation time by imparting *stealth* characteristics to nanoparticles. Polycaprolactone (PCL), known for its non-toxic profile and high drug permeability, is used in sustained and controlled-release systems. When conjugated with PEG, PCL-based NPs have been shown to improve therapeutic outcomes. Poly(lactic-co-glycolic acid) (PLGA) is another synthetic polymer that offers favorable properties for drug delivery, including tunable degradation rates and biocompatibility. PLGA can be tailored through manipulation of its lactic-to-glycolic acid ratio and molecular weight, influencing degradation kinetics. Advanced formulations using PLGA-PEG nanoparticles have been designed for targeted

delivery. Other synthetic polymers with unique capabilities, such as polyethyleneimine (PEI), poly(vinylimidazole) (PVI), and poly(amidoamine) (PAMAM), are being explored for applications such as gene delivery. The adaptability of these polymers enables the design of a variety of nanoparticle architectures, supporting diverse biomedical applications.

Polymeric Micelles

Polymeric micelles [20] are a class of nanocarriers recognized for their versatility in delivering therapeutic agents and, in some cases, acting as bioactive substances themselves. Structurally, they typically consist of a core-shell architecture formed through the self-assembly of amphiphilic block copolymers in aqueous environments. This structure provides a hydrophobic core suitable for encapsulating poorly water-soluble drugs, surrounded by a hydrophilic shell that enhances solubility and stability in biological fluids. Their design offers significant flexibility for functionalization, making them adaptable to various drug delivery needs.

Amphiphilic block copolymers such as Pluronic® and Tetronic® surfactants are commonly used to form these micelles, especially when conditions surpass the critical micellar concentration or temperature.

Several polymeric micelle-based nanomedicines have successfully entered the pharmaceutical market. Genexol-PM® is a polymeric micellar formulation of paclitaxel composed of monomethoxy poly(ethylene glycol)-block-poly(D,L-lactide), which has received approval for the treatment of metastatic breast cancer, non-small cell lung cancer, and ovarian cancer in various countries including South Korea, the Philippines, India, and Vietnam. Another example, NanoxelTM, utilizes a di-block copolymer system comprising poly(vinylpyrrolidone)-block-poly(N-isopropylacrylamide) and paclitaxel. It is formulated as a liquid and approved for refrigerated storage, in contrast to Genexol-PM®, which is available as a lyophilized powder. NanoxelTM has been approved for the treatment of metastatic breast cancer, non-small cell lung cancer, and AIDS-related Kaposi Sarcoma.

Paclical®, also known as Apealea® in some regions, represents another example of a micelle-based formulation of paclitaxel. Developed using XR17 micelle platform technology, it is free of Cremophor EL and has been authorized in several jurisdictions for the treatment of ovarian cancer.

Dendrimers

Dendrimers [20] are highly branched, 3D polymeric nanostructures characterized by multiple functional groups located both within internal cavities and on their outer surface. Their well-defined architecture allows for precise molecular control, making them promising candidates for advanced drug delivery systems. Among these, polyester dendrimers are often regarded as *smart carriers* due to their ability to release therapeutic agents selectively in response to specific physiological conditions, potentially minimizing off-target effects and improving treatment outcomes.

These nanostructures have also been explored as an alternative route for transdermal

drug administration, which may be particularly advantageous for patients who are unable or unwilling to take oral medications, such as those experiencing nausea or unconsciousness. For example, dendrimers approximately 4 nm in size were shown to be efficiently eliminated via renal excretion, with no detectable accumulation in the kidney glomeruli after one day.

In preclinical studies, certain dendrimer formulations have shown selective cytotoxicity against cancer cells while sparing healthy cells.

Inorganic Nanoparticles

Inorganic NPs [20] include a broad category of materials such as metal-based nanoparticles - commonly composed of iron, gold, silver, or zinc - as well as rare-earth metal nanoparticles like lanthanum oxide and ytterbium oxide, and silica NPs. These systems have been extensively explored for their potential in diagnostic and therapeutic applications, particularly in conditions such as atherosclerosis and cancer. The primary reason for adopting gold and silver NPs as nanomaterials for drug delivery is because they exhibit potential drug transport and imaging properties [86].

Venofer® consists of iron oxide NPs coated with sucrose, enabling a controlled release of iron after intravenous administration, thereby minimizing the risk of a sudden increase in free iron levels in the bloodstream. Ferrlecit® represents a stable complex of sodium ferric gluconate within a sucrose matrix, also intended for intravenous use.

Hybrid NP systems have shown particular promise. One such example is the development of multifunctional gold-based NPs conjugated with targeting ligands and therapeutic agents, such as a formulation incorporating Angiopep-2, polyethylene glycol (PEG), and doxorubicin. This system demonstrated the ability to cross the blood brain barrier (BBB) and selectively accumulate in glioma cells, highlighting the therapeutic potential of engineered inorganic nanocarriers in oncology.

Literature Search Strategy

This thesis focuses on articles published from the past decade to the present, examining the broader landscape of medical drug research. The choice to concentrate on this timeframe allows for an in-depth exploration of recent advancements, trends, and innovations, ensuring the analysis remains relevant to current developments in the field.

A comprehensive literature search was conducted across major scientific databases, including Google Scholar, PubMed, and others. This approach was aimed at gathering a wide range of peer-reviewed studies and authoritative sources to support a thorough and up-to-date review of methodologies, findings, and emerging directions in medical drug research.

The main keywords searched are "Drug delivery", "Medical drug", "Diffusion in drug delivery", "Drug delivery and medical imaging", "Pedritian drug delivery", "MATLAB drug delivery".

Chapter 3

Overview of Results and Representative Examples

The literature available in this context is very large. In this section, some relevant articles have been chosen for the evaluation of this work. The articles have been selected mainly for the use of MATLAB software within the work. Furthermore, another aspect considered was the fact that they were topics covered in the Materials and methods section 2.

Graphs

The graphs presented in this chapter were generated using MATLAB code developed by the author (unless otherwise indicated), based on the mathematical models described in the various papers reported. The parameters used correspond to those proposed in the original article, in order to verify their dynamic behaviors.

3.1 Applications of Fick's Law

In the context of the bibliographic analysis on the mechanisms of drug diffusion in human tissues, the models proposed by Khanday et al. [38] were considered, which represent a significant basis for the mathematical modeling of pharmaceutical distribution in biological compartments. They treated the different parts of the body as compartments.

The movement of drugs within the body is modeled by dividing the body into different compartments and monitoring the drug as it moves in and out of each one. The drug leaves one compartment and enters another at a rate proportional to the drug concentration in the original compartment. This transfer of the drug between compartments follows first-order kinetics.

Three distinct models were analyzed.

Model I - Oral Administration

This model considers two compartments: the gastrointestinal tract (GI) and the blood flow. The drug is absorbed from the GI into the blood, with an absorption rate k_1 and an elimination rate from the blood k_e. The differential equations are:

$$\frac{dc_1}{dt} = -k_1 c_1(t), \qquad c_1(0) = c_0 \tag{3.1}$$

$$\frac{dc_2}{dt} = k_1 c_1(t) - k_e c_2(t), \qquad c_2(0) = 0 \tag{3.2}$$

Where:

- c_1 is the concentration of drug in stomach or GI tract.
- c_2 is the concentration of drug in blood stream.
- c_0 is the initial concentration of drug dose.

Each equation reports the change in drug concentration in their respective compartments over time, as shown in the figure 3.1a.

The analytical solution shows that the concentration in the GI compartment decreases exponentially, while that in the blood increases to a peak, and then decreases.

Therefore, the amount of drug absorbed by the body is not always consistent. Oral medication can sometimes be less effective due to factors such as stomach sensitivity, liver dysfunction, or delayed absorption. In these situations, intravenous administration is preferred because it delivers the drug more efficiently and rapidly. Additionally, in emergency cases, medication often needs to be absorbed quickly by body tissues, making intravenous delivery the most suitable method.

Model II - Intravenous Administration (Two Compartments)

In this model, the drug is directly injected into the blood and then diffuses into the tissue. Two compartments (blood and tissue) are included, with constants k_b,k_t, and k_e.

The equations solved by Laplace transform are:

$$\frac{dc_b(t)}{dt} = -(k_b + k_e)c_b + k_t c_t, \qquad c_b(0) = c_0 \tag{3.3}$$

$$\frac{dc_t(t)}{dt} = k_b c_b - k_t c_t, \qquad c_t(0) = 0 \tag{3.4}$$

Where:

- $c_b(t)$ is the concentration of drug in the compartment blood.
- $c_t(t)$ is the concentration of drug in the compartment tissue.
- c_0 is the initial concentration of drug injected.

The model is shown in the graph 3.1b.

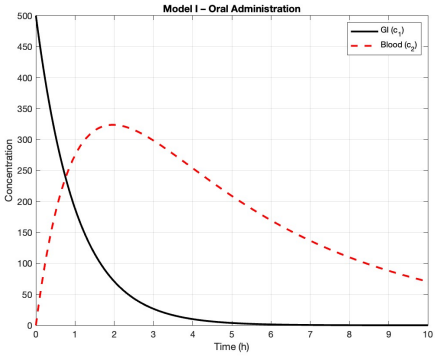

(a) Model I

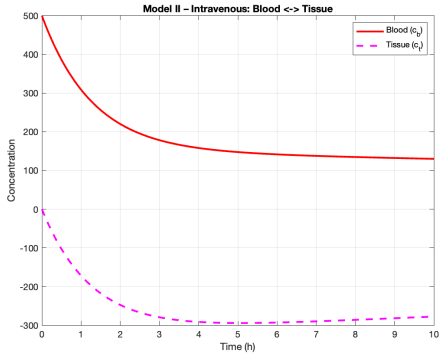

(b) Model II

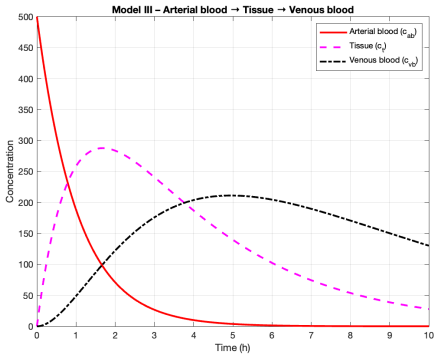

(c) Model III

Figure 3.1: MATLAB simulations of Model I, II, III. Graphs made by the author based on Khanday et al. [38].

Model III - Administration via Arterial/Venous Circulation (Three Compartments)

This more complex model introduces the concept of unidirectional flow: the drug enters via arterial blood, passes into the tissues, and from there into venous blood, from where it is eliminated. In this case, the authors considered the therapeutic effect.

Since blood flow in the cardiovascular system is unidirectional, drug administration through the venous blood follows a specific pattern. The drug carried by the venous blood reaches the target site via the capillary bed, while the remaining drug is either eliminated or returned to the circulatory system by the arterial blood. Assume that the drug consumption by arterial blood as it moves toward the tissue occurs at a rate of k_b, and the transfer of the drug from the tissue compartment back to the venous blood happens at a rate of k_t. k_e represent the clearance rate of the drug from the blood.

System of equations:

$$\frac{dc_{ab}(t)}{dt} = -k_b c_{ab}(t), \qquad c_{ab}(0) = c_0 \tag{3.5}$$

$$\frac{dc_t(t)}{dt} = k_b c_{ab}(t) - k_t c_t(t), \qquad c_t(0) = 0 \tag{3.6}$$

$$\frac{dc_{vb}(t)}{dt} = k_t c_t t - k_e c_{vb}(t), \qquad c_{vb}(0) = 0 \tag{3.7}$$

Where:

- $c_{ab}(t)$ is the concentration of drug in the arterial blood.
- $c_t(t)$ is the concentration of drug in the compartment tissue.
- $c_{vb}(t)$ is the concentration of drug in the venous blood.
- c_0 is the initial drug dosage.

Three curves over time 3.1c: concentration in arterial blood, tissue, venous blood.

The models highlight how the variation of the kinetic parameters affects the efficacy and persistence of the drug. Increasing k_1 or k_b, a faster diffusion is observed, while a low k_e prolongs the presence of the drug in the organism, potentially increasing the risk of side effects.

It is interesting to note that these models are based on Fick's law, previously described in detail. There is also a reference to the Laplace transform.

The study by Hong et al. [31] was taken as a reference, which characterized the controlled diffusion of a contrast agent (gadobutrol that is a gadolinium-based MRI contrast agent) from a calcium sulfate matrix in agar by quantitative MRI. The multi-echo gradient echo (GRE) MRI data were processed using MATLAB scripts in order to obtain R2* and magnetic susceptibility maps (QSM). Starting from the average of the R2* values in an annular region surrounding the central core, a drug release curve was obtained, based on a model derived from Fick's laws for cylindrical geometries. The model used is the following:

$$\frac{M(t)}{M(\infty)} = 1 - \frac{4}{\lambda_1^2} \cdot \exp\left(-\frac{\lambda_1^2 \cdot D \cdot t}{R^2}\right) \tag{3.8}$$

where $\lambda_1^2 = 2.405$ is the first root of the Bessel function $J_0(\lambda) = 0$, D is the diffusion coefficient (in m^2/s), R the radius of the cylinder, and t the time. The experimental data were normalized as a function of R2* and fitted to the model to extract D.

The figure 3.2 shows the normalized cumulative release of the drug (gadobutrol) over time, estimated indirectly through the mean R2* values measured in an annular region around the calcium sulfate core. The experimental data (black dots) were successfully fitted to the theoretical controlled release model for cylindrical geometries, based on Fick's laws, by nonlinear regression. The fitting curve (pink line) shows an excellent fit

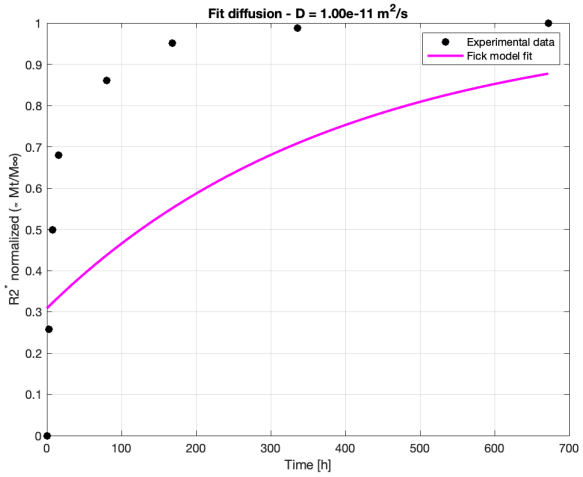

Figure 3.2: MATLAB processing by the author on Hong et al. [31] data.

to the data ($R^2 \approx 0.991$), confirming the validity of the adopted model. The estimated diffusion coefficient is $D = 4.59 \times 10^{-11}$ m^2/s, a value consistent with that reported in previous studies for the diffusion of small water-soluble agents inside porous matrices. The analysis therefore allows a precise quantification of the release of the active principle from biocompatible carriers, through MATLAB processing applied to quantitative MRI data.

To analyze the influence of geometric and physical parameters on drug release in tissues, the mathematical models proposed by Yahya et al. [93] for diffusion-controlled release devices were reproduced in MATLAB. The models are based on Fick's second law in non-steady state conditions and were applied to three geometric configurations: slab, spherical and cylindrical.

In the case of the slab geometry, the release profile was simulated using the following analytical expression:

$$\frac{M(t)}{M_0} = 1 - \frac{8}{\pi^2} \sum_{n=0}^{\infty} \frac{1}{(2n+1)^2} \exp\left(-\frac{(2n+1)^2 \pi^2 D t}{4L^2}\right) \tag{3.9}$$

where D is the diffusion coefficient, L the thickness of the device, $M(t)$ the cumulative amount of drug released at time t, and M_0 the initial amount.

Different experimental conditions were considered by varying the thickness L at a constant diffusion coefficient, and subsequently varying the diffusion coefficient D at a fixed thickness. The results are reported in the graphs 3.3.

The results show that a reduction in thickness determines an increase in the velocity of release, in agreement with the inverse relationship between L and the exponential term. Similarly, an increase in the diffusion coefficient leads to an acceleration of the release, as predicted by theoretical models.

These simulations confirm the effectiveness of the mathematical approach to predict and modulate the release kinetics in polymeric systems and can be extended to the analysis of diffusion in human tissues, assuming appropriate boundary conditions and values of physiological parameters.

An relevant factor is the geometry of the drug delivery system. It can be:

- slabs with flat surfaces delivery device,
- spherical delivery device,
- cylinders delivery device.

The authors of the paper tested this factor with a mathematical model to demonstrate its importance.

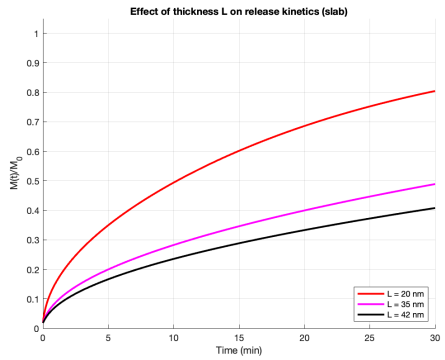

(a) Cumulative release profile versus time for three different thicknesses L in a slab geometry. An inverse relationship between thickness and release rate is observed.

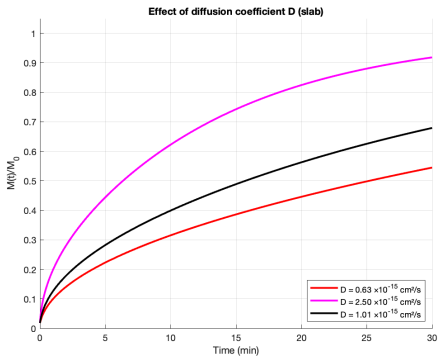

(b) Effect of diffusion coefficient D on the release profile at constant thickness (L). The increase in diffusivity accelerates the release of the drug from the matrix.

Figure 3.3: MATLAB simulations. Graphs made by the author based on Yahya et al. [93].

Simulations conducted in MATLAB reproduced the release profiles for diffusion-controlled systems with planar geometry (slab), using the analytical solution derived from Fick's second law in non-steady regime. The two graphs obtained (3.3) show respectively the effect of the variation of the thickness of the device L and of the diffusion coefficient D on the release kinetics.

In 3.3a it is observed how, with the same diffusion coefficient, a reduction of the thickness of the device from 42 to 20 nm leads to a significant increase in the release rate: this result is consistent with the fact that the diffusion path is shortened, allowing the drug to cross the polymer matrix more rapidly.

In 3.3b, the effect of the diffusion coefficient is highlighted, keeping the thickness constant at 22 nm. The increase of D from 0.63×10^{-15} to 2.50×10^{-15} cm^{-2}/s produces an acceleration of the release, consistent with what was theoretically expected: a higher value of D corresponds to a greater mobility of the drug in the matrix, and therefore to a faster release.

The results obtained are perfectly in line with those reported by Yahya et al., both for qualitative trend and for the values of the parameters used. In the article, in addition to the slab geometry, the spherical and cylindrical geometries were also analyzed, showing similar effects: the reduction of the radius or height of the device increases the release speed, as well as the increase in diffusivity. However, the mathematical dependence on the parameters changes depending on the geometry, as highlighted by the differential equations used in the paper.

This analysis confirms that mathematical modeling can represent an effective predictive tool to design controlled release devices, allowing to optimize the shape and size of the system based on the drug to be delivered and the characteristics of the target tissue.

3.2 Applications of Nanoparticles

In the context of anticancer drug delivery systems (DDS), magnetic nanomaterials offer a range of multifunctional properties beyond simple drug transport. These include photothermal activity, magnetically targeted hyperthermia, and serving as MRI contrast agents, which collectively enable real-time monitoring of tumor treatment. This multifunctionality enhances the precision and effectiveness of cancer therapy by allowing both targeted treatment and simultaneous imaging.

However, despite their potential, magnetic nanomaterials face several challenges that limit their broader application. Issues such as long and complex fabrication processes, low surface area, and high reaction temperatures contribute to high production costs and poor scalability. Overcoming these limitations is essential for transitioning these advanced materials from experimental settings to widespread clinical use.

A relevant study by Waqas et al. [86] proposes a numerical analysis of the dynamics of blood nanofluids containing gold (Au) and silver (Ag) nanoparticles (NPs) injected into a stenoses artery. *Nanofluids* are ultrafine nanoparticle suspensions in ordinary liquids.

The NPs, considered as drug carriers, are modeled in the context of magnetohydrodynamic (MHD) flow, including also thermal radiation effects and heat sources. The system of partial differential equations is transformed into dimensionless ordinary equations, solved by the bvp4c numerical method in MATLAB.

Table 3.1 summarizes the key thermophysical properties of blood, gold, and silver, which are relevant in the modeling of nanofluid-based drug delivery systems. As shown, gold and silver NPs have significantly higher thermal conductivity compared to blood (314 W/m·K and 429 W/m·K vs. 0.492 W/m·K, respectively), which can enhance heat transfer in biological environments. Moreover, their much higher electrical conductivity may influence magnetohydrodynamic (MHD) behavior under external magnetic fields. These properties justify their use as carriers in magnetically assisted drug delivery. The low specific heat capacity of metals compared to blood also implies a faster thermal response, which may be beneficial or destructive depending on the application. Overall, these differences highlight the importance of accurately incorporating nanoparticle properties into numerical models.

The results, reported in the article, show that increasing the volumetric fraction of

Table 3.1: Thermophysical properties of base fluid and nanoparticles [55]

Property	**Blood**	**Gold (Au)**	**Silver (Ag)**
Density ρ [kg/m^3]	1063	19320	10500
Specific heat c_p [J/(kg·K)]	3594	129	235
Thermal conductivity k [W/(m·K)]	0.492	314	429
Thermal expansion coefficient $\alpha \times 10^{-5}$ [1/K]	0.18	1.4	–
Electrical conductivity σ [S/m]	0.667	4.10×10^7	–

NPs reduces the flow velocity, while parameters such as thermal radiation and Biot number significantly influence the temperature profile. These parameters can be related to the diffusive behavior and thermal distribution of the drug in the blood. The approach highlights the importance of multiphysics modeling in predicting the efficacy of intravascular drug delivery, and suggests that metal NPs may improve localization and tissue penetration in specific regions.

The results show that increasing the magnetic parameter M, which represents the intensity of the applied magnetic field, induces a decrease in the velocity of the nanofluid (blood + NPs). This effect is due to the Lorentz force, which acts as a resistance to the flow. The behavior is consistent both in the case of gold and silver NPs, and is particularly relevant for applications in magnetically assisted drug delivery, where the drug localization can be controlled by reducing the flow in certain regions.

This fact is visible in the graph 3.4. Figure shows the velocity profile f' as a function of the similarity variable η, for the blood-based nanofluid containing the metal NPs, in the cases of stretching and shrinking of the lamina. The curves are plotted for different values of the magnetic parameter ($M = 0.5$, 1.0, 1.5), with the aim of highlighting the influence of the magnetic field on the flow. The solid lines represent the stretching case, while the dashed lines correspond to the shrinking condition. It is observed that as M increases, the braking effect of the magnetic field tends to reduce the fluid velocity, making the profile f' less steep. Furthermore, a difference is noted between the two types of NPs: the suspensions with Au show a higher intensity of the profile than those with Ag, suggesting a different influence of the thermophysical properties of the two metals on the fluid dynamics. Overall, the graph confirms that both the nature of the NPs and the intensity of the magnetic field play a determining role in the behavior of the laminar flow.

Although the magnetic field studied in the present work is idealized and used in a magnetohydrodynamic context, it is interesting to hypothesize a connection with magnetic resonance imaging. In particular, the application of high-intensity static magnetic fields, as occurs in MRI, could locally influence the flow of conductive nanofluids, modifying their distribution. This opens potentially interesting scenarios for magnetic field-assisted drug delivery, in which the clinical magnetic environment, in addition to allowing imaging, could be exploited to guide or slow down the diffusion of the drug in specific regions.

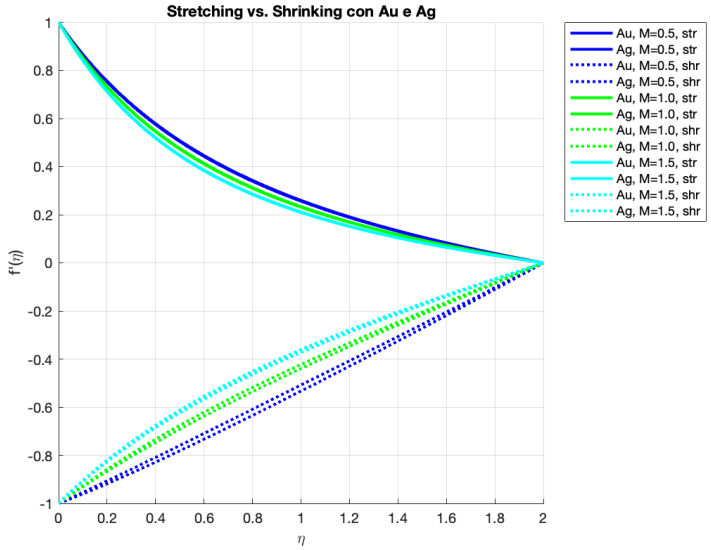

Figure 3.4: Curves of magentic parameter (M) vs velocity profile (f') [86].

Another relevant example is that of Gharehdaghi et al. [26] and represents an application of the Higuchi model (chapter 2). In this work the induction of apoptosis is proposed as the main the mechanism in most anticancer drugs.

In recent years, the integration of therapeutic and diagnostic functionalities in nanomaterials has led to the development of theranostic systems, capable of combining controlled drug release and real-time monitoring via medical imaging. A promising example is represented by magnetic metal-organic frameworks (MOFs), which combine high loading capacity, stimuli responsiveness and MRI contrast.

In the work of Gharehdaghi et al., a composite based on Fe_3O_4@Cu-BTC was developed, where:

- Fe_3O_4 provides the magnetic properties for T_2-weighted MRI imaging.
- Cu-BTC (HKUST-1) acts as a porous matrix for loading and releasing doxorubicin (DOX).
- The system is pH-sensitive: it releases the drug preferentially in acidic environment, typical of tumor tissues.

The efficiency of the contrast agent is expressed by the cross-sectional relaxivity r_2, defined as:

$$r_2 = \frac{1}{T_2 \cdot [\mathrm{Fe}]} \tag{3.10}$$

where T_2 is the relaxation time and [Fe] the iron concentration.

In the analyzed work, a value of $r_2 = 137.6\,\mathrm{mM}^{-1}\mathrm{s}^{-1}$ was obtained, higher than those of clinical agents (ferumoxsil ~ 72, ferumoxide ~ 98.3), suggesting a much more marked MRI response and a potential for real-time monitoring of tumor distribution.

The system was tested at three representative pHs:

pH	**DOX release after 48h**
5.0	83.2%
6.5	60.3%
7.4	30.5%

The release profile was modeled with the Higuchi equation:

$$\frac{M_t}{M_\infty} = K_h t^{\frac{1}{2}} \tag{3.11}$$

with correlation coefficient $R^2 = 0.969$, indicating a non-Fickian diffusion-controlled release.

The DOX@Fe_3O_4@Cu-BTC system showed much lower IC_{50} than free DOX:

Sample	**IC_{50} HeLa** (μg/mL)	**IC_{50} MCF-7** (μg/mL)
Free DOX	17.7	18.0
DOX@MOF	4.45	6.8

The system also proved to be less toxic towards healthy cells (3T3), demonstrating tumor selectivity.

The Fe_3O_4@Cu-BTC nanocomposite has been shown to be an effective candidate for the simultaneous treatment and monitoring of neoplasms, thanks to:

- high MRI efficiency (high r_2),
- pH-dependent release,
- low toxicity on healthy cells.

These results pave the way for the clinical use of magnetic MOFs in precision oncology.

The values of T_2 as a function of iron concentration, although not represented graphically in the article, were reconstructed on the basis of the definition of relaxivity r_2, obtaining a linear curve with a slope equal to 137.6 $\text{mM}^{-1}\text{s}^{-1}$, consistent with the declared results.

The graph 3.5 shows the trend of the transverse relaxation rate $\frac{1}{T_2}$ as a function of the iron concentration [Fe], simulated on the basis of the classical definition of magnetic relaxivity r_2. The simulated data follow a linear behavior, as expected theoretically, and the interpolation by linear regression provides a slope value equal to:

$$r_2^{estimated} = 137.6 \text{ mM}^{-1}\text{s}^{-1} \tag{3.12}$$

this value coincides with that reported in the original work by Gharehdaghi et al., validating the numerical reconstruction.

The physical meaning of this slope is clear: the higher the [Fe] concentration in the medium, the greater the local dephasing effect of the protons, and therefore the shorter the T_2 time (faster decay of the signal). A high value of r_2 therefore indicates a high

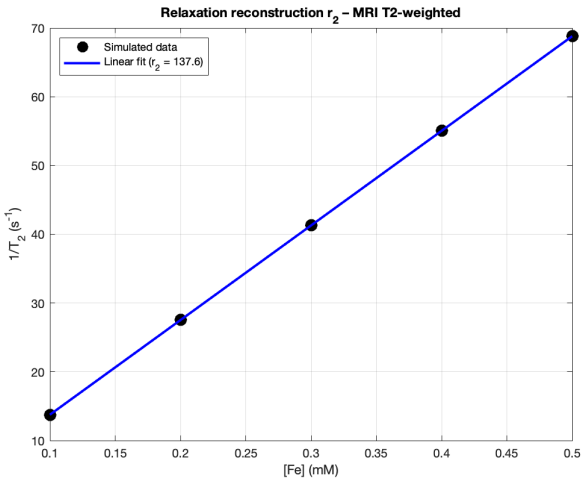

Figure 3.5: Trend of transversal relaxivity r_2 reconstructed from the experimental data reported by Gharehdaghi et al. [26]. MATLAB processing by the author.

efficiency as a T_2-weighted contrast agent, higher even than known clinical products such as ferumoxsil and ferumoxide.

From the application point of view, this parameter is fundamental for the in vivo monitoring of the vector and allows to follow the distribution and tumor accumulation of the nanocomposite by magnetic resonance, confirming the dual therapeutic and diagnostic function of the magnetic MOF system.

3.3 Applications of MRI-DWI

Granata et al. [28] present a very significant application: they conducted a study to test a new class of targeted agents, specifically bevacizumab. This chemotherapy drug has several different mechanisms of action that result in inhibition of new vessel growth, regression of newly formed tumor vasculature, normalization of tumor blood flow, and direct effects on tumor cells.

Diffusion weighted imaging (DWI) (for more information see chapter 2) is a magnetic resonance imaging (MRI) technique that is sensitive to the motion of water molecules in tissues. It provides a quantitative measure called apparent diffusion coefficient (ADC), which represents a global parameter of diffusion, influenced by both actual tissue diffusion and microvascular perfusion, variations in the microstructure of the implant (e.g. porosity, viscosity, degradation) modify the molecular mobility and are reflected in the parameter.

To separate these contributions, the intravoxel incoherent motion (IVIM) model was introduced, which uses a DWI sequence with multiple b (diffusion gradient intensity) values and fits the signals with a bi-exponential function.

The ADC calculation is based on the Stejskal-Tanner equation:

$$\text{ADC} = \frac{1}{b} \ln \left(\frac{S_0}{S_b} \right) \tag{3.13}$$

$$S(b) = S_0[f_p e^{-bD_p} + (1 - f_p)e^{-bD_t}] \tag{3.14}$$

Where:

- D_t is 'true' (tissue) diffusion.
- D_p: is pseudorandom diffusion associated with capillary flow.
- f_p is perfusion fraction (blood volume per unit of tissue).
- $f_p D_p$ is proxy for microvascular blood flow.
- ADC is apparent mean (not deconvoluted) of the entire signal.

In the study, 25 patients with liver metastases from colorectal cancer underwent MRI with multi-b DWI (values of b from 0 to 800 s/mm^2). The protocol allowed to obtain:

- Global ADC: calculated with two points ($b = 0$ and $b = 800$).
- IVIM parameters: D_t, D_p, f_p, and $f_p D_p$ obtained by nonlinear bi-exponential fitting.

The comparison was performed before and after the administration of bevacizumab, an anti-angiogenic monoclonal antibody.

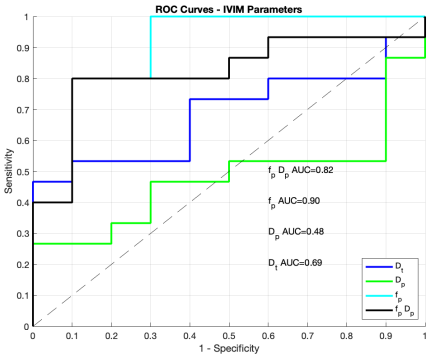

(a) ROC curves of IVIM parameters. The parameter $f_p D_p$ shows the best discriminating ability (AUC = 0.76), followed by f_p (AUC = 0.70).

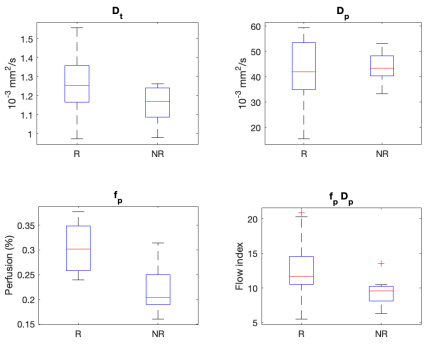

(b) Boxplot of IVIM parameters in responder (R) and non-responder (NR) patient groups.

Figure 3.6: MATLAB simulations. Graphs made by the author based on Granata et al. [28].

Figure 3.6a shows the ROC curves of the four IVIM parameters. Among them, $f_p D_p$ is the one with the best diagnostic ability, with an area under curve (AUC) of about 0.76, followed by fp (AUC $\approx$ 0.70). The parameters D_t and D_p show AUCs lower than 0.65.

These results confirm what was observed in the original work: the parameters related to microvascular perfusion are more correlated with the early response to anti-angiogenic treatment. In particular, f_p reflects the reduction of vascularization induced by the drug, while f_pD_p represents an indicator of the residual microcirculatory flow

Figure 3.6b shows the boxplots of the parameters D_t, D_p, fp and f_pD_p in the two groups of patients: responders (R) and non-responders (NR) to anti-angiogenic treatment with bevacizumab. The data were simulated starting from the means and standard deviations reported in the work of Granata et al., in order to verify their distribution and compare their visual significance. Among the parameters analyzed, the perfusion fraction fp is significantly higher in responder patients. Also the product f_pD_p, considered a surrogate indicator of flow, shows a clear difference between the groups. On the contrary, the parameters D_t and D_p show overlap between R and NR, confirming their lower discriminating capacity.

In the work, the most sensitive parameter to the response to treatment was found to be f_p, since bevacizumab acts on angiogenesis and therefore modifies perfusion early, even before the morphological variation.

- Boxplots and t-tests show a significant reduction in f_p and f_pD_p after treatment in responders.
- ROC curves show that: f_p AUC $= 0.70$, f_pD_p AUC $= 0.76$, high specificity ($\sim$90%) for both.
- No significant changes in D_p or D_t between responders and non-responders.

This study demonstrates the utility of DWI-derived IVIM parameters in the early assessment of therapeutic response. In particular, microvascular perfusion (f_p) and flow (f_pD_p) were shown to be sensitive indicators of response to bevacizumab, confirming the biological rationale of anti-angiogenic treatment. The simple ADC parameter, although useful, is less specific in this context.

Some problematics are the sample size of the lesions and, even more, of the patients in our series was small. Respiratory artifacts may have an impact on the images evaluation.

For analysis, a region-of-interest (ROI) approach was used. Median signal values from individual voxels within each ROI were calculated for every b-value to improve signal-to-noise ratio and reduce fitting errors. Tumor ROIs were manually delineated by an experienced radiologist (14 years of experience), focusing on hyperintense regions at $b =$ 800 s/mm. ROIs were carefully drawn to exclude areas affected by motion artifacts or blurring, though no automated motion correction algorithms were applied.

The main parameters derived from IVIM-DWI analysis were simulated and compared in patients affected by liver metastases from colorectal carcinoma treated with bevacizumab. Patients were classified into two groups: *responder* (R) and *non-responder* (NR).

Among the analyzed parameters, f_p and f_pD_p are significantly higher in responders than in non-responders. The ROC curves show that f_pD_p is the best discriminator of early therapeutic response, in agreement with what was reported in the work.

In Situ forming implants (ISFIs) represent a promising strategy for controlled drug delivery. These systems are injected as a liquid solution containing a biodegradable polymer (e.g. PLGA) and a drug, and solidify in situ through a solvent/nonsolvent phase inversion process, forming a solid depot with sustained release.

However, understanding the release mechanism and diffusional properties within the implant is complex and often invasive. The study by Hopkins et al. [32] proposes the use of diffusion-weighted MRI (DWI) to non-destructively and non-invasively characterize the spatial and temporal variations of apparent diffusivity within ISFIs.

In the analyzed work, two types of ISFI implants were studied, both based on PLGA but with different molecular weight (15 kDa vs. 52 kDa). DWI was used to:

- Create spatial maps of diffusivity (ADC) inside the implant.
- Monitor mean diffusivity (MD) over time both globally and in polymeric regions only.
- Correlate DWI maps with microstructure (SEM), drug release, erosion and degradation.

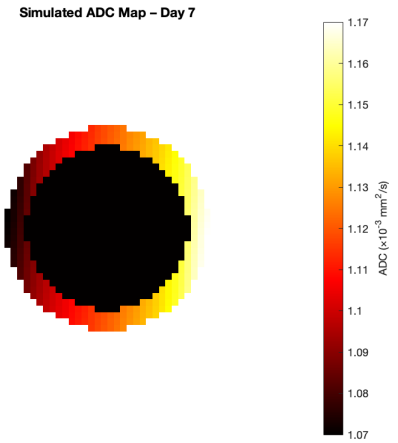

Figure 3.7: ADC map simulation in an ISFI, day 7. MATLAB processing by the author.

Results showed:

- A constant diffusivity in the outer shell of the implant ($\sim 1.17 \times 10^{-3}$ mm^2/s).
- A progressive increase of diffusivity in the inner core from 0.26×10^{-3} to 1.88×10^{-3} mm^2/s in 14 days.
- A spatial transition visible as a ring of high diffusivity (shell-core transition) between 2 and 6 days.

The MRI-DWI approach therefore allows to monitor: the burst release phase, associated with initially low ADC values in the core but high in the shell; the diffusion release phase, where the core ADC increases with time; the degradation release phase, evidenced by the complete homogenization of the ADC to values similar to the aqueous medium.

This study demonstrates the potential of DWI as a tool for:

- Quantifying intracellular diffusion and interstitial in implantable devices.
- Predict drug release behavior non-invasively.
- Support implant design with customized release profile.

The methodology could be extended to other controlled release systems or preclinical models of intratumoral release, with direct impact on precision medicine.

A ADC map in figure 3.7 was generated using a radial model to describe the ISFI. The central region exhibits lower diffusivity, while the periphery shows higher values, consistent with the experimentally observed profile by Hopkins et al. The transition between core and shell over time reflects the progress of polymer release and degradation.

3.4 Comparison Between Machines and AI

Prolonged MRI acquisition times have driven the adoption of AI-powered deep learning (DL) image reconstruction techniques aimed at accelerating scan workflows while preserving diagnostic image fidelity. These reconstruction algorithms enhance signal-to-noise ratio (SNR), suppress artifacts, and enable significant scan time reductions without compromising image quality.

Leading MRI manufacturers have integrated these DL reconstruction solutions into clinical systems [59]. GE Healthcare offers DL Recon, which facilitates up to a 50% reduction in scan time while improving edge sharpness and noise suppression. Philips incorporates its Compressed SENSE and SmartSpeed DL reconstruction technologies, enabling scan acceleration of up to 66% across various anatomies, with a focus on maintaining spatial resolution and contrast integrity. Siemens Healthineers has implemented its Deep Resolve^{TM} suite-deployed across its entire MRI portfolio-capable of achieving up to 70% scan time reductions. When paired with simultaneous multi-slice (SMS) imaging and parallel acquisition techniques, total acceleration can reach up to 80%. For example, a standard knee protocol on a 3T system that previously required approximately 10 minutes can now be completed in under 2 minutes using DL-enhanced imaging.

In parallel, these vendors are advancing AI-based workflow automation to minimize operator dependency and inter-user variability. GE's AIRTM Workflow integrates intelligent patient positioning and coil selection, reducing setup time and standardizing exam preparation. Philips' SmartWorkflow^{TM} automates patient isocenter alignment, protocol selection, and planning key steps in reducing scan variability. Siemens' myExam Companion^{TM} leverages rule-based and AI-driven logic to guide users through exam setup, optimize scan parameters, and deliver real-time adaptive instructions, including automated breath-hold guidance when necessary.

These systems are increasingly capable of automating complex decision points such as slice prescription, protocol matching, and timing synchronization. By integrating AI into both image acquisition and operational workflow, OEMs are significantly enhancing throughput, reproducibility, and consistency in clinical MRI practice.

AI-powered synthetic contrast CT methods allow the generation of contrast-enhanced images from non-enhanced scans, reducing the need for intravenous contrast agents. This has strong implications for drug diffusion studies, as it enables indirect visualization of vascular and tissue permeability without direct drug administration. The integration of AI in radiology, including MRI and CT, facilitates high-resolution, low-dose imaging and may help quantify or simulate drug-related contrast enhancement in tissues. These advancements could enhance computational models of drug diffusion by providing richer, real-time anatomical and perfusion data.

Chapter 4

Discussion

This part will try to give a more discursive overview of the problem, also integrating an interpretation of the case studies in the results section.

4.1 New Era: On-demand and Nanomedicine

In the last decades, long-acting controlled release systems, including smart and on-demand release [51], have represented a major evolution in drug delivery, especially for the treatment of chronic diseases. Unlike passive release techniques, which feature predefined temporal profiles and limited spatial control, smart drug delivery systems offer advanced spatiotemporal resolution, allowing for targeted and personalized drug release. These systems are designed to respond to endogenous stimuli such as pH, concentration gradients, enzymes, or the EPR (enhanced permeability and retention) effect or exogenous ones, such as electric, magnetic, electromagnetic fields, temperature variations, or ultrasound.

Among exogenous mechanisms, electric fields have been widely explored to activate both invasive and non-invasive drug delivery systems (DDS). In particular, conductive polymers, capable of volumetric expansion or contracting in response to redox processes, have proven effective in modulating drug release. For topical or transdermal application, however, techniques such as electroporation and iontophoresis have shown considerable potential. Electroporation allows for temporary permeabilization of cell membranes, while iontophoresis which is based on electromigration and electroosmotic flow is particularly suitable for small molecules.

Numerous studies have demonstrated its clinical efficacy for various indications, including the transdermal administration of heterogeneous drugs such as lidocaine (local anesthetic), fentanyl (opioid analgesic), and acyclovir (antiviral), and even for the ophthalmic administration of corticosteroids. More recently, iontophoresis has also shown promising applications in the treatment of solid tumors, such as pancreatic and breast tumors.

Another emerging approach is represented by low-intensity alternating electric fields, known as tumor treating fields (TTFs). This non-invasive technique interferes with the

mitosis process of tumor cells, inducing selective apoptosis of rapidly dividing cells, without affecting quiescent ones. TTFs have demonstrated significant clinical efficacy in the treatment of glioblastoma multiforme and represent a potential synergistic strategy to be integrated with controlled DDS.

The use of magnetic fields in controlled drug delivery systems represents a particularly promising strategy, especially in the oncology and transdermal fields. Static or low-frequency magnetic fields, generated by permanent magnets or electromagnets, have been successfully used to trigger the mechanical deformation of polymeric matrices or liposomes containing active ingredients. A relevant example is the engineering of liposomes loaded with chemotherapeutic drugs and functionalized with chains of magnetic nanoparticles. When exposed to a low-frequency alternating magnetic field (10 kHz), the vibrations induced by the chains cause the controlled rupture of the liposomal membrane, releasing the drug directly into the tumor site. This approach allows for localized release and significantly reduces systemic side effects.

In addition to oncology applications, magnetic fields have also been explored for transdermal drug delivery, through a technique known as magnetophoresis. In this case, a static magnetic field (<450 mT) applied to the skin surface promotes the transport of hydrophilic diamagnetic molecules through the stratum corneum, even without a net electric charge. Unlike techniques based on electric fields, such as iontophoresis, the transport does not depend on the polarity of the drug, nor does it disturb the ionic charges already present in the tissues, making it a safe and non-invasive method for a wide range of molecules.

However, the efficacy and versatility of magnetically activated DDS are limited by several technological factors. First, the generation of magnetic fields strong enough to activate the systems in depth requires the use of bulky and expensive coils or magnets, which limits portability and often requires the presence in equipped hospital environments. This condition compromises the full *on-demand* potential of the system, preventing its use at home or on the move with all the problems can be connected but also many advantages.

Recent research has therefore focused on high-frequency magnetic fields (>20 kHz), which can generate localized heat in magnetic particles through different mechanisms (hysteresis losses, Néel or Brown relaxations). This heating can be exploited to trigger thermal release of the drug, for example through the contraction of thermoresponsive hydrogels or the controlled fusion of polymeric membranes. These strategies, in addition to promoting release, can be combined with hyperthermic therapy for the destruction of tumor tissue.

Despite its potential, this technology presents significant challenges in terms of safety and process control. To date, there is no direct method to monitor in real-time the temperature reached by magnetic NPs inside the body. This requires the adoption of very accurate open-loop control systems, capable of avoiding overheating of surrounding tissues and the induction of unwanted side effects. To reduce the risk of necrosis or thermal damage, particles can be engineered to have a predefined Curie temperature, beyond which they lose their magnetic properties, automatically stopping heating.

Another critical issue concerns the stability of the active ingredients. Not all drugs

tolerate the high temperatures generated locally: proteins, enzymes and vaccines are particularly sensitive to heat, which can denature their structure and compromise their efficacy. Furthermore, even in the absence of the stimulus, passive release of the drug by diffusion can occur, with potential off-target effects.

From an application point of view, numerous in vitro studies have shown precise and reproducible release profiles. However, translation in vivo remains an open challenge, since the biological environment introduces complex variables that can compromise the efficiency, specificity and safety of the system. In addition, there are further fundamental considerations, such as the biocompatibility and biodegradability of the materials used, the useful life of the system (i.e. its effective cycle life, determined by the frequency and stability of activations, and by the amount of drug per cycle), and the possibility of scaling up production for large-scale clinical applications.

Finally, the use of magnetic and electromagnetic fields in the clinical setting must take into account possible interference with implantable medical devices, such as pacemakers or neurostimulators, which could be negatively affected by the signals generated to activate the DDS and may also prevent other therapy-related examinations.

Nanomedicine [8, 83] represents an innovative and increasingly relevant approach in clinical pharmacology, thanks to the possibility of delivering drugs in a targeted and controlled manner to specific body districts. NPs in particular liposomes, polymers, and inorganic NPs are designed to modify the pharmacokinetics of drugs, prolonging their systemic circulation, improving their stability, and reducing their systemic toxicity.

One of the key principles on which oncological nanomedicine is based is the EPR effect, which allows NPs to preferentially accumulate in tumor tissues due to the anomalous permeability of capillaries and inefficient lymphatic drainage. However, as demonstrated by numerous clinical studies analyzed by Man et al. [47], the intensity of the EPR effect is highly variable between patients and even between lesions within the same patient, making an individual assessment of drug distribution necessary.

To this end, the use of molecular imaging techniques (PET, SPECT, MRI) has allowed to directly quantify the biodistribution of nanoparticles and, in some cases, the release of the drug in tissues. For example, studies with liposomes radiolabeled with ^{111}In or ^{99m}Tc have shown visible tumor accumulations up to 7 days after administration, demonstrating prolonged retention times and a high variability between subjects. The clinical study with [64Cu]MM-302, a PEGylated liposome containing doxorubicin and labeled with copper-64, has quantified the amount of drug accumulated in the metastases of patients with HER2-positive breast cancer, revealing a poor correlation with blood concentration, but a potential correlation with therapeutic response. The use of superparamagnetic iron-based NPs (Ferumoxytol) in magnetic resonance imaging has provided an alternative means to assess tumor penetration, paving the way for the development of companion diagnostics.

These approaches allow not only to map the spatial diffusion of the drug in the human body, but also to evaluate the percentage of dose absorbed in the target tissues, with the possibility of customizing the treatment based on the actual tissue exposure. In this sense, nanomedicine is configured as an ideal platform for the application of quantitative imaging in the assessment of drug diffusion.

4.2 Artificial Intelligence: Personalized Medicine

Artificial intelligence (AI) [8] has revolutionized the medical field, radically transforming the way drugs are discovered, developed and administered. Personalized medicine which aims to provide tailored treatments based on the genetic, phenotypic and environmental profile of the patient benefits greatly from the predictive, analytical and generative capabilities offered by AI algorithms.

AI technologies allow us to address individual biological complexity with an unprecedented level of precision and speed. In literature there are many articles that talk about artificial intelligence, a very useful tool in this field nowadays but also controversial and at the center of many discussions. A very significant aspect is that AI is applicable to the vast majority of aspects of this scenario but not only. In figure 4.1 there is a diagram that represents the application of AI to drug development demonstrating the wide potential for use.

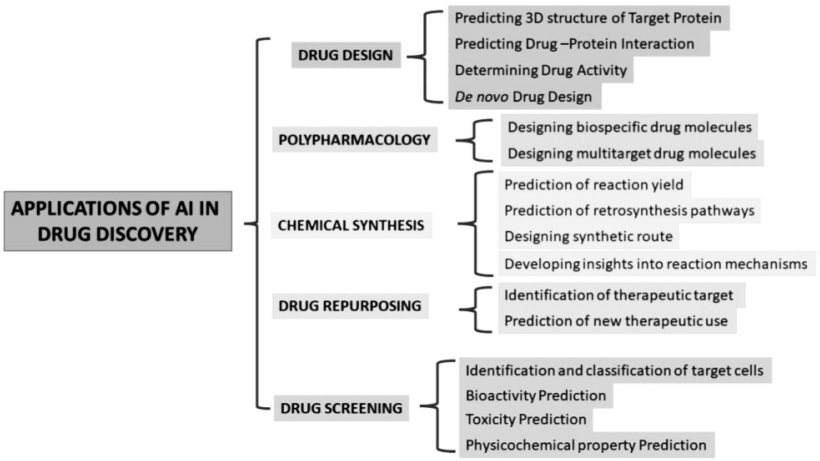

Figure 4.1: Applications of AI in drug duscovery. Diagram made by Visan et al. [84].

The current era of big data [66] is marked by an extraordinary volume and variety of digital information, transforming how we collect, analyze, and interpret data to support decision-making across numerous fields. This transformation is especially evident in medical imaging, where there's a growing trend of combining data from multiple centers and imaging systems to conduct high-impact research, and Seoni et. discuss this in depth.

Integrating data from diverse sources in medical imaging is essential for demonstrating the generalizability and applicability of specific methods across different datasets. Additionally, including a wider and more varied sample population enhances the statistical power of studies, making it possible to detect smaller but clinically meaningful effects.

However, a major challenge in multi-center and multi-device studies - those involving two or more imaging centers or systems - is the presence of unwanted variability in the images. This variability includes differences in image intensity, coding formats (such as uint8 or int16), pixel spacing, and other factors that may affect the consistency and comparability of the data. These discrepancies often stem from variations in imaging

protocols, hardware configurations, and environmental conditions.

Reducing this unwanted variability is critical to ensuring reliable and consistent outcomes, particularly when utilizing AI systems for analysis. AI-based methods have demonstrated increasingly strong performance across a wide range of tasks in medical image analysis. These include core applications such as image segmentation and classification, as well as broader uses like supporting drug therapy decisions. By leveraging large datasets and complex algorithms, AI systems can identify patterns and insights that may not be easily detectable by human experts, ultimately contributing to more accurate diagnoses and personalized treatment strategies.

Image harmonization techniques in medical imaging can vary widely depending on the clinical context and the imaging modalities involved. These methods are essential for aligning and standardizing images obtained from different sources, ensuring they are comparable and suitable for analysis - especially in multi-center or multi-device studies.

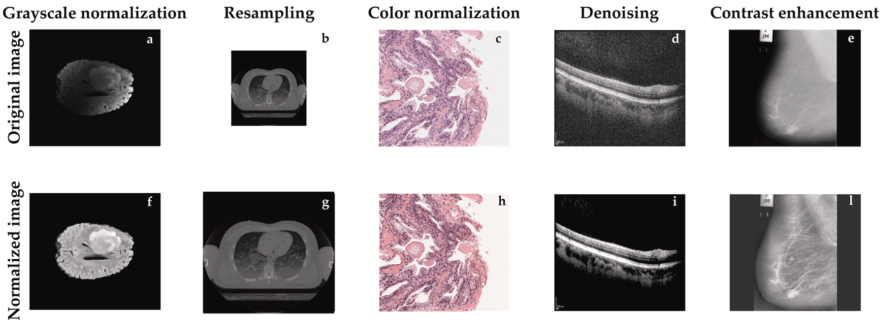

Figure 4.2: Examples of images resulting from data preparation approaches in healthcare: (a, f) grayscale normalization in MR, (b, g) resampling in CT, (c, h) color normalization in digital pathology, (d, i) noise reduction in OCT, (e, l) contrast enhancement in mammography. These images were collected by Seoni et al. [66].

Most image harmonization approaches can be grouped into five main categories and in the figure 4.2 there are some examples reported by Seoni et al.

- Grayscale normalization. This technique standardizes the intensity levels of grayscale images to ensure consistent brightness and contrast across different devices or acquisition settings. This facilitates fair comparison and accurate analysis of image features.

- Resampling. These methods involve adjusting the spatial resolution of images through scaling, resizing, or interpolation. Resampling ensures consistent image dimensions and spatial properties, improving alignment and compatibility between datasets.

- Color normalization. Applied primarily in color imaging modalities, this approach standardizes color appearance across images taken under varying lighting conditions or using different color representations. It helps maintain consistency in color-based features, improving interpretability and analysis.

- Denoising. Denoising techniques are used to reduce unwanted noise or artifacts in images, enhancing overall image quality. This makes it easier to extract meaningful features and improves the accuracy of image interpretation.

- Contrast enhancement. These methods adjust contrast levels to make anatomical structures or abnormalities more distinguishable. Enhanced contrast helps reveal subtle details, supporting more effective visual assessment and analysis.

These harmonization strategies are vital for ensuring consistency, comparability, and quality in medical images, particularly when dealing with data from multiple sources. They play a key role in enabling AI models to perform reliably and accurately by minimizing irrelevant variability. By focusing the AI system on clinically meaningful differences rather than technical inconsistencies harmonized images support more robust diagnoses and advance research outcomes in healthcare applications.

Nowadays, it is important to have the ability to create something personalized for each specific patient, something tailored made [1, 8, 86]. This is to educe the risk of adverse effects to improve patients' quality of life.

Recent advances in medical imaging have facilitated the acquisition of patient-specific characteristics of the intratumoral microenvironment. When integrated with multiphysics modeling, these imaging-derived features enable the simulation and optimization of drug delivery protocols both prior to and during treatment. Multiphysics models employ a system of governing equations to represent the complex processes involved in drug transport and interaction within the tumor. By utilizing individual tumor properties extracted from diagnostic medical images as input parameters, these models can predict drug delivery outcomes and therapeutic responses under various administration scenarios. This approach supports the timely and cost-effective optimization of treatment strategies, which is often impractical through conventional clinical practice [8].

Advances in medical imaging and image processing have emerged as powerful tools for deriving patient-specific parameters, which can be integrated into computational models to enhance their predictive capabilities. In particular, image-based computational modeling has gained significant attention for its role in simulating drug delivery mechanisms. This approach has opened new avenues for personalized medicine, enabling more accurate and individualized treatment predictions.

The adoption of AI in the medical field dates back to the 1950s [84], with the development of the first expert systems (e.g. DENDRAL, MYCIN). In the following years, with the advent of machine learning (ML), deep learning (DL) and natural language processing (NLP), applications have extended to diagnosis, assisted surgery, clinical data management and, more recently, precision medicine.

Machine learning uses computational algorithms to make predictions from pools of data and learn patterns and it is used to predict drug properties, identify potential drug candidates, and optimize chemical structures. Deep learning is used to analyze large-scale biological data, predict drug properties, and identify potential drug candidates. In addition to these, there are many other techniques summarized in the table 4.1.

AI enables the analysis of large amounts of multi-omics (genomics, proteomics, metabolomics), clinical and epidemiological data to predict individual response to treatments.

Table 4.1: Artificial intelligence techniques used in drug discovery and development [84].

AI Technique	**Application in Drug Discovery and Development**
Supervised Learning (SL)	Classification of active/inactive compounds, prediction of ADMET properties, toxicity profiling. Includes methods such as linear regression, logistic regression, decision trees, support vector machines (SVM), random forests, and neural networks.
Unsupervised Learning (UL)	Clustering of chemical structures or biological data, dimensionality reduction, pattern recognition in omics data. Includes techniques such as k-means, hierarchical clustering, PCA, and t-SNE.
Deep Learning (DL)	Feature extraction from large and complex datasets such as images, molecules, and genomic sequences. Includes convolutional neural networks (CNNs), recurrent neural networks (RNNs), and graph neural networks (GNNs).
Reinforcement Learning (RL)	Optimization of molecular structures and synthesis routes; used for de novo drug design and lead optimization.
Transfer Learning (TL)	Leveraging pre-trained models on similar tasks to improve performance with small datasets; applied in target identification and property prediction.
Generative Models (GM)	Generation of novel drug-like molecules with desired properties. Includes variational autoencoders (VAEs), generative adversarial networks (GANs), and transformer-based models.
Natural Language Processing (NLP)	Extraction of knowledge from scientific literature and patents; identification of drug-disease relationships and named entity recognition (NER).

Main applications include the use of ML algorithms to analyze biological data and identify proteins involved in specific pathologies and validation through computational simulations, genetic manipulation (knockdown, overexpression), mutagenesis, etc.

Neural networks analyze three-dimensional molecular structures to evaluate the interaction with protein targets, AI technologies (GNN, molecular docking, RL) enable the design of tailored molecules with optimal properties and software such as DeepChem, DeltaVina and ORGANIC supports the entire development cycle. Predictive models for solubility, bioavailability, toxicity and DL algorithms and quantum computing to optimize pharmacokinetics and reduce clinical failures.

AI also finds application in the discovery of new materials for drug delivery (e.g. polymeric nanoparticles). The techniques used include:

- Supervised Learning: linear regression, SVM, CNN, RNN.
- Unsupervised Learning: clustering, PCA, t-SNE.
- Generative Adversarial Networks (GANs): to generate new molecules.
- Reinforcement Learning and Transfer Learning: to optimize processes and reuse

knowledge from pre-trained models.

Multimodal molecular imaging consists of the synergistic combination of different imaging techniques - anatomical, functional, and molecular - to obtain complementary information on the structure, function and distribution of target molecules in biological tissues. Examples include PET/CT, PET/MRI that combine anatomical resolution and functional sensitivity, MSI + Optical Imaging that integrate high-resolution chemical-spatial information, hardware-based that integrated instrumentation (e.g. PET/CT scanner) and software-based that co-registration and fusion of separately acquired datasets (e.g. MSI + optical images).

Despite significant progress, several critical challenges persist in the application of AI to personalized medicine. Data interoperability remains a major hurdle, with difficulties integrating heterogeneous sources such as clinical records, imaging, and genomic data. Equally important is the interpretability of AI models, as transparent and explainable systems are essential for clinical adoption. Experimental validation is also crucial to confirm that in silico predictions translate into real-world outcomes. Furthermore, ethical concerns - ranging from privacy and data bias to medico-legal liability - must be carefully addressed. Nevertheless, the potential of AI in personalized medicine is immense. AI can enable timely clinical decision-making, identify patients most likely to respond to treatment, and optimize therapies to reduce adverse events. Looking ahead, promising innovations include smart multimodal probes that are detectable across imaging modalities, integrated databases that combine clinical, imaging, and genomic data for model training, and *smart* clinical trials with continuous monitoring and outcome prediction. Additionally, developing interpretable AI-human interfaces will be essential to foster trust and ensure transparency in clinical workflows.

The integration of artificial intelligence and multimodal imaging represents a strategic turning point in personalized medicine and in the development of new drugs. From target discovery to the evaluation of therapeutic efficacy, these technologies improve the efficiency, precision and safety of the entire process. Their systematic implementation is destined to define the future of precision medicine, enabling faster, more targeted and personalized treatments.

4.3 Medical Drugs and Children

In pediatrics, the processes of pharmacokinetics (PK) - absorption, distribution, metabolism and elimination of drugs - and pharmacodynamics (PD) [62] undergo substantial changes compared to adulthood, requiring specific and adapted therapeutic management [18, 20]. These differences depend on factors related to physiological maturation, the development of excretory organs and changes in body composition. The age of the pediatric patient is therefore a critical parameter for determining the efficacy and safety of drug therapy.

Considerable overlap exists across pediatric age subcategories [20] in terms of physical, cognitive, and psychosocial development, leading to intrinsic heterogeneity within this population. This variability, coupled with the limited number of pediatric subjects in

clinical trials, has historically resulted in children being labeled as *therapeutic orphans* and the widespread off-label use of adult medications in pediatric patients. The PK and PD of active pharmaceutical ingredients differ significantly between children and adults, making direct extrapolation of adult dosages inappropriate. Factors such as gut function, which varies with age and clinical condition, influence the choice of oral dosage forms, while the selection of excipients requires careful consideration due to potential toxicological risks in children. PK parameters, including area under the curve (AUC), maximum concentration (C_{max}), clearance, half-life, and volume of distribution (V_d), reflect the absorption, distribution, metabolism, and excretion (ADME) processes that differ widely across pediatric subgroups. Variables such as gastric acidity, gastric emptying rates, intestinal surface area, enzyme activity, and organ blood flow further complicate drug absorption and disposition in children. To minimize unnecessary in vivo studies and better predict pediatric drug behavior, alternative approaches like in vitro - in vivo correlation (IVIVC) and physiologically based pharmacokinetic-pharmacodynamic (PBPK-PD) modeling are increasingly utilized. Pediatric drug formulations must address multiple factors, including age-appropriate API dosing, acceptability, palatability, dosing frequency, and cultural preferences. Additionally, despite many excipients being generally regarded as safe, adverse reactions and varying tolerability profiles across different pediatric ages have been reported, highlighting the need for comprehensive data on excipient safety. Initiatives such as the European pediatric formulation initiative (EuPFI) and its STEP (Safety and Toxicity of Excipients for Paediatrics) database aim to fill these knowledge gaps. Emerging technologies like nanomedicine also offer innovative solutions for pediatric treatment across diverse fields, including oncology, infection, dentistry, dermatology, and nutrition.

The anatomical and physiological variables, that strongly influence the process of drug absorption in children, newborns, and infants, are:

- Gastric acid secretion: is reduced in newborns, increasing the bioavailability of drugs that are unstable in an acidic environment (e.g. penicillins), but reducing it for weakly acidic drugs (e.g. phenobarbital).
- Formation of bile salts: still immature, compromises the absorption of lipophilic drugs such as diazepam.
- Intestinal motility and gastric emptying: slowed in neonates, delay the achievement of therapeutic concentration for drugs administered orally.
- Bacterial flora and presence of intestinal enzymes: immature, limit the absorption and local metabolism of some drugs.

Alternative routes of administration, such as transdermal, may lead to greater absorption due to the thinner stratum corneum and the greater body surface/weight ratio. The rectal route is reserved for emergency cases, with variability in absorption related to the site of placement. Finally, pulmonary absorption of inhaled drugs varies less with age, but can be influenced by factors such as the type of delivery and neonatal respiratory conditions.

The volume of distribution of drugs in children is altered by different body composition. In neonates, the higher percentage of total body water requires higher doses (per

kg) of water-soluble drugs. With growth, the reduction in body water requires a recalculation of dosages to avoid toxicity. Lower levels of albumin and plasma binding proteins in neonates increase the amount of free drug in circulation, increasing the risk of adverse effects. In obese subjects, the volume of distribution may be further altered due to the greater fat and lean mass.

Drug metabolism occurs mainly in the liver via the cytochrome P450 (CYP450) enzyme system. In neonates, enzyme activity (phase I) is initially reduced, increases in the first months and may exceed that of adults in the first years for some drugs (e.g. phenytoin, barbiturates). Phase II, which includes conjugation processes, has a variable development: enzymes for the conjugation of bilirubin and paracetamol mature more slowly, while those for morphine are already active in preterm infants. External factors, such as diet and co-administration of other drugs, can induce or inhibit CYP450 activity, altering pharmacokinetics and increasing the risk of drug interactions.

The major route of elimination of drug is renal, which is less efficient in the first months of life. Renal plasma flow at birth is approximately 12 mL/min, reaching adult levels (140 mL/min) by the first year. Glomerular filtration rate increases from 2-4 mL/min at birth to approximately 120 mL/min by 3-5 months. Tubular secretion and protein binding processes are also immature in neonates, affecting renal clearance of drugs.

Pharmacokinetic differences require individualized dosing, often based on body weight, chronological age, and functional maturation of organs. When possible, monitoring plasma concentrations is a more accurate method of therapeutic optimization, although systemic concentration does not always correspond to target site concentration. A recent report revealed that of 103 drugs approved for adult patients, only 19 were approved for pediatric patients [20]. The appendix table 5 contains some clinical trials with their results.

This is what is reported on the European website [37]:

> *Paediatric medicinal products are also specifically regulated (Regulation (EC) No 1901/2006, amended by Regulation (EU) 2019/5) to ensure that they have been tested specially for children in an ethical way, that they meet the needs of children and that they have age-appropriate doses and formulations. Pharmaceutical companies carry out studies on children to obtain evidence about the safety and efficacy of new medicines before requesting marketing authorisation. The EMA's Paediatric Committee assesses those studies and the data generated by them.*

According to the American academy of pediatrics (AAP), the upper age limit of pediatrics is considered 21 years, with a proposed subcategorization [20] of adolescence into three main groups: early, represented by adolescents from 11 to 14 years old; middle, for adolescents with ages between 15 and 17 years old; and late adolescence ranging from 18 to 21 years old. In figure 4.3 there is a scheme of the division.

In children, and particularly in patients younger than 5 years, drug delivery and tissue diffusion represent a significant clinical and technological challenge. The difficulties are due not only to anatomical and physiological limitations (such as organ immaturity,

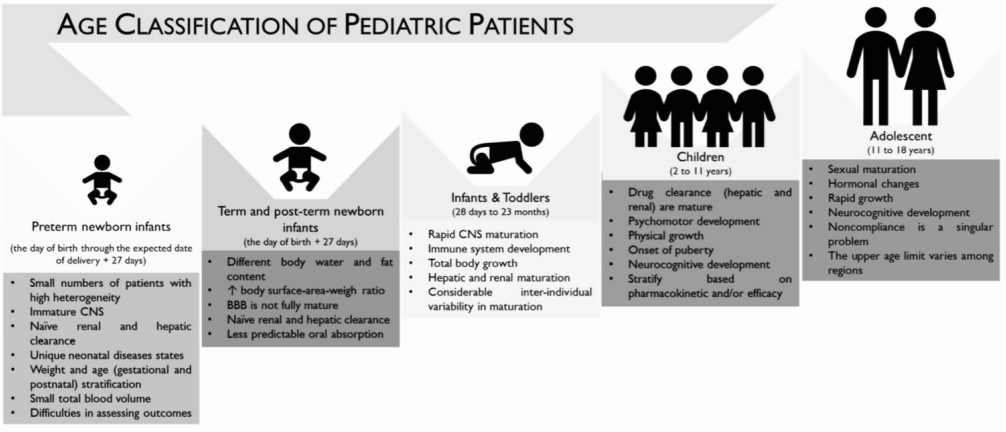

Figure 4.3: Categorization of pedriatric patients by Domingues et al. [20].

different tissue composition, and variability of hepatic and renal metabolism), but also to practical limitations in delivery systems, especially in low socio-demographic conditions.

In the work of Kirtane et al. [39] an innovative oleogel system for oral and rectal drug delivery in children is proposed. Although the work does not directly analyze drug diffusion in pediatric tissues, it offers relevant contributions in this context, in particular the formulations adaptable to pediatric physiology. Oleogels are designed to bypass common problems in children such as difficult swallowing, thus avoiding potentially dangerous solid formulations (e.g. risk of choking). The thermal stability and biochemical compatibility: the formulations are stable up to 40°C and use food oils and gelling agents, proving safe even for immature tissues. Improved absorption and bioavailability: studies in porcine models have shown that the absorption of some drugs (such as azithromycin) was even higher than that of tablet formulations, suggesting effective systemic diffusion from the intestinal or rectal mucosa. Although a direct evaluation of diffusion in the organ parenchyma is lacking, the ability of oleogels to effectively convey drugs of different solubilities (both hydrophilic and lipophilic) indicates a potential application also to reach tissue targets in pediatric age. Furthermore, the association with controlled-dose administration systems (such as multidose applicators) ensures greater precision in the treatment of children, in whom even minimal dose variations can have significant clinical consequences.

A particularly important application of drug diffusion assessment in the pediatric setting is represented by inhalation therapy in asthmatic children. The use of devices such as valved holding chambers (VHCs) has improved the administration and pulmonary deposition of inhaled corticosteroids, reducing oropharyngeal deposition and optimizing local tissue diffusion. As reported by Panda [55], the correct choice of chamber volume and patient respiratory conditions directly influences the drug distribution profile in the pediatric respiratory system. Inhaled drug delivery is one of the most common approaches to treat asthma and wheezing in children. Devices such as spacers and VHCs play a crucial role in drug delivery to the lungs, with direct impacts on drug diffusion to tissue levels.

The article highlights that the use of VHCs with metered-dose inhalers (pMDIs) optimizes drug delivery to the lower respiratory tract without requiring complex respiratory coordination, which is particularly important in children under 5 years of age.

The efficiency of drug diffusion also depends on:

- the volume of the chamber (spacer),
- the particle size,
- the flow turbulence,
- and the child's ability to generate inspiratory pressure.

These factors influence the amount of drug that actually reaches the lung epithelium and can therefore penetrate into the tissues. The effect is distinguished between small volume (100 ml) and large volume (>700 ml) spacers. The former tend to produce an initial burst of aerosol with high concentration but followed by air almost devoid of drug. The latter generate a more uniform distribution of particles during the entire inspiratory cycle, favoring better pulmonary diffusion. Although the article does not directly examine drug diffusion in tissues at the molecular level (as MRI or spectrometry techniques would do), it does offer a clinically relevant model of controlled drug distribution through a technological interface. This is an essential component in the study of pediatric drug diffusion, as it determines local (pulmonary) efficacy and reduction of systemic deposition (e.g. reduced oropharyngeal exposure). The document also highlights the importance of proper technique of use, priming of devices and regular maintenance, all of which indirectly influence the consistency and predictability of drug diffusion in each administration.

4.3.1 Pediatric Medical Imaging

Various imaging techniques, such as MRI, ultrasound, and others, offer no-invasive tools to monitor and quantify drug distribution in tissues in vivo. These techniques are particularly useful in the pediatric setting, where tissue access is limited and patient safety is a priority.

In the pediatric setting, diffusion-weighted imaging (DWI) [15] has been used to assess drug distribution in various organs, including the liver, kidney, and brain. However, the application of DWI in children presents challenges, such as lower signal-to-noise ratio and susceptibility to physiological motion, which can compromise image quality. The adoption of motion compensation techniques and the use of free-breathing or respiratory-triggered sequences have improved the reliability of DWI in pediatric patients.

Perfusion-weighted imaging (PWI) [34] assesses blood flow in tissues, providing information on tissue perfusion and drug distribution. PWI techniques, such as dynamic susceptibility contrast (DSC) and arterial spin labeling (ASL), have been used to study cerebral perfusion in children, contributing to understanding drug distribution in the brain.

The use of gadolinium-based contrast agents improves the visualization of vascularization and tissue permeability. Clinical studies by Hahn et al. [30] have shown that

gadobutrol has a favorable pharmacokinetic and safety profile in pediatric patients aged 2 to 17 years, making it a valid option for assessing drug diffusion into tissues in this population.

Contrast-enhanced ultrasound (CEUS) uses gas microbubbles as contrast agents to improve the visualization of blood flow and tissue perfusion. In pediatric settings, CEUS has been used to assess renal, hepatic, and intestinal perfusion, providing valuable information on drug distribution in these organs [27]. Focused ultrasound (FUS) [8] can be used to increase the permeability of the blood-brain barrier (BBB), facilitating drug delivery to the brain. Preclinical studies have shown that the application of FUS in combination with microbubbles can improve drug diffusion into brain tissue, offering new possibilities for the treatment of pediatric neurological diseases. Sonoporesis [58], or phonophoresis, is a technique that uses ultrasound to increase the permeability of the skin and facilitate transdermal drug penetration. The use of ultrasound frequencies, both high (0.7 MHz) and low (20-100 kHz), has been shown to improve drug diffusion through the skin, making this technique promising for noninvasive drug delivery in children. Multispectral optoacoustic tomography (MSOT) [49] combines optical and ultrasound imaging to provide high-resolution images of drug distribution in tissues. This emerging technique offers the potential to monitor drug pharmacokinetics in children in real-time, improving the understanding of their distribution and metabolism.

Brain tumors are the second most frequent cancers in children, following leukemia. Timely and precise diagnosis is essential to enhance treatment outcomes. So neuroimaging [53] is the answer for this practice and advanced techniques, with the conventional medical imaging of CT and MRI, can help to find tumor characteristics (incidence, location, and type). Nikam et al. provided a detailed account of the techniques used to treat brain cancer in children, many of which have been cited previously and shown in table 4.2.

Pediatric brain tumors represent a heterogeneous group of central nervous system neoplasms. This is why many different techniques are used. The most common of which include gliomas, embryonal tumors, and ependymomas. Gliomas account for nearly half of all pediatric brain tumors and can range from benign low-grade forms, such as pilocytic astrocytoma, to highly malignant high-grade variants like diffuse midline glioma. Embryonal tumors, including medulloblastoma and atypical teratoid/rhabdoid tumor (AT/RT), are aggressive neoplasms that typically arise in the posterior fossa and demonstrate characteristic imaging features such as restricted diffusion and elevated choline peaks on MR spectroscopy. Ependymomas commonly originate from the ependymal lining of the ventricles and can be identified through their typical ventricular location and perfusion patterns. Accurate imaging-based differentiation of these tumor types is critical for diagnosis, treatment planning, and prognostication in pediatric patients.

Non-invasive imaging techniques are a fundamental tool to indirectly assess drug diffusion in human tissues, especially in the pediatric population, where direct approaches are often impractical or risky. In particular, DCE-MRI and DWI-MRI provide quantitative information on perfusion and cellular density, useful for estimating drug penetration and distribution within the tumor or target tissue. These parameters can be used to model tissue pharmacokinetics or to assess response to drug treatment. Similarly, CEUS

Table 4.2: Medical Imaging Approaches for Pediatric Brain Tumors [53].

Imaging Modality	**Description**
Computed Tomography (CT)	Useful for detecting hemorrhage, calcifications, and hydrocephalus. Limited soft tissue contrast compared to MRI.
Magnetic Resonance Imaging (MRI)	Standard structural imaging with excellent soft tissue contrast. Primary tool for diagnosis and monitoring.
Diffusion-Weighted Imaging (DWI)	Evaluates water diffusion; useful for identifying hypercellular tumors and distinguishing tumor grades.
Diffusion Tensor Imaging (DTI)	Measures anisotropic diffusion to visualize white matter tracts; aids in surgical planning.
Functional MRI (fMRI)	Maps active brain regions during specific tasks using BOLD signal; essential for pre-surgical planning.
Resting-State fMRI (RS-fMRI)	Detects intrinsic brain activity and functional networks without requiring patient cooperation.
Arterial Spin Labeling (ASL)	Non-invasive perfusion imaging using magnetically labeled blood water; estimates cerebral blood flow.
Magnetic Resonance Spectroscopy (MRS)	Assesses metabolic changes by detecting brain metabolites such as choline, lactate, and NAA.
Magnetic Resonance Elastography (MRE)	Evaluates tissue stiffness; emerging tool for non-invasive assessment of tumor mechanical properties.
Positron Emission Tomography (PET)	Measures metabolic activity using radiotracers (e.g., FDG); helps detect recurrence and monitor response.
Single Photon Emission Computed Tomography (SPECT)	Functional imaging using gamma-emitting isotopes; less commonly used than PET but still valuable.
Radiomics	Quantitative feature extraction from imaging data to aid in tumor classification and prognosis.
Radiogenomics	Links imaging phenotypes with molecular and genetic characteristics; supports non-invasive *virtual biopsy*.

allows real-time analysis of microvascular perfusion, proving particularly useful in the pediatric setting due to the lack of exposure to ionizing radiation, greater tolerability, and the possibility of serial monitoring. The use of radiolabeled tracers via PET/CT or PET/MRI, although limited by radiation exposure, offers an additional way to assess the systemic distribution and metabolic activity associated with certain drugs, especially in oncology. However, the use of imaging in children requires a balance between diagnostic

efficacy and safety: the sedation required for some techniques (e.g. prolonged MRI) can alter physiology, interfering with drug diffusion dynamics; furthermore, reduced body size and organic development significantly influence the distribution and elimination of the active ingredient. For these reasons, the choice of the most appropriate imaging must consider not only the technical characteristics but also the physiological and pharmacokinetic specificities of the pediatric patient (Frush et al. [25]).

4.3.2 Nanoparticles in Pediatric Pharmacotherapy

Nanoparticles (NPs) [20] represent a strategic innovation in pediatric pharmacotherapy, addressing the numerous unique challenges to treating children, who are not simply *small adults*. Historically, the scarcity of pediatric-specific formulations has led to widespread off-label use of adult medications, posing safety and efficacy concerns.

NP-based drug delivery systems offer tangible solutions by enhancing the oral bioavailability of poorly soluble drugs and enabling administration via more acceptable dosage forms such as suspensions, orodispersible films, and transdermal applications. Encapsulation techniques also allow taste-masking of bitter drugs, thereby improving therapeutic adherence in younger patients. Clinically, liposomal formulations of vincristine and doxorubicin have demonstrated improved pharmacokinetics in pediatric leukemia treatment, while chitosan nanoparticles are being explored for delivering antiepileptics, antivirals, and antibiotics. The recent approval of mRNA vaccines utilizing lipid nanoparticles for children underscores the clinical potential of nanomedicine.

Despite these advances, several obstacles remain. Pediatric-specific clinical data are limited, age-related physiological variability complicates dosing, and regulatory challenges hinder widespread adoption. The long-term effects of NPs on the developing organism are not yet fully understood, necessitating further toxicological and pharmacodynamic studies. Moreover, most preclinical research focuses on adult models and intravenous delivery, whereas oral administration predominates in pediatrics, limiting the translational accuracy of pharmacokinetic assessments. Ethical considerations, such as informed consent and socioeconomic disparities, alongside high costs and insufficient pediatric-focused research, further complicate development. Environmental exposure to NPs and their potential impact on children's health also warrant careful investigation. Given these factors, nanomedicine should be viewed as a complementary tool to existing therapies, offering personalized and safer treatment options within a multidisciplinary framework integrating pharmacology, chemistry, biology, and regulatory science.

Parallel to nanomedicine, advanced therapy medicinal products (ATMPs) - including gene therapies, somatic cell therapies, tissue-engineered products, and combined therapies - represent a transformative frontier in pediatric medicine. Gene therapy approaches, whether ex vivo or in vivo, hold promise for treating genetic disorders, while cell-based therapies harness pluripotent, adult, or cancer stem cells for regenerative medicine, immunotherapy, and cancer treatment. Tissue-engineered products aim to regenerate or replace damaged tissues through substantially manipulated or functionally novel cells. Stem cell therapies can be grouped into three categories: pluripotent stem cells (PSCs), adult stem cells (ASCs), and cancer stem cells (CSCs).

Despite their potential for complete disease remission, ATMPs face significant challenges related to safety, immunogenicity, high development costs, and complex regulatory pathways summarized by the *four As*: authorization, availability, assessment, and affordability. Additionally, pharmacovigilance concerns and limited market incentives impede clinical translation and accessibility. In the figure 4.4 the phases that comprise the creation of a drug are represented.

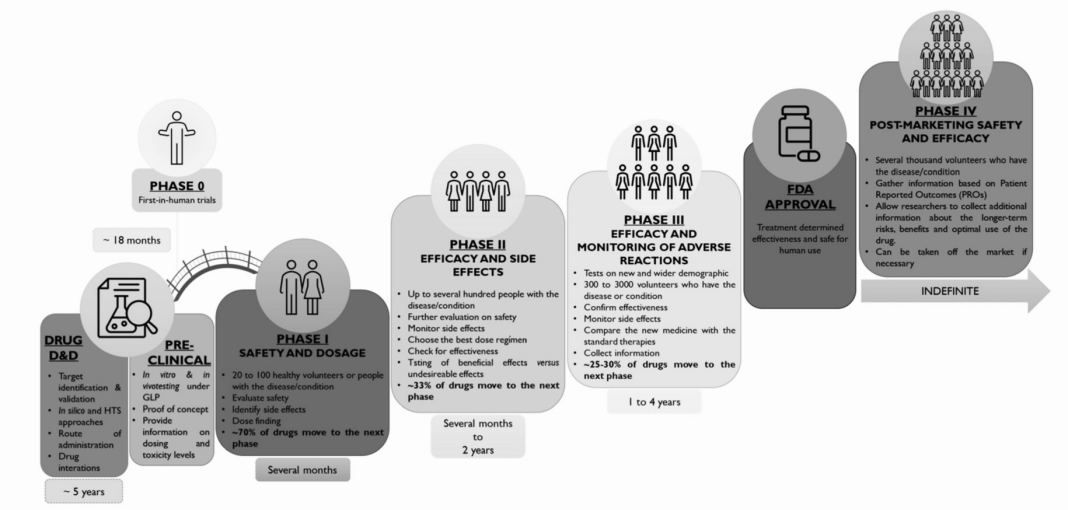

Figure 4.4: Schematic representation of the phases of clinical development of a drug. The process includes several stages: preclinical research and development, clinical trials (Phases 0-III), FDA approval, and post-marketing monitoring (Phase IV). Each phase has specific goals for safety, efficacy, dosing, and monitoring of adverse effects, with a progressive reduction in the number of drugs advancing to subsequent phases. Phase IV continues indefinitely to evaluate long-term safety [20].

Nanomedicine and ATMPs provide promising avenues to overcome these challenges but require coordinated efforts between pharmaceutical developers and clinicians to standardize pediatric formulations within a quality, efficacy, and safety framework. As the field advances, critical questions remain regarding the readiness of healthcare systems, regulatory agencies, and society to embrace personalized pediatric medicine and manage the ethical, economic, and scientific complexities inherent in these innovative therapies.

Pediatric medicine continues to be a hot and challenging topic to be investigated and the role of pharmaceutical developers is undoubtedly crucial in the pre-conception, design, and formulation, to the clinical phase of them, taking into consideration a common international framework established in the trinomial pillars of quality, efficacy, and safety in a fit-by-design perspective.

4.3.3 Racial and Ethnic Differences

In addition to age differences, racial and ethnic differences may arise. Indeed, Marin et al. [48] conducted a research in the emergency departments of some American hospitals between 2016 and 2019 with 13 milion visits consider. They found significant racial

and ethnic disparities in imaging use. Specifically, non-Hispanic white children were significantly more likely to receive at least one diagnostic test (X-ray, US, CT scan, or MRI, was chosen because they are the most common tests) than non-Hispanic black children and Hispanic children. It is also relevant to the above-mentioned fact that the patterns that may appear in these studies are not the same in the pediatric field.

After adjusting for confounding variables such as age, sex, insurance type, diagnosis, and clinical complexity, black and Hispanic children still underwent less imaging than their white peers. Differences were consistent across nearly all diagnostic categories analyzed and even when the analysis was limited to patients discharged from the emergency department. Hypothesized causes include implicit clinician bias, cultural or communication differences, language barriers, and structural inequalities in access to care. These findings suggest that race and ethnicity may independently influence clinical decisions in pediatric emergency settings, with potential implications for both overdiagnosis in white patients and underdiagnosis in minority patients. The study highlights the need for further research and targeted interventions to promote equitable and appropriate use of diagnostic imaging in children.

The Canadian CALIPER study [74] of healthy children (Caucasian, Asian, South Asian, Black) analyzed 52 biomarkers. Most (86%) showed no ethnic differences, but seven biomarkers (including vitamin D, amylase, ferritin, FSH, IgA, IgG, IgM) had significant variations that required ethnicity-specific reference ranges.

A limitation that has arisen in this context is the fact that there are not many specific studies but more on the socio-economic aspect than on the biological level.

4.4 Which One is the Best?

In the field of assessing drug diffusion in human tissues, there is no universally *best* technique, but rather a range of tools with specific advantages and limitations. The choice of methodology strongly depends on the type of drug, the target tissue, the patient population (e.g. adults vs. children) and the clinical objective (diagnostic, therapeutic or experimental).

MRI, particularly in its variants Diffusion Weighted Imaging (DWI) and Dynamic Contrast Enhanced (DCE), is currently one of the most effective techniques to non-invasively assess drug distribution in tissues. It offers an excellent combination of spatial and functional resolution, allowing a quantitative assessment of diffusivity and perfusion. However, access to this technology can be limited by high costs, long acquisition times and the need for patient cooperation, making it less suitable in pediatric or critically ill patients.

Nuclear imaging techniques, such as PET and SPECT, are extremely sensitive and allow precise tracking of radiolabeled molecules even at very low concentrations. They are widely used in oncology research and practice, but have significant disadvantages such as poor spatial resolution, high infrastructural complexity and potential radiotoxicity, a particularly critical factor in pediatric patients.

Ultrasound, especially in its contrast-enhanced variant (CEUS), represents a more accessible and safe technology, particularly suitable for the pediatric field. Although it

cannot compete in terms of anatomical detail or molecular visualization, it offers the advantage of portability and the possibility of real-time acquisitions. Furthermore, techniques such as sonoporation are opening new perspectives for the controlled release of drugs.

Optical techniques, such as optical coherence tomography (OCT), offer exceptional resolution but limited penetration depth, proving useful only in very localized contexts (skin, mucosa, eye). Finally, molecular imaging with fluorophores or bioluminescent agents is mainly used in the preclinical phase on animal models.

In fact, very often the choice is made to adopt an approach that involves combining multiple techniques to be more effective and precise in the therapy. But at this juncture the problem of costs arises, but also of the time needed and of the technologies adopted in the various structures.

From a modeling perspective, pharmacokinetic models provide a simplified but functional picture of the systemic distribution of drugs, while physical-mathematical models based on diffusion and convection laws (Fick, Darcy, Navier-Stokes) allow more accurate simulations in complex tissues but require a high number of parameters and computational capacity. Data-driven models, such as physics-informed neural networks (PINNs), represent a promising frontier for personalization and prediction, although still in the clinical validation phase.

In conclusion, the answer to the question *which is the best?* is necessarily contextual. The most promising trend emerges from the synergic integration of multiple technologies, in which imaging provides experimental data to calibrate advanced computational models. This strategy allows not only to improve the understanding of the diffusion process, but also to build personalized tools for therapeutic planning, especially in delicate areas such as pediatrics, where invasiveness must be minimized and efficacy maximized.

Chapter 5

Conclusion

This work aimed to provide an in-depth review of the methods currently used to quantify drug diffusion in human tissues, with particular attention to clinical and pediatric applications and the integration of physical-mathematical modeling and advanced imaging techniques.

The analysis highlighted how the multidisciplinary approach - which includes pharmacokinetics, thermodynamics, laws of transport physics and magnetic resonance - is essential to understand and predict the behavior of drugs in the human body. In particular, the use of models based on laws such as those of Fick or Darcy, combined with non-invasive technologies such as DWI or DCE-MRI, today represents one of the most promising tools to evaluate the efficacy of drug administration in vivo, but also reveals, at times, related problems and limitations. Consider the chapter on laws and models that explains how simplifications are adopted to make models functional and able to produce results. In this sense, an important help is given by technological and IT progress, specifically by artificial intelligence. This can never replace the personnel in charge but becomes a valid help if used correctly.

However, many challenges remain, especially related to the complexity of biological tissues, interindividual variability and ethical and technical limits, the fear of the advent of new technologies, but also economic problems. In this sense, it has emerged very clearly that combining this multidisciplinarity is very complex and creates interesting challenges for various professional figures. In this context, a starting point for reflections and insights but also new connections to develop the impossible can often be seen. The role of emerging technologies, such as targeted release nanoparticles, nanomedicine that can also become telemedicine to help people who are far away or with limited access to care, is of great interest for the future.

The contribution of this thesis lies in the systematization of the different existing approaches, in the highlighting of the current methodological limits and in the proposal of an integrated vision, useful both in the clinical field and in the design of new therapeutic protocols. Particular importance was given to the problems of pharmacotherapy in pediatric age, a topic also addressed for personal reasons, was supported by significant scientific evidence but revealed many critical aspects, difficulties at a global level and

other facets. Even more relevant is the contribution of artificial intelligence, whose growing computational power and machine learning capacity allow it to increasingly effectively support the entire therapeutic process: from the design and personalization phase of the treatment, to real-time monitoring, up to the early identification of any critical issues in the overall clinical picture. The vastness of the data that can be analyzed, combined with the speed of processing, makes artificial intelligence an essential tool for the evolution of precision medicine and for the continuous improvement of clinical outcomes.

For the future, it will be crucial to develop increasingly personalized models, based on individual clinical data and that combine all the resources available today to create something unique, also accessible at an economic level. Furthermore, it will be essential to strengthen the interaction between computational simulation and real data, thanks to the support of neural networks and predictive algorithms. Only through this integration will it be possible to progress towards precision medicine, truly effective and safe for all segments of the population, including the most fragile patients.

Appendix A: Table

Table 1: Challenges for Each Class of Therapeutic and Delivery Technology Examples [80]

Class of therapeutic	Challenge	Example
Small molecules	Controlling PK parameters	Osmotically controlled-release oral-delivery system of methylphenidate HCl (Concerta)
	Improving solubility	Ritonavir (Norvir), thiazole-modified for improved stability and solubility
	Improving permeability	Benazepril (Lotensin), an alkyl ester prodrug
	Target development	Ezetimibe (Zetia), discovered via library screening
	Reducing off-target toxicity	Naloxegol (Movantik), PEGylated naloxone derivative
Proteins and peptides	Improving physicochemical stability	Desmopressin (DDAVP), with non-natural amino-acid substitution
	Controlling PK parameters	Leuprolide acetate (Lupron Depot), a sustained-release microsphere formulation
	Non-invasive administration	Insulin human inhalation powder (Afrezza)
	Bypassing biological barriers	Semaglutide (Rybelsus), oral GLP-1 agonist with SNAC
	Reducing immunogenicity	Pegademase bovine (Adagen), PEGylated protein
	Improving target selectivity	Belatacept (Nulojix), fusion protein with amino acid substitutions
Antibodies	Controlling PK parameters	Certolizumab pegol (Cimzia), PEGylated antibody fragment
	Improving physicochemical stability	Blinatumomab (Blincyto), lyophilized with trehalose

Continued on next page

Continued from previous page		
Class of therapeutic	**Challenge**	**Example**
	Non-invasive administration	Trastuzumab + hyaluronidase (Herceptin Hylecta), subcutaneous depot
	Bypassing biological barriers	Same as above
	Reducing immunogenicity	Panitumumab (Vectibix), fully human antibody
	Achieving high-dose requirements	Tocilizumab (Actemra), subcutaneous high-concentration delivery
Nucleic acids	Controlling PK parameters	Patisiran (Onpattro), siRNA-lipid nanoparticles
	Improving stability	Fomivirsen (Vitravene), with phosphorothioate modification
	Bypassing cell membrane	Givosiran (Givlaari), GalNAc-siRNA conjugate
	Accessing cytosol/nucleus	Patisiran (Onpattro), enables endosomal escape
	Reducing immunogenicity	Nusinersen (Spinraza), with 2'-O-methoxyethyl modification
	Preventing off-target gene editing	CRISPR-edited $CD34^{+}$ cells for HIV (NCT03164135)
Live-cell therapies	Controlling unpredictable PK	Alginate-based biopolymer implants for CAR T cells
	In vivo persistence	SIG-001, factor-VIII cells in antifibrotic matrix (NCT04541628)
	Reducing immunogenicity	Fludarabine conditioning for CAR T cells (NCT01865617)
	Maintaining phenotype	Sipuleucel-T (Provenge), dendritic cell therapy
	Targeting to disease location	Matrix-induced chondrocyte implantation
	Manufacturing and scale-up	Tisagenlecleucel (Kymriah), CAR T-cell therapy

Table 2: Mathematical models of drug release from microspheres [4]

Mechanism	**System type**	**Condition**	**Main equation**	**Notes**
Diffusion	Reservoir (spherical shell)	C_r costant; perfect sink	$\frac{\partial C}{\partial t} = \frac{1}{r^2}\frac{\partial}{\partial r}\left(Dr^2\frac{\partial C}{\partial r}\right)$	Release through a polymeric shell
	Matrix (dissolved drug)	$C_0 < C_s$	$\frac{M_t}{M_\infty} = 1 - \frac{6}{\pi^2}\sum_{n=1}^{\infty}\frac{1}{n^2}e^{-Dn^2\pi^2 t/R^2}$	Classical Fickian model
	Matrix (dispersed drug)	$C_0 > C_s$	$\frac{M_t}{M_\infty} = 1 - \left(\frac{r'(t)}{R}\right)^3$	Mobile interface between saturated and diffusing zone
Swelling	Empirical model (Korsmeyer)	Abnormal transport	$\frac{M_t}{M_\infty} = kt^n$	$n = 0.43$ (diffusion), $n = 1$ (constant release)
	Movable front model	Front R, S	$\frac{M_t}{M_\infty} = \frac{\sqrt{B}(t_d^*+t_d)}{2l}\left(\sqrt{2\alpha t} + \sqrt{B}t\right)$	Combination of diffusion and dissolution
Erosion	Biodegradable matrices	Chemical degradation	$\frac{\partial C}{\partial t} = D\nabla^2 C - kC$	k represents the degradation of the polymer
Diffusion in tissue	Brain, liver, bone tissue	With local deletion	$\frac{\partial C}{\partial t} = \nabla\cdot(D\nabla C) - k_{\text{elim}}C$	Includes tissue metabolism

Table 3: Main mathematical models for drug release [77].

Model	**Description**	**Application Area**	**Mathematical Formula**
Classical Fick	Based on Fick's diffusion law.	Systems with homogeneous membranes; diffusion-controlled release.	$\frac{dM(t)}{dt} = \frac{ADK}{LV}(M_0 - M(t))$
Higuchi	Release proportional to the square root of time from solid matrices.	Homogeneous, saturated matrices.	$\frac{M(t)}{M_\infty} = \sqrt{D(2A - C_s)C_s t}$
Hixson-Crowell	Considers changes in surface area over time.	Systems where the particle shape evolves (e.g., tablets).	$M_0^{1/3} - M(t)^{1/3} = K_{HC}t$
Peppas (Korsmeyer-Peppas)	Semi-empirical power law model.	Systems with undefined or complex mechanisms.	$\frac{M(t)}{M_\infty} = Kt^n$
Peppas-Sahlin	Combines diffusion and polymer relaxation mechanisms.	Swelling polymeric matrices.	$\frac{M(t)}{M_\infty} = K_1 t^n + K_2 t^{2n}$
Baker-Lonsdale	Extension of Higuchi's model for spherical matrices.	Spherical microcapsules and nanoparticles.	$\left(1 - \frac{M(t)}{M_\infty}\right)^{2/3} + \frac{2}{3}\frac{M(t)}{M_\infty} = Kt$
Hopfenberg	Describes surface erosion-controlled drug release.	Degradable polymeric systems.	$\frac{M(t)}{M_\infty} = 1 - \left(1 - \frac{k_0 t}{C_0 a_0}\right)^n$
Corrigan	Two-phase model: initial diffusion, followed by polymer degradation.	Biodegradable polymers (e.g., PLGA).	$F_{TOT} = F_B + F_{Deg}$ $F_B = F_{BIN}(1 - e^{-k_b t})$ $F_{Deg} = (1 - F_{BIN})\left(\frac{e^{k(t-t_{max})}}{1 + e^{k(t-t_{max})}}\right)$
Weibull	Flexible empirical model; sigmoid/parabolic release curve.	Generic fitting; model comparison.	$\frac{M(t)}{M_\infty} = 1 - e^{-(k(t-t_c))^d}$
Sivak	Experimental model for dual drug release from polyurethane foams.	Dual-drug systems in foams.	$mol_{drug} = \frac{1}{MW}\left[\sum_i 3\left(\frac{m}{V}\right)_i + \left(\frac{m}{V}\right)_j (V_T - 3V_j)\right]$
Pulsatile	Release occurs only during external stimulus.	Smart DDS with on-off activation.	$\begin{cases} C(t) = f(t) & \text{for } 0 < t < k \\ C(t) = 0 & \text{for } k < t < m \end{cases}$

Table 4: FDA-approved lipid-based nanoformulations.

Commercial Name	**Active Agent**	**Indication**	**Approval Year**
Doxil®	Doxorubicin	Kaposi's sarcoma, ovarian cancer, multiple myeloma	1995
DaunoXome®	Daunorubicin	Kaposi's sarcoma	1996
DepoCyt®	Cytarabine	Lymphomatous meningitis	1999
Myocet®	Doxorubicin	Metastatic breast cancer	2000
Mepact®	Mifamurtide	Osteosarcoma	2004
Marqibo®	Vincristine	Acute lymphoblastic leukemia	2012
Onivyde™	Irinotecan	Metastatic pancreatic adenocarcinoma	2015
Vyxeos®	Daunorubicin:Cytarabine (1:5)	Acute myeloid leukemia	2017
Arikayce®	Amikacin	Mycobacterium avium complex infections	2018
Abelcet®	Amphotericin B	Fungal infections	1995
AmBisome®	Amphotericin B	Fungal/protozoal infections	1997

Table 5: Example of completed clinical trials using chitosan in pediatric populations [20].

NCT Number	**Brief Summary**	**Condition**	**Completion Date**	**Results Available**
NCT00707486	HemCon Dental Dressing to stop bleeding during dental surgeries	Tooth Extractions	1 July 2009	Yes
NCT01597817	Textile coated with chitosan for treatment of atopic dermatitis	Atopic Dermatitis	1 Dec 2012	No
NCT01950546	Nanosilver fluoride for control of *S. mutans* in dental plaque	Dental Caries	1 Jan 2015	No
NCT02789033	Isosorbide dinitrate spray and chitosan in diabetic foot ulcers	Diabetic Foot Ulcers	1 Aug 2015	Yes
NCT02668055	Slow-release Tb4 collagen and chitosan sponge for wound healing	Wounds	1 Dec 2015	No
NCT05475444	PLGA nanoparticles coated with chitosan for endodontic infections	Oral Bacterial Infections	15 Mar 2020	No
NCT04365270	Chitosan-modified glass ionomers vs chlorhexidine in primary molars	Caries	5 Jan 2021	No
NCT03421717	Chitosan application for peri-implantitis treatment	Peri-implantitis	8 Apr 2021	No
NCT04906291	Toothpaste with hydroxyapatite vs fluoride in children	Caries	31 Oct 2021	No
NCT04481945	Antimicrobial activity of nanosilver and chitosan sealer	Endodontic Disease	1 Jan 2022	No
NCT04005872	Management of deep carious lesions	Deep Caries	30 Nov 2022	No

Acknowledgements

A mamma. Con la tua forza silenziosa, il tuo amore (e la tua ansia) mi sei stata sempre vicina. Questo traguardo é anche un po' tuo.

A papá. Grazie per avermi fatta testarda. Spero tu possa essere un pochino fiera di me. Mi manchi.

Ai miei nonni. Marisa, Silvana, Giovanni e Giancarlo.

Agli zii. Simona, Francesca e Franco (o meglio Gian Franco).

Alle mie cugine. Agata, Alina, Marta e Sara.

Ad Alice. Fidata ascoltatrice.

Agli altri parenti. Siete troppi e costa stampare queste pagine. :)

Ad Alessia. Sorella che non ho mai avuto. Abbiamo inziato insieme questo inferno e in qualche modo l'abbiamo finito. Grazie per il supporto, la soportazione e per la presenza costante.

A Fiocco (Chiara). Compagna di questo viaggio dall'inizio alla fine.

A Chiara. Compagna di avventure fin dal liceo.

A Lorenzo. Anche se tu non mi hai messo nei ringraziamenti della tua tesi, io lo faccio.

Ad Alessandro. Tu sai.

A Francesca. Piú di una psicologa.

Al professore Umberto Lucia e alla dottoressa Giula Grisolia. Grazie per il tempo che mi avete dedicato e dell'aiuto datomi.

Grazie a chiunque abbia partecipato a questo percorso, se ho dimenticato qualcuno mi scuso.

Alle mie Puzzine. Sempre al mio fianco.

Infine, grazie a me stessa.

Bibliography

[1] Chapter 2 nanoparticles types, classification, characterization, fabrication methods and drug delivery applications. doi:10.1007/978-3-319-41129-3_2.

[2] K. Ammer. The glamorgan protocol for recording and evaluation of thermal images of the human body. *Thermology International*, 2008. URL: https://www.researchgate.net/publication/233420893.

[3] Anonymous. Metalli in medicina 2022-2023 parte 5 radiofarmaci, 2022. URL: https://moodle2.units.it/pluginfile.php/561357/mod_resource/content/1/Metalli%20in%20medicina%202022-2023%20parte%205%20Radiofarmaci.pdf.

[4] Davis Yohanes Arifin, Lai Yeng Lee, and Chi-Hwa Wang. Mathematical modeling and simulation of drug release from microspheres: Implications to drug delivery systems. *Advanced Drug Delivery Reviews*, 2006. URL: 10.1016/j.addr.2006.09.007.

[5] S. et al. Bagavathiappan. Infrared thermal imaging for detection of peripheral vascular disorders. *Journal of Medical Physics*, 2013. URL: https://doi.org/10.4103/0971-6203.48720.

[6] Matteo Baudino. Studio di sistemi per il rilascio controllato di principi attivi da tessuti. Master's thesis, Politecnico di Torino, 2017.

[7] Luca Benci. *La prescrizione e la somministrazione dei farmaci. Responsabilità giuridica e deontologica*. Coppini - Firenze, 2014.

[8] Ajay Bhandari, Boram Gu, Farshad Moradi Kashkooli, and Wenbo Zhan. Image-based predictive modelling frameworks for personalised drug delivery in cancer therapy. *Journal of Controlled Release*, 2024. URL: https://doi.org/10.1016/j.jconrel.2024.05.004.

[9] Marcello Bracale. Gli ultrasuoni, 2002.

[10] Francesco Branciforti, Massimo Salvi, Filippo D'Agostino, Francesco Marzola, Sara Cornacchia, Maria Olimpia De Titta, Girolamo Mastronuzzi, Isotta Meloni, Miriam Moschetta, Niccolò Porciani, Fabrizio Sciscenti, Alessandro Spertini, Andrea Spilla, Ilenia Zagaria, Abigail J. Deloria, Shiyu Deng, Richard Haindl, Gergely Szakacs, Agnes Csiszar, Mengyang Liu, Wolfgang Drexler, Filippo Molinari, and Kristen M. Meiburger. Segmentation and multi-timepoint tracking of 3d cancer organoids from optical coherence tomography images using deep neural networks. *Diagnostics*, 2024. URL: https://doi.org/10.3390/diagnostics14121217.

[11] Kevin M. Brindle and Iain D. Campbell. Nmr studies of kinetics in cells and tissues. *Q Rev Biophys*, 1987. doi:10.1017/s003358350000411x.

[12] Jerrold T. Bushberg, J. Anthony Seibert, Edwin M. Leidholdt, and John M. Boone. *The Essential Physics of Medical Imaging*. Lippincott Williams & Wilkins, 2011.

[13] Jerrold T. Bushberg, J. Anthony Seibert, Edwin M. Leidholdt Jr, and John M. Boone. *The Essential Physics of Medical Imaging*. Lippincott Williams & Wilkins, 2011.

[14] Luisa Camorani. Tecnologie innovative per la diagnosi e la terapia oncologica: Risonanza magnetica ad alto campo e ultrasuoni focalizzati ad alta intensità, 2015 - 2016.

[15] Govind B. Chavhan, Zehour AlSabban, and Paul S. Babyn. Diffusion-weighted imaging in pediatric body mr imaging: Principles, technique, and emerging applications. *Radiographics*, 2014. doi:10.1148/rg.343135047.

[16] José Guilherme de Almeida, Nuno M. Rodrigues, Ana Sofia Castro Verde, Ana Mascarenhas Gaivão, Carlos Bilreiro, Inês Santiago, Joana Ip, Sara Belião, Celso Matos, Sara Silva, Manolis Tsiknakis, Kostantinos Marias, Daniele Regge, and Nikolaos Papanikolaou. Impact of scanner manufacturer, endorectal coil use, and clinical variables on deep learning–assisted prostate cancer classification using multiparametric mri. *Radiology: Artificial Intelligence*, 2025. URL: https://doi.org/10.1148/ryai.230555.

[17] Agenzia Italiana del Farmaco (AIFA), 2025. URL: https://www.aifa.gov.it.

[18] Dott.ssa S. Dell'Orco, Dott.ssa A. Verzino, Dott.ssa V. Cilia, Dott.ssa S. Caruso, Dott.ssa R. Tallarico, and Ing. T. Colizzi. Approfondimento di appropriatezza farmaceutica, 2022. URL: https://www.aslroma6.it/documents/20143/2169514/Approfondimento+n.+24+-+Farmaci+in+Pediatria.pdf.

[19] Nirupama Deshpande, Andrew Needles, and Jürgen K. Willmann. Molecular ultrasound imaging: Current status and future directions. *Nature Reviews Drug Discovery*, 2008. doi:10.1038/nrd2482.

[20] Cátia Domingues, Ivana Jarak, Francisco Veiga, Marília Dourado, and Ana Figueiras. Pediatric drug development: Reviewing challenges and opportunities by tracking innovative therapies. *Pharmaceutics*, 2023. URL: https://www.mdpi.com/1999-4923/15/10/2431, doi:10.3390/pharmaceutics15102431.

[21] Karen A. Esmonde-White, Maryann Cuellar, Bruno Lenain, and Ian R. Lewis. Raman spectroscopy as a process analytical technology for pharmaceutical manufacturing and bioprocessing. *Anal Bioanal Chem*, 2016. doi:110.1007/s00216-016-9824-1.

[22] Karen A. Esmonde-White, Maryann Cuellar, Bruno Lenain, Ian R. Lewis, and Carsten Uerpmann. Raman spectroscopy as a process analytical technology for pharmaceutical manufacturing and bioprocessing. *Anal Bioanal Chem*, 2016. doi:10.1007/s00216-016-9824-1.

[23] Riccardo Fesce and Guido Fumagalli. *Farmacologia Molecolare e cellulare*. UTET, 2018.

[24] Ernesto Freire. Do enthalpy and entropy distinguish first in class from best in class? *Drug Discov Today*, 2009. doi:10.1016/j.drudis2008.07.005.

[25] Donald P. Frush, Michael J. Callahan, Brian D. Coley, Helen R. Nadel, and R. Paul Guillerman. Comparison of the different imaging modalities used to image pediatric

oncology patients: A cog diagnostic imaging committee/spr oncology committee white paper. *Pediatr Blood Cancer*, 2023. doi:10.1002/pbc.30298.

[26] Zahra Gharehdaghi, Seyed Morteza Naghib, Rahmatollah Rahimi, Atin Bakhshi aand Amirhosein Kefayat, Armin shamaeizadeh, and Fatemeh Molaabasi. Highly improved ph-responsive anticancer drug delivery and t2-weighted mri imaging by magnetic mof cubtc-based nano/microcomposite. *Frontiers in Molecular Biosciences*, 2023. URL: https://doi.org/10.3389/fmolb.2023.1071376.

[27] Antonio Granata, Irene Campo, Paolo Lentini, Francesco Pesce, Loreto Gesualdo, Antonio Basile, Vito Cantisani, Matthias Zeiler, and Michele Bertolotto. Role of contrast-enhanced ultrasound (ceus) in native kidney pathology: Limits and fields of action. *Diagnostics*, 2021. doi:10.3390/diagnostics11061058.

[28] Vincenza Granata, Roberta Fusco, Orlando Catalano, Salvatore Filice, Daniela, Maria Amato, Guglielmo Nasti, Antonio Avallone, Francesco Izzo, and Antonella Petrillo. Early assessment of colorectal cancer patients with liver metastases treated with antiangiogenic drugs: The role of intravoxel incoherent motion in diffusion-weighted imaging. *Plos One*, 2015. doi:10.1371/journal.pone.0142876.

[29] Yair Granot and Boris Rubinsky. Mass transfer model for drug delivery in tissue cells with reversible electroporation. *Int J Heat Mass Transf*, 2008. URL: 10.1016/j.ijheatmasstransfer.2008.04.041.

[30] Gabriele Hahn, Ina Sorge, Bernd Gruhn, Katja Glutig, Wolfgang Hirsch, Ravi Bhargava, Julia Furtner, Mark Born, Cornelia Schroder, Hakan Ahlstrom, Sylvie Kaiser, Jorg Detlev Moritz, Christian Wilhelm Kunze, Manohar Shroff, Eira Stokland, Zuzana Jirakova Trnkova, Marcus Schultze-Mosgau, Stefanie Reif, Claudia Bacher-Stier, and Hans-Joachim Mentzel. Pharmacokinetics and safety of gadobutrol-enhanced magnetic resonance imaging in pediatric patients. *Investigative radiology*, 2009. doi:10.1097/RLI.0b013e3181bfe2d2.

[31] Greg Hong, Tina Khazaee, Santiago F. Cobos, Spencer D. Christiansen, Junmin Liu, Maria Drangova, and David W. Holdsworth. Characterizing diffusion-controlled release of small-molecules using quantitative mri in view of applications to orthopedic infection. *NMR in Biomedicine*, 2024. URL: https://doi.org/10.1002/nbm.5254.

[32] Kelsey A. Hopkins, Nicole Vike, Xin Li, Jacqueline Kennedy, Emma Simmons, Joseph Rispoli, and Luis Solorio. Noninvasive characterization of in situ forming implant diffusivity using diffusion-weighted mri. *Journal of Controlled Release*, 2019. URL: https://doi.org/10.1016/j.jconrel.2019.07.019.

[33] Shah Hussain, Iqra Mubeen, Niamat Ullah, Syed Shahab Ud Din Shah, Bakhtawar Abduljalil Khan, Muhammad Zahoor, Riaz Ullah, Farhat Ali Khan, and Mujeeb A. Sultan. Modern diagnostic imaging technique applications and risk factors in the medical field: A review. *BioMed Research International*, 2022. doi:10.1155/2022/5164970.

[34] Geon-Ho Jahng, Ka-Loh Li, Leif Ostergaard, and Fernando Calamante. Perfusion magnetic resonance imaging: A comprehensive update on principles and techniques. *Korean Journal of Radiology*, 2014. URL: https://doi.org/10.3348/kjr.2014.15.5.554.

[35] Rakesh K. Jain. Barriers to drug delivery in solid tumors. *Scientific American*, 1994.

doi:10.1038/scientificamerican0794-58.

[36] Jesse V. Jokerst and Sanjiv S. Gambhir. Molecular imaging with theranostic nanoparticles. *Accounts of Chemical Research*, 2011. doi:10.1021/ar200106e.

[37] Filip Karan and Christian Kurrer. Medicines and medical devices, 2025. URL: https://www.europarl.europa.eu/factsheets/en/sheet/50/medicines-and-medical-devices.

[38] M.A. Khanday, Aasma Rafiq, and Khalid Nazir. Mathematical models for drug diffusion through the compartments of blood and tissue medium. *Alexandria Journal of Medicine*, 2016. URL: http://dx.doi.org/10.1016/j.ajme.2016.03.005.

[39] Ameya R. Kirtane, Christina Karavasili, Aniket Wahane, Dylan Freitas, Katelyn Booz, Dao Thi Hong Le, Tiffany Hua, Stephen Scala, Aaron Lopes, Kaitlyn Hess, Joy Collins, Siddartha Tamang, Keiko Ishida, Johannes L. P. Kuosmanen, Netra Unni Rajesh, Nhi V. Phan, Junwei Li, Annlyse Krogmann, Jochen K. Lennerz, Alison Hayward, Robert Langer, and Giovanni Traverso. Development of oil-based gels as versatile drug delivery systems for pediatric applications. *S C I E N C E A D V A N C E S*, 2022. URL: https://science.org/doi/10.1126/.

[40] Edward Klatt. *Robbins and Cotran Pathologic Basis of Disease*. Elsevier, 2016.

[41] Timo Koch, Martin Schneider, Rainer Helmig, and Patrick Jenny. Modeling tissue perfusion in terms of 1d-3d embedded mixed-dimension coupled problems with distributed sources. *Journal of Computational Physics*, 2020. URL: https://doi.org/10.1016/j.jcp.2020.109370.

[42] K. Kooiman, H. J. Vos, M. Versluis, and N. de Jong. Ultrasound and microbubble guided drug delivery. *Advanced Drug Delivery Reviews*, 2014. doi:10.1016/j.addr.2014.03.003.

[43] B. B. Lahiri, S. Bagavathiappan, T. Jayakumar, and J. Philip. Medical applications of infrared thermography: A review. *Infrared Physics & Technology*, 2012. doi:10.1016/j.infrared.2012.03.007.

[44] David G. Levitt. Physiologically based pharmacokinetic modeling of amino acid and peptide drugs delivered by intravenous infusion. *Journal of Pharmacokinetics and Pharmacodynamics*, 37(2):143–162, 2010.

[45] Umberto Lucia. *Elementi di Ingegneria delle terapie termiche*. Cult, 2022.

[46] Dr. Martin Makary. U.s. food and drug administration (fda), 2025. URL: https://www.fda.gov.

[47] Francis Man, Twan Lammers, and Rafael T. M. de Rosales. Imaging nanomedicine-based drug delivery: a review of clinical studies. *Mol Imaging Biol*, 2018. doi:10.1007/s11307-018-1255-2.

[48] Jennifer R. Marin, Jonathan Rodean, Matt Hall, Elizabeth R. Alpern, Paul L. Aronson, Pradip P. Chaudhari, Eyal Cohen, Stephen B. Freedman, Rustin B. Morse, Alon Peltz, Margaret Samuels-Kalow, Samir S. Shah, Harold K. Simon, and Mark I. Neuman. Racial and ethnic differences in emergency department diagnostic imaging at us children's hospitals, 2016-2019. *JAMA Network Open*, 2021. doi:10.1001/jamanetworkopen.2020.33710.

[49] Lacey R. McNally, Megan Mezera, Desiree E. Morgan, Peter J. Frederick, Eddy S.

Yang, Isam-Eldin Eltoum, and William E. Grizzle. Current and emerging clinical applications of multispectral optoacoustic tomography (msot) in oncology. *Clin Cancer*, 2016. doi:10.1158/1078-0432.CCR-16-0573.

[50] Constantin Mircioiu, Victor Voicu, Valentina Anuta, Andra Tudose, Christian Celia, Donatella Paolino, Massimo Fresta, Roxana Sandulovici, and Ion Mircioiu. Mathematical modeling of release kinetics from supramolecular drug delivery systems. *Pharmaceutics*, 2019. URL: 10.3390/pharmaceutics11030140.

[51] Seyed M. Mirvakili and Robert Langer. Wireless on-demand drug delivery. *NatuRE ELEctronics*, 2021. doi:10.1038/s41928-021-00614-9.

[52] Arman Namvar, Bill Lozanovski, David Downing, Tom Williamson, Endri Kastrati, Darpan Shidid, David Hill, Ulrich Buehner, Stewart Ryan, Peter F Choong, Reza Sanaei, Martin Leary, and Milan Brandt. Customized additive-manufactured implants for ovine femora: A finite element and experimental study. *Frontiers in Bioengineering and Biotechnology*, 2023. doi:10.3389/fbioe.2024.1386816.

[53] Rahul M. Nikam, Xuyi Yue, Gurcharanjeet Kaur, Vinay Kandula, Abdulhafeez Khair, Heidi H. Kecskemethy, Lauren W. Averill, and Sigrid A. Langhans. Advanced neuroimaging approaches to pediatric brain tumors. *Cancers*, 2022. doi:10.3390/cancers14143401.

[54] Ronan O'Brien, Natalia Markova, and Geoffrey A. Holdgate. *Applied Biophysics for Drug Discovery*. John Wiley and Sons Ltd., 2017.

[55] Mamata Panda. Inhalation therapy in children with wheezing and asthma: Spacer or valved holding chamber (vhc) is an optimal drug delivery system. *Research and Reviews in Pediatrics*, 2024. URL: https://journals.lww.com/rrp/Fulltext/2024/24030/Inhalation_therapy_in_children_with_wheezing_and.5.aspx, doi:10.4103/rrp.rrp_1_24.

[56] European Parliament and Council. Directive 2001/83/ec of the european parliament and of the council of 6 november 2001 on the community code relating to medicinal products for human use, 2025. URL: https://eur-lex.europa.eu/legal-content/EN/TXT/?uri=CELEX%3A32001L0083.

[57] Yun Peng, Zeting Zhang, Lichun He, Conggang Li, and Maili Liu. Nmr spectroscopy for metabolomics in the living system: recent progress and future challenges. *Analytical and Bioanalytical Chemistry*, 2024. URL: https://doi.org/10.1007/s00216-024-05137-8.

[58] Baris E. Polat, Douglas Hart, Robert Langer, and Daniel Blankschtein. Ultrasound-mediated transdermal drug delivery: Mechanisms, scope, and emerging trends. *J Control Release*, 2011. doi:10.1016/j.jconrel.2011.01.006.

[59] Jaka Potočnik, Shane Foley, and Edel Thomas. Current and potential applications of artificial intelligence in medical imaging practice: A narrative review. *Journal of Medical Imaging and Radiation Sciences*, 2023. doi:10.1016/j.jmir.2023.03.033.

[60] Giacomo Ricci. Principi di funzionamento di spect e pet e recenti evoluzioni tecnologiche, 2012-2013.

[61] E. F. J. Ring and K. Ammer. Infrared thermal imaging in medicine. *Physiological Measurement*, 2012. doi:10.1088/0967-3334/33/3/R33.

[62] Malcolm Rowland and Thomas N. Tozer. *Clinical Pharmacokineticsand Pharmacodynamics: Concepts and Applications*. Lippincott Williams and Wilkins, 2011.

[63] Val M. Runge. Safety of magnetic resonance contrast media. *Topics in Magnetic Resonance Imaging*, 2018. doi:10.1097/00002142-200108000-00007.

[64] Suliman Salih, Aisyah Elliyanti, Hasina Khan, Ajnas Alkatheeri, Fatima AlYafei, and Bashayer Almarri. The role of molecular imaging in personalized medicine. *Journal of Personalized Medicine*, 2023. doi:10.3390/jpm13020369.

[65] James F. Schenk, Gregory C. McKinnon, and Mark A. Griswold. Mri techniques for perfusion imaging. *European Radiology*, 14(3):383–393, 2004.

[66] Silvia Seoni, Alen Shahini, Kristen M. Meiburger, Francesco Marzola, Giulia Rotunno, U. Rajendra Acharya, Filippo Molinari, and Massimo Salvi. All you need is data preparation: A systematic review of image harmonization techniques in multicenter/device studies for medical support systems. *Computer Methods and Programs in Biomedicine*, 2024. URL: https://doi.org/10.1016/j.cmpb.2024.108200.

[67] Silvia Seoni, Alen Shahini, Kristen M. Meiburger, Francesco Marzola, Giulia Rotunno, U. Rajendra Acharya, Filippo Molinari, and Massimo Salvi. All you need is data preparation: A systematic review of image harmonization techniques in multicenter/device studies for medical support systems. *Computer Methods and Programs in Biomedicine*, 2024. doi:10.1016/j.cmpb.2024.108200.

[68] Y. Shu, H. Liang, and Y. et al. Liu. Bioinspired microneedles with enhanced tissue penetration and minimal pain. *Acta Biomaterialia*, 135:179–193, 2021. doi:10.1016/j.actbio.2021.07.015.

[69] Siemens Healthcare. Magnetom prisma the 3t powerpack for exploration., 2013. URL: www.siemens.com/healthcare.

[70] Siemens Healthcare. Symbia intevo, 2014. URL: www.siemens.com/symbia-intevo.

[71] Siemens Healthcare. Clearly going beyond, 2023. URL: siemens-healthineers.com/biographmCT.

[72] Richard F. Spaide, James M Klancnik Jr., and Michael J. Cooney. Retinal vascular layers imaged by fluorescein angiography and optical coherence tomography angiography. *JAMA Ophthalmology*, 2015. doi:10.1001/jamaophthalmol.2014.3616.

[73] Petra Stohanzlova and Radim Kolar. Tissue perfusion modelling in optical coherence tomography. *BioMedical Engineering OnLine*, 2017. doi:10.1186/s12938-017-0320-4.

[74] Houman Tahmasebi, Shervin Asgari, Alexandra Hall, Victoria Higgins, Ashfia Chowdhury, Rebecca Thompson, Mary Kathryn Bohn, Joseph Macri, and Khosrow Adeli. Influence of ethnicity on biochemical markers of health and disease in the caliper cohort of healthy children and adolescents. *Clin Chem Lab Med*, 2019. URL: https://doi.org/10.1515/cclm-2019-0876.

[75] Henrik S. Thomsen and Sameh K. Morcos. Contrast media and the kidney: European society of urogenital radiology (esur) guidelines. *The British Journal of Radiology*, 2009. doi:10.1259/bjr/26964464.

[76] Paul S. Tofts. Modeling tracer kinetics in dynamic gd-dtpa mr imaging. *Journal of Magnetic Resonance Imaging*, 1997. doi:10.1002/jmri.1880070113.

[77] Paolo Trucillo. Drug carriers: A review on the most used mathematical models for drug release. *Processes*, 2022. URL: https://doi.org/10.3390/pr10061094.

[78] unknown. Capitolo 2. studio della diffusione mediante immagini di risonanza magnetica. URL: http://www.etsrm.it/doc_rubriche/154-012-02Capitolo2.pdf.

[79] Rudolf L.M. van Herten, Amedeo Chiribiri, Marcel Breeuwer, Mitko Veta, and Cian M. Scannell. Physics-informed neural networks for myocardial perfusion mri quantification. *Medical Image Analysis*, 2022. doi:10.1016/j.media.2022.102399.

[80] Ava M. Vargason, Aaron C. Anselmo, and Samir Mitragotri. The evolution of commercial drug delivery technologies. *Nature Biomedical Engineering*, 2021. URL: https://doi.org/10.1038/s41551-021-00698-w.

[81] Diego Vásquez, Luis Medina, and Gabriela Martínez. Finite element optimization of 3d-printed pla scaffolds for bone tissue engineering using taguchi method. *Acta Bioengineering and Biomechanics*, 2025. doi:10.37190/abb-02572-2024-03.

[82] Isabeau Vermeulen, Emre M. Isin, Patrick Barton, Berta Cillero-Pastor, and Ron M.A. Heeren. Multimodal molecular imaging in drug discovery and development. *Drug Discovery Today*, 2022. URL: https://doi.org/10.1016/j.drudis.2022.04.009.

[83] V. Vighetto, E. Pascucci, N.M. Percivalle, A. Troia, K.M. Meiburger, M.R.P. van den Broek, T. Segerse, and V. Cauda. Functional nanocrystal as effective contrast agents for dual-mode imaging: Live-cell sonoluminescence and contrast-enhanced echography. *Ultrasonics Sonochemistry*, 2025. doi:10.1016/j.ultsonch.2025.107242.

[84] Anita Ioana Visan and Irina Negut. Integrating artificial intelligence for drug discovery in the context of revolutionizing drug delivery. *Life*, 2024. doi:10.3390/life14020233.

[85] VisualSonics. Redefining preclinical imaging, 2008. URL: www.visualsonics.com.

[86] Hassan Waqasa, Umar Farooq, Dong Liu, Metib Alghamdi, Sobia Noreen, and Taseer Muhammad. Numerical investigation of nanofluid flow with gold and silver nanoparticles injected inside a stenotic artery. *Materials and Design*, 2022. doi:10.1016/j.matdes.2022.111130.

[87] Julia Welzel, Maike Bruhns, and Helmut H. Wolff. Optical coherence tomography in contact dermatitis and psoriasis. *Archives of Dermatological Research*, 2003. doi:10.1007/s00403-003-0390-y.

[88] Wikipedia contributors. Contrast-enhanced ultrasound, 2025. URL: https://en.wikipedia.org/wiki/Contrast-enhanced_ultrasound.

[89] Wikipedia contributors. Cytosol, 2025. URL: https://en.wikipedia.org/wiki/Cytosol?utm_source=chatgpt.com.

[90] Wikipedia contributors. In vivo magnetic resonance spectroscopy, 2025. URL: https://en.wikipedia.org/wiki/In_vivo_magnetic_resonance_spectroscopy.

[91] Wikipedia contributors. Matrix-assisted laser desorption/ionization, 2025. URL: https://en.wikipedia.org/wiki/Matrix-assisted_laser_desorption/ionization.

[92] Wikipedia contributors. Sonoporation, 2025. URL: https://en.wikipedia.org/wiki/Sonoporation.

[93] Ibtihag Yahya, Razan Atif, Lina Ahmed, Tahleel Salah Eldeen, Akram

Omara, and Megdi Eltayeb. Mathematical modeling of diffusion controlled drug release profiles from nanoparticles. *International Journal of Research and Scientific Innovation (IJRSI)*, 2019. URL: https://www.researchgate.net/profile/Ibtihag-Yahya/publication/342902966_Mathematical_Modeling_of_Diffusion_Controlled_Drug_Release_Profiles_from_Nanoparticles/links/5f0cd3f892851c38a51ccae8/Mathematical-Modeling-of-Diffusion-Controlled-Drug-Release-Profiles/-from-Nanoparticles.pdf.

[94] Yuqi Yang, Huazheng Liang, Chun Tang, Yuan Cheng, and Liang Cheng. Exploration of ultrasound-sensitive biomaterials in cancer theranostics. *Advanced Functional Materials*, 2024. URL: https://doi.org/10.1002/adfm.202313454.

[95] Tian Yuan, Wenbo Zhan, Michele Terzano, Gerhard A. Holzapfel, and Daniele Dini. A comprehensive review on modeling aspects of infusion-based drug delivery in the brain. *Acta Materialia*, 2024. doi:10.1016/j.actbio.2024.07.015.